(NASA-CR-156776) ADVANCED MICROWAVE RADIOMETER ANTENNA SYSTEM STUDY Final Report, Sep. 1974 - Jan. 1976 (Hughes Aircraft Co.) 143 p HC A07/MF A01 CSCL 20N

N78-29304

Unclas
G3/32 27519

ADVANCED MICROWAVE RADIOMETER ANTENNA SYSTEM STUDY

W. H. Kummer
A. T. Villeneuve
A. F. Seaton
Antenna Department, Radar Systems Group
Hughes Aircraft Company
Culver City, California 90230

August 1976

Final Report for Period September 1974 — January 1976

Prepared for

GODDARD SPACE FLIGHT CENTER

Greenbelt, Maryland 20771

TECHNICAL REPORT STANDARD TITLE PAGE

1. Report No.	2. Government Accession No.	3. Recipient's Catalog No.

4. Title and Subtitle	5. Report Date
ADVANCED MICROWAVE RADIOMETER ANTENNA SYSTEM STUDY	August 1976
	6. Performing Organization Code

7. Author(s)	8. Performing Organization Report No.
W.H. Kummer A.T. Villeneuve A.F. Seaton	Dept. Ref. 2153/872 P76-429; HAC Ref. D2444

9. Performing Organization Name and Address	10. Work Unit No.
Antenna Department, Radar Systems Group Hughes Aircraft Company Culver City, CA 90230	11. Contract or Grant No. NAS 5-20738
	13. Type of Report and Period Covered Final Report 11/74 through 1/76
12. Sponsoring Agency Name and Address L. R. Dod/GSFC Technical Officer National Aeronautics and Space Administration Goddard Space Flight Center Greenbelt, Maryland 20771	14. Sponsoring Agency Code

15. Supplementary Notes

16. Abstract

The practicability of a multi-frequency antenna for spaceborne microwave radiometers was considered in detail by the Hughes Aircraft Company as an alternative to multiple antennas. The program consisted of a comparative study of various antenna systems, both mechanically and electronically scanned, in relation to specified design goals and desired system performance. The study involved several distinct tasks: definition of candidate antennas that are lightweight and that, at the specified frequencies of 5, 10, 18, 22, and 36 GHz, can provide conical scanning, dual-linear polarization, and simultaneous multiple-frequency operation; examination of various feed systems and phase-shifting techniques; detailed analysis of several key performance parameters such as beam efficiency, sidelobe level, and antenna beam footprint size; and conception of an antenna/feed system that could meet the design goals. Candidate antennas examined include phased arrays, lenses, and optical reflector systems. Mechanical, electrical, and performance characteristics of the various systems were tabulated for ease of comparison. It was concluded that a system comprised of an offset paraboloidal reflector, a dichroic mirror, and two corrugated feed horns is the candidate to cover the entire frequency range and provide both components of linear polarization. Scanning would be accomplished by mechanical movement of the entire system. With careful attention to mechanical tolerances, the recommended system would have an estimated beam efficiency of greater than 85 percent.

17. Key Words (Selected by Author(s))		18. Distribution Statement
radiometer	multi-frequency operation	
feed horns	electronic scanning	
arrays	dichroic mirrors	
lenses	beam efficiency	
reflectors	mechanical scanning	
sidelobes		

19. Security Classif. (of this report)	20. Security Classif. (of this page)	21. [illegible]	22. Price*
Unclassified	Unclassified		

PREFACE

Future remote sensing of the atmosphere and the earth's surface by spaceborne microwave radiometers will require an antenna that can provide conical scanning for high-resolution mapping, dual-linear polarization for precise signal discrimination, high beam efficiency for large target contrast, and multiple frequency operation over a range from 3 to 40 GHz. In the straightforward approach, which has been followed to date, one antenna is utilized for each frequency of interest; the resulting multiple antennas create problems in weight, deployment, and dynamic balancing of the spacecraft, when mechanical scanning is employed. An attractive alternative is the use of one antenna that can operate at more than one frequency. The practicability of such a multi-frequency antenna, specifically, one that can operate simultaneously at five frequencies with both vertical and horizontal linear polarization, was considered in detail by the Hughes Aircraft Company. The program consisted of a comparative study of various antenna systems, both mechanically and electronically scanned, in relation to specified design goals and desired system performance; the results are reported in this document.

The study involved several distinct tasks: definition of candidate antennas that are lightweight and that, at the specified frequencies of 5, 10, 18, 22, and 36 GHz, can provide the desired conical scanning, dual-linear polarization, and simultaneous multiple-frequency operation; examination of various feed systems and phase-shifting techniques; detailed analysis of several key performance parameters such as beam efficiency, sidelobe level, and antenna beam footprint size; and conception of an antenna/feed system that could meet the design goals. Candidate antennas examined include phased arrays, lenses, and optical reflector systems. Mechanical and electrical

performance characteristics of the various systems were tabulated for ease of comparison.

It was concluded that a system comprised of an offset dichroic parabolic reflector, a dichroic planar surface, and two corrugated feed horns is the candidate to cover the entire frequency range and provide both components of linear polarization. Scanning would be accomplished by mechanical movement of the entire system. With careful attention to mechanical tolerances, the recommended system would have an estimated beam efficiency of greater than 85 percent.

CONTENTS

CONTENTS (Continued)

LIST OF ILLUSTRATIONS

LIST OF ILLUSTRATIONS (Continued)

LIST OF ILLUSTRATIONS (Continued)

LIST OF ILLUSTRATIONS (Continued)

LIST OF TABLES

1.0 INTRODUCTION

Remote sensing of the atmosphere and the earth's surface by microwave radiometric techniques poses a difficult antenna system design problem. For example, the microwave radiometer onboard COSMOS 243 has four channels ranging from 3.5 to 37.5 GHz, and the Scanning Multispectral Microwave Radiometer to be flown on Nimbus-G has five channels ranging from 4.99 to 36 GHz. Similar multiple operating frequencies have been proposed for radiometric systems for inclusion on the Earth Observation Satellite and on SEASAT; present plans involve sampling of the frequency band in the range from 3 to 40 GHz at five discrete frequencies so that at least five scanned antennas might be deployed on one satellite. This proliferation of antennas creates problems in their deployment as well as in the dynamic balancing of the satellite itself, if mechanical scanning techniques are utilized.

Future research and development in microwave radiometry, as a spaceborne remote sensing technique, requires an antenna that can provide conical scanning for high-resolution mapping, dual-linear polarization for precise signal discrimination, high beam efficiency for large target contrast, and multiple frequency operation over a range from 3 to 40 GHz. Ideally, such an antenna must also be lightweight. An interesting solution is the use of one antenna or only a few antennas that operate at more than one frequency. The practicability of such a multi-frequency antenna was considered in detail by the Hughes Aircraft Company through a comparative study of various antenna systems, both mechanically and electronically scanned, in relation to specified design goals and desired system performance. The results of this study are reported in this document.

1.1 DESIGN GOALS

The ultimate goal for the microwave radiometric antenna system studied during the program is simultaneous operation at five frequencies with either vertical or horizontal polarization at each frequency. The center frequencies specified for the initial design are 5, 10, 18, 22 and 36 GHz, and the RF bandwidth of each channel should be greater than or equal to 500 MHz. The parameters desired at each frequency are indicated in Table 1-1.

The linear size of the 3-dB antenna beam footprint on the earth's surface, from an altitude of 1000 km, is to be approximately equal to the instantaneous field-of-view values given in Table 1-1. (It should be noted that the values for this parameter and for several others are provided for two aperture sizes: 1 and 2 meters.) The footprint size constraint should hold for any antenna beam scan angle. The linear size of the antenna footprint is the length, L_i, in the in-track (with respect to the spacecraft orbital velocity vector) direction and the length, L_c, in the cross-track direction, when the antenna is in the non-scanning position. The antenna system must also provide coaxially oriented beams, with respect to the radiating aperture, at each of the five operating frequencies.

TABLE 1-1. MICROWAVE RADIOMETER ANTENNA SYSTEM DESIGN GOALS*

Parameter	Center Operating Frequency (GHz)									
	5		10		18		22		36	
Wavelength, cm	6		3		1.67		1.36		0.84	
RF bandwidth, MHz	500		500		500		500		500	
Aperture size, m	1	2	1	2	1	2	1	2	1	2
3rd B beamwidth, deg degrees	4.3	2.1	2.1	1.1	1.9	0.6	1.0	0.5	0.6	0.3
Scan time, seconds	30	15	15	7.5	8	4	7	3.5	4	2
Instantaneous field of view, km	1	2	1	2	1	2	1	2	1	2
In-track	201.65	100.88	190.4	50.23	55.72	27.87	45.58	22.80	27.86	13.96
Cross-track	115.36	57.71	57.66	28.84	32.03	16.02	26.21	13.11	16.02	8.01

*Based on an orbital altitude of 1000 km, an earth radius of 6371 km, an orbital period of 100 minutes, an orbital velocity of 7.72 km/s, and a ground track velocity of 6.67 km/s.

Antenna scan times are for contiguous coverage at each frequency.

It is desired that the antenna beams execute approximately conical scanning with the cone axis parallel to the local vertical. The half-angle of the cone, θ_c, is to be 45 degrees, and an angle of incidence at the surface of the earth, θ_i, of 55 ±2 degrees is to be maintained. The minimum total scan angle, θ_s, in the azimuthal direction is to be ±35 degrees with respect to the spacecraft velocity vector.

The maximum sidelobe level of the antenna system in the scanned direction (cross-track) is to be more than 25 dB below the major lobe for all beam angular positions, and the maximum level of all sidelobes in the cross-scan (in-track) direction is to be more than 15 dB below the major lobe. Cross-polarization isolation between the two linearly polarized components must be greater than 25 dB.

Mechanically scanned systems, if utilized, must be statically and dynamically balanced about the scan axis so that gyroscopic torques that might wobble the spacecraft are avoided. In addition, the net angular momentum of the scanning antenna must also be reduced to a negligible value by some means of compensation. Perturbations to the spacecraft are to be held below a rate of 0.01 degree per second.

The exposed surfaces of the antenna system will be subject to the extreme temperature ranges encountered in spaceflight (-200 to +100°C), and at any time, the antenna system may experience temperature differentials across the structure within this range. Consequently, the structure of the antenna system must be so designed that the operating characteristics of the antenna are not appreciably degraded by the stresses resulting from these differentials.

The question of antenna system losses was not addressed in detail; losses are directly correlated with the sensitivity and the range of temperatures that can be obtained with any one system, and detailed discussions are available in the literature. Beam efficiency, however, which is considered to be the most critical parameter, was studied extensively. Because of its prime importance, it must be as high as is practicable; consequently, the design goal is set at 85 percent for all scan angles. General aspects of this parameter as related to radiometric antennas are considered in the next subsection.

1.2 BEAM EFFICIENCY

As mentioned above, the most critical parameter of a radiometric antenna is its beam efficiency. Beam efficiency may be defined as the percentage of the total radiated power that lies within the main beam with the desired polarization when the antenna is viewed as a transmitting antenna. Alternatively, it is the percentage of the total received power from a uniform distribution of sources, all at one temperature, that comes through the main beam with the desired polarization. It is a measure of how well the antenna discriminates against sources outside the main beam and is related to the average sidelobe level. If the beam is essentially circular out to the first null, then it can be shown that the average gain of the sidelobes is given by

$$G_{sav} = \frac{1 - \alpha}{\left(\cos \frac{\textcircled{H}_0}{2}\right)^2} \tag{1-1}$$

where α is the fraction of power in the main beam with the desired polarization (beam efficiency) and $\textcircled{H}_0$ is the null-to-null beamwidth. For apertures with distributions of the form

$$f(r) = b + \left[1 - \left(\frac{2r}{D}\right)^2\right]^P \tag{1-2}$$

where D is the aperture diameter, b is the pedestal, and r is the radius from the aperture center, the relationship between half-power beamwidth $\textcircled{H}$ and null-to-null beamwidth is given in Table 1-2. If 2.65 is taken as a representative value of the ratio, the values in Table 1-3 then give the acceptable average sidelobe gain relative to isotropic. It is evident that, for the narrow beamwidths considered, the acceptable average sidelobe gain is very insensitive to the beamwidth and depends primarily on the required efficiency. In the absence of errors in the aperture distribution,

TABLE 1-2. RATIO OF NULL-TO-NULL BEAMWIDTH AND HALF-POWER BEAMWIDTH
(See Equation 1-2)

Exponent (p)	Pedestal (b)	
	0	1/4
0	2.39	2.39
1	2.57	2.55
2	2.76	2.73

TABLE 1-3. ACCEPTABLE AVERAGE GAINS OF SIDELOBES RELATIVE TO ISOTROPIC

Half-Power Beamwidth (degrees)	Average gain of Sidelobes (dB)	
	With 0.85-Beam Efficiency	With 0.90-Beam Efficiency
0.29	-8.24	-10.0
0.59	-8.24	-10.0
0.97	-8.24	-10.0
2.13	-8.23	- 9.99
4.27	-8.20	- 9.96

the mean sidelobe level can be made extremely low and the corresponding beam efficiency can be very high. For example, for the case b = 0 and p = 1, the beam efficiency in the absence of errors is 98.3 percent (Hansen, 1964). For uniform illumination, the beam efficiency is 83.8 percent. However, random errors produced by manufacturing and component tolerances can cause a significant reduction of this ideal efficiency by

introducing phase errors into the aperture distribution that remove some of the main beam energy and scatter it into the sidelobe region.

Another aspect that affects a dual-polarized microwave radiometric antenna is the cross-polarization isolation; the relationship of this parameter to the overall beam efficiency is shown in the derivation that follows.

As stated previously, beam efficiency is defined as the ratio of the power received by the antenna within the first null of the major lobe in a given polarization to the total power received by the antenna for all polarizations. Let

P_{mb-v} = power in wanted polarization (vertical polarization as an example) in main beam

P_{t-v} = total received power by antenna for vertical polarization

P_{t-h} = total received power by antenna for horizontal polarization

Then the beam efficiency can be expressed as

$$BE_v = \left(\frac{P_{mb-v}}{P_{t-v} + P_{t-h}} \right) = \left(\frac{P_{mb-v}}{\text{total received power}} \right) \tag{1-3}$$

The cross-polarization isolation (CPI) is defined as the ratio of the power received by the antenna system within the first null of the major lobe in a given (wanted) polarization to the total power received by the antenna from all angles in the other polarization (unwanted):

$$CPI = \frac{P_{mb-v}}{P_{t-h}} \tag{1-4}$$

Then, from Equation (1-3),

$$(BE_v)\,(P_{t-v} + P_{t-h}) = P_{mb-v}$$

$$CPI = \frac{BE_v}{P_{t-h}} \times (\text{total power received}) \qquad (1\text{-}5)$$

Thus, the cross-polarization isolation is the ratio of the beam efficiency and the fraction of the total power appearing as cross-polarized power.

In the design of a dual linearly polarized antenna, definition of the cross-polarized isolation provides some indication of the way in which the beam efficiency could be improved, i.e., by reduction of the cross polarization. However, it is only a necessary condition in specification of the beam efficiency. As an example, for a cross-polarization isolation of 25 dB and a beam efficiency of 85 percent, the fraction of cross-polarized power would be

$$P_{t-h}/P_{total} = -26\ dB$$

1.3 PROGRAM SUMMARY

The study program performed by Hughes involved several distinct tasks. Candidate antennas, both mechanically and electronically scanned, were defined that, at the specified frequencies, can provide the desired general performance: conical scanning, dual-linear polarization, and simultaneous multiple-frequency operation. Various feed systems were also examined, as were different phase-shifting techniques. The candidate systems included phased arrays, lenses, and optical reflector systems that are extensions of single-frequency systems with multiple or broadband feeds.

In general, the use of arrays directly as the main antenna aperture provides the most flexibility and aperture control. In addition, arrays suffer little pattern degradation aa a function of scan angle. However, because they may require many large modules and complex feeding systems, arrays may be quite heavy. If the array is large, the weight can be reduced by thinning the aperture, but at the expense of a rise in the far-out sidelobe level and a decrease in beam efficiency. Arrays are most naturally single steered-beam systems but can be made into multiple-beam systems by the addition of appropriate feeding networks. Phased arrays present three specialized areas of concern: the design of radiating branch lines to handle both senses of polarization and/or multiple frequencies, the design of a feeding network that includes phase shifters, and the interleaving of arrays to cover multiple frequencies from a single aperture.

Reflectors are light and broadband, with bandwidths limited only by type of feed. They can be unfurled so that large apertures can be obtained. Large symmetrical systems have better polarization characteristics than offset systems, but aperture blockage is reduced or eliminated with the latter. Depending on the feed system used, reflectors can be either single steered-beam antennas or multiple-beam antennas. When fed by arrays, they are more naturally single, steered-beam systems. Use of a feed array provides considerable control over the aperture distribution so that good sidelobes can be maintained when the beam is moved. Such antennas can be made into multiple-beam systems by the addition of beam-forming networks, but this approach adds significant complexity. Feeds formed from clusters of horns are more naturally multiple-beam systems with separate terminals. The sidelobes of the secondary patterns, however, may be less easily controllable for the various beams in the coverage region compared with those generated by an array feed.

Lens antennas are not subject to aperture blockage effects and, because of their large number of degrees of freedom, can be designed to provide relatively little pattern degradation for off-axis beams. They tend to be heavier than reflectors. Depending on their type and construction,

they may be broadband or narrowband. The bandwidth of the bootlace lens is limited primarily by the bandwidth of the elements at the faces of the lens; the bandwidth of the waveguide lens is inherently somewhat narrow, but this type of system can be made lighter in weight than the bootlace lens.

It was concluded that a system comprised of an offset parabolic reflector, a dichroic mirror, and two corrugated feed horns is a candidate to cover the entire frequency range and provide both components of linear polarization. Scanning will be accomplished by moving the entire system mechanically. With careful attention to mechanical tolerances, the system would have a beam efficiency estimated at greater than 85 percent.

2.0 PHASE-SCANNED ARRAYS

Several different types of arrays that are amenable to phase-scanning techniques were examined; the results of these substudies are presented in this section. The problem of maintaining the desired polarization over the scan angle is germane to all the arrays studied and is discussed first.

2.1 POLARIZATION CONSIDERATIONS

When phased arrays are used to scan a radiometric beam electronically, care must be taken to ensure that the desired polarization is maintained over the scan angle. Vertical and horizontal polarizations are defined in this discussion with respect to Figure 2-1. The horizontally polarized

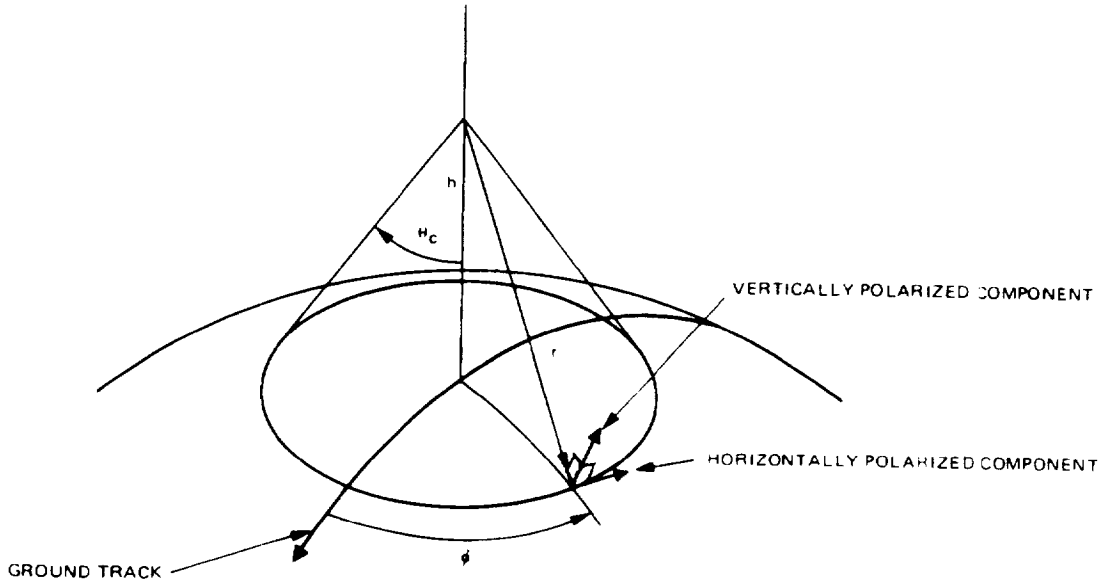

Figure 2-1. Vertical and horizontal components of polarization.

component of the electric field strength vector lies perpendicular to the plane formed by r and h. The "vertical" component of the electric field strength vector lies in the plane formed by r and h and is perpendicular to r.

For true vertical polarization to be obtained over the scan track by means of electronically scanned beams, the radiating elements themselves must provide true vertical polarization on the scan track. Radiators that provide vertically directed electric currents, such as vertical dipoles, fall into this category. Similarly, for true horizontal polarization to be provided over the scan track by means of electronically scanned beams, the radiating elements must provide true horizontal polarization on the scan track. Vertical slots or current loops with vertical axes fall into this category. For example, if vertical slots are used to obtain horizontal polarization, the proper polarization is maintained as the beam is scanned over a cone about the vertical axis, because the electric field vector lies on circles concentric with the slot axes and hence is everywhere horizontal. However, if horizontal slots are used to obtain vertical polarization (i.e., in the plane of incidence), the correct polarization is obtained only along the ground track. As the beam is scanned through angles ϕ on a cone on either side of the ground track, the polarization becomes tilted until, in the limit as ϕ approaches 90 degrees, the polarization becomes purely horizontal. The ratio of the vertically polarized component to the horizontally polarized component is given by

$$\left|\frac{E_v}{E_h}\right|^2 = \left(\frac{\cot \phi}{\cos \theta_c}\right)^2$$

This function is plotted in Figure 2-2 for a cone angle, θ_c, of 45 degrees. It is apparent that the desired polarization isolation is not maintained.

The polarization problem could be corrected if the appropriate fraction of signal from the horizontally polarized array were subtracted from the "vertically" polarized array to cancel out the contribution from the horizontal component in its output. Such a cancellation scheme would be

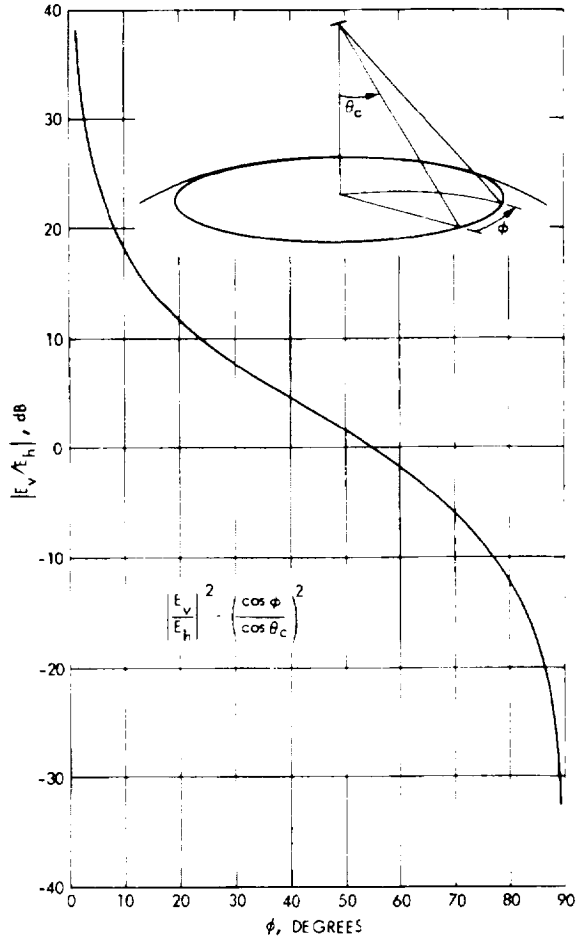

Figure 2-2. Relative vertically and horizontally polarized radiation from horizontal slot as a function of ϕ for a 45-degree ($\pi/4$) cone angle.

scan-dependent. The remaining vertically polarized component would then vary as

$$E_v = \frac{E \cos\phi}{\sqrt{\cos^2\theta_c + \sin^2\theta_c \cos^2\phi}}$$

At ϕ = 35 degrees and θ_c = 45 degrees, a signal loss of 0.95 dB results, compared with that obtained with a true vertically polarized antenna, such as

a vertical dipole. An analogous situation occurs if horizontal dipoles are used to obtain horizontal polarization over the coverage cone.

For arrays in which crossed slots are utilized, the maximum cross-track scan angle that can be achieved is 4.55 degrees, if vertical polarization with a cross-polarized level less than -25 dB is to be maintained without a cancellation scheme. Because the cross polarization is known for a particular array, it can be removed in the signal processing system of the radiometer if the two received components are added properly in phase and amplitude as the array is scanned. This cancellation might be performed using a two dimensional array composed of vertical arrays similar to that discussed in Section 2.2.1. The horizontally polarized output of the arrays of vertically directed slots would be divided into two parts. The first part is used as the horizontally polarized output. The second part would be weighed by an electronically controlled attenuator that is synchronized with the scan controller. This weighed signal is combined with the output of the horizontal slots in such a way as to cancel the horizontal components generated by the slots, leaving only the vertical component. The signal combining would be accomplished in circuitry that came after the S/N of the system was established. If this processing is performed at IF, it precludes the use of a single receiver that switches sequentially between the two components. However, the processing could also be performed at RF by means of variable power dividers controlled in synchronism with the antenna scan; in this case, a single switched receiver could be used.

The polarization problem should be kept in mind during a review of the various arrays discussed in the following pages because some of the antennas require some type of cancellation scheme for the desired polarization purity to be obtained.

2.2 SINGLE FREQUENCY ARRAYS

For the case in which a separate phased array is used to cover each of the five frequency bands, the requirement for dual polarization still mandates use of a specialized array. Because of volume limitations, however, it is highly desirable that the vertical and horizontal components of the signal at a given frequency come from the same aperture. Therefore, only dual-polarized arrays are discussed here. At the millimeter-wave frequencies for which this radiometric system is intended, either slot or round-hold radiators are highly desirable because of the small dimensions involved. In the 5- and 10-GHz bands, dipoles might also be considered practical.

2.2.1 Square-Waveguide Dual-Mode Array

One method by which a dual-polarization capability can be obtained from a slot array is by the launching of two orthogonal modes, TE_{01} and TE_{10}, into square waveguide. Nonresonant crossed slots cut into one wall of this waveguide would couple to the two modes in a controllable fashion. One arm of the crossed slot couples to one mode and the other arm to the other mode. Hence, orthogonally polarized signals can be separated at the ends of the arrays by orthomode transducers. A linear X-band array that operates on this principle (Figure 2-3) was built and tested successfully at Hughes (Goebels and Fong, 1965). A number of these linear arrays can be paralleled to form a planar array. A nonscanning array of this type that directed four different beams into four different quadrants was also built and tested at Hughes (Miller and Forman, 1966). It performed very well.

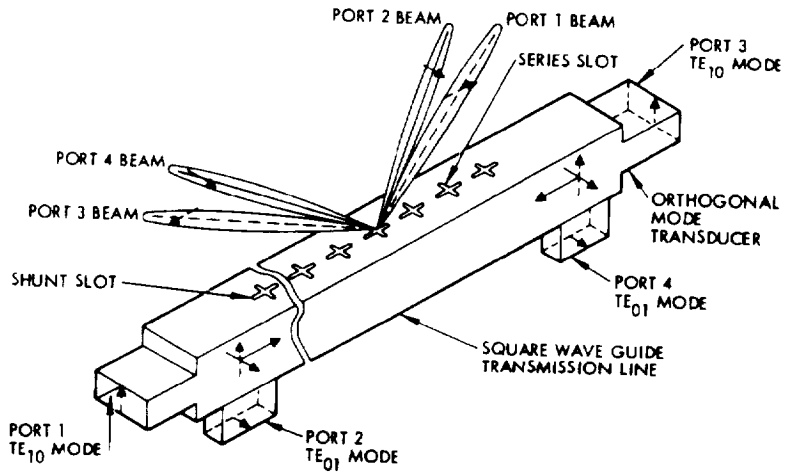

Figure 2-3. Four-port, four-beam linear array.

A phased array composed of dual-mode square waveguides can be obtained by incorporation of orthomode transducers on the end of each branch line. Two sets of terminals are thus made available, one for each orthogonal component of signals received by the array. Two corporate feeds and two sets of phase shifters are then required to complete the antenna. The two

sets of phase shifters must be very nearly identical and driven in the same manner to make the two orthogonally polarized beams track precisely. An array similar to this configuration was built and tested at 37 GHz (Pascalar, 1974). The aperture, which is square, is comprised of 109 individual linear arrays; orthomode transducers at each array output separate the two polarization components of the received radiation into two individual rectangular waveguide outputs. The beam of each polarization component is then individually steered by two groups of current-controlled phase shifters. The phase-shifter outputs are summed in separate edge-slotted waveguide arrays. The electronics are mounted on the back surface of the antenna. Some of the pertinent characteristics are given in Table 2-1.

TABLE 2-1. CHARACTERISTICS OF 37-GHz RADIOMETER

Parameter	Value
Beamwidth, degrees	1.17 x 0.73
Beam efficiency, percent	>90
Dimensions, inches	Length - 39, width - 39, depth - 4
Weight (including receiver and electronics), pounds	99
Deployment	39-inch square faces forward
Power consumption	55 watts at 24.5 volts

With the addition of circulators, a single phase shifter could be used to scan both polarizations simultaneously and thereby eliminate the need for two sets of drivers. At 5 GHz, this type of array can be implemented by means of dipoles and stripline feeding systems.

2.2.2 Overlaid Linearly Polarized Arrays

Another type of waveguide slot array that radiates dual-polarized energy is shown in Figure 2-4. This array, an experimental K_a-band model built at Hughes, consists of two, independent, standing-wave arrays, one

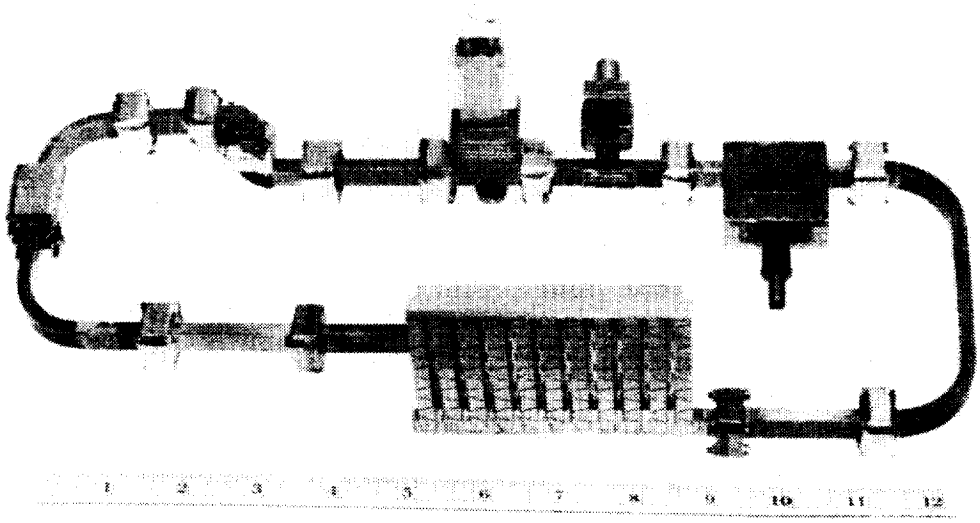

Figure 2-4. 35-GHz variable-polarization array.

overlaid on the other (Strider, 1974). The lower half consists of 10 linear arrays, each with 10 shunt slots cut in the broad wall. Feeding is accomplished via shunt-series slots from the broad wall of a centrally located input waveguide. The upper half of the antenna consists of 11 linear arrays, each having 10 inclined shunt slots cut in the narrow wall. The inclination of the slots with respect to the waveguide "b" dimension is alternated from slot to slot to achieve in-phase radiation for slots spaced at 0.7 free-space wavelength. These upper arrays are orthogonally polarized compared with the polarization of the arrays in the lower half of the antenna and are endfed via narrow-wall shunt-series slots. The use of broad walls for the lower arrays and narrow walls for the upper arrays facilitates the overlaid arrangement; radiation from the lower linear arrays can pass freely between the upper linear arrays.

Measured performance data for the antenna are in close agreement with the theoretical. The maximum VSWRs over the 200-MHz frequency band for the upper and lower halves of the antenna are 1.22:1 and 1.35:1, respectively. Sidelobe levels for both sections are 12.1 dB maximum, and the half-power beamwidth varies from 6 to 7.5 degrees. The measured gain of each half of the antenna exceeds 27 dB.

For operation of the overlaid array as a phased array, the two feed lines are replaced by corporate feed and phase-shifter networks similar to those utilized in the square waveguide array. No orthomode transducers are needed because each waveguide branch line carries only one mode.

2.3 MULTIMODE DUAL-POLARIZED ARRAYS

Two versions of a new type of dual-polarized array were devised during this program. In the first version, the broad walls of the waveguides are in the aperture plane; in the second version, the narrow walls of the waveguides are in the aperture plane. Both types of arrays are of the standing-wave variety.

2.3.1 Broad-Wall Multimode Arrays

Both the broad-wall and the narrow-wall type of multimode array require the use of a number of parallel waveguides with common walls. For one polarization, adjacent waveguides are excited in phase, called "even-mode excitation." For the other polarization, adjacent waveguides are excited 180 degrees out of phase, called "odd-mode excitation." The currents peculiar to each type of excitation are discussed below.

2.3.1.1 Even-Mode Excitation

With even-mode excitation of the broad-wall multimode array, the waveguides are arranged as shown in Figure 2-5 with common narrow walls. Each waveguide is required to carry only the dominant TE_{10} mode and is not large enough to carry higher order modes; consequently, there is no spurious mode problem. When the currents in the top walls of the guides are all driven in phase, they are as shown in Figure 2-6. If short

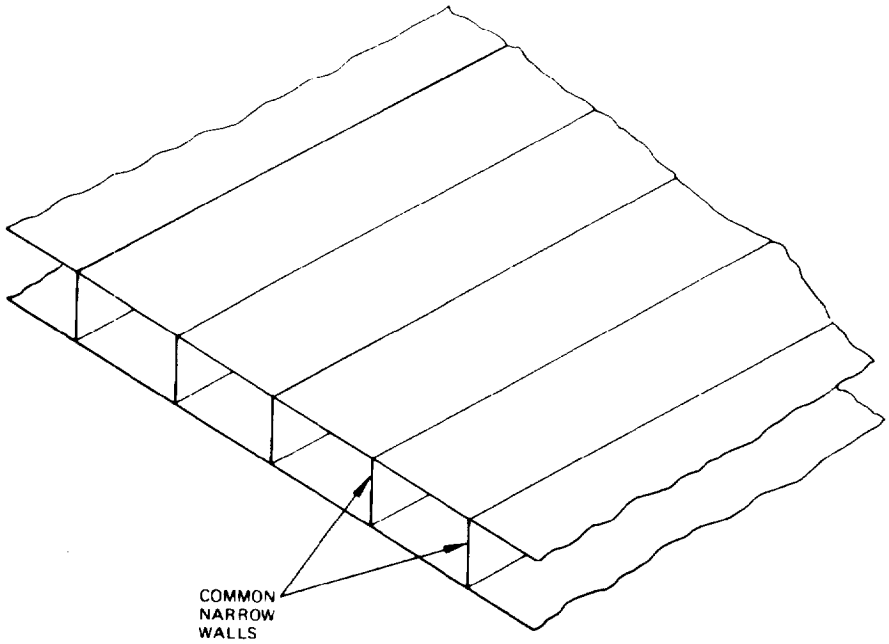

Figure 2-5. Broad-wall multimode array section.

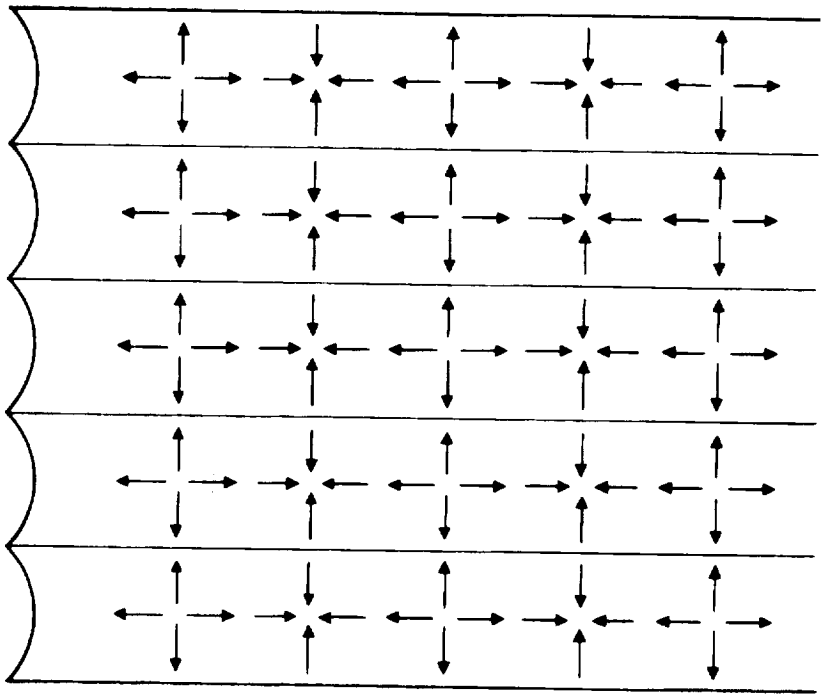

Figure 2-6. Currents in top walls of waveguide for even-mode excitation of broad-wall array.

nonresonant transverse slots are placed over the common walls and quarter-wave chokes cut into the wall under the slots as shown in Figure 2-7, it is possible to couple to the longitudinal component of the current in the top walls of the guides. The slots are called "common-wall" slots and are a variation of "virtual-wall" slots developed at Hughes for a circularly polarized array (Hughes, 1964; Seaton, 1971). The quarter-wave choke in the common wall is necessary to prevent the wall from shorting out the slot, but it does not interrupt any current flow in the narrow walls of the guides. For the present application, the slots would be perfectly centered over the common walls and would thus draw power equally from the two adjacent waveguides. They are made nonresonant to control the amount of coupling at each point along the guide. Because the slots are perpendicular to the wall, they do not couple to the transverse component of current in the top wall of the waveguide.

The phasing of the longitudinal currents in this even-mode excitation is such that, for the generation of a broadside beam, the slots must lie in vertical columns that are a guide wavelength apart. This spacing is undesirable because the guide wavelength in normal waveguide is always greater

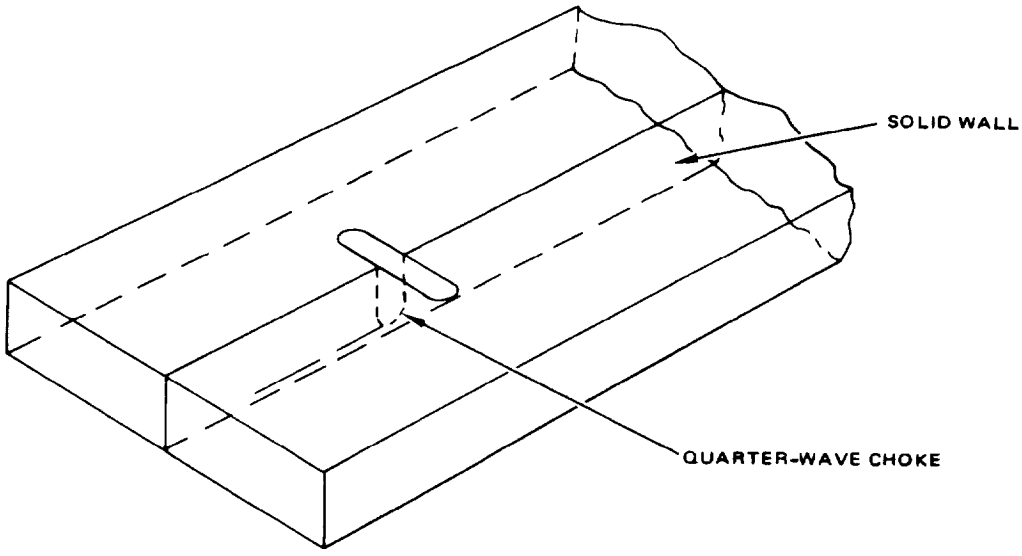

Figure 2-7. Transverse slot centered on the common wall between two waveguides.

than the free-space wavelength and grating lobes will be generated in the forward and backward directions.

One solution to the problem is use of dielectrically loaded slots that are physically short but electrically longer than resonance and that effect a 180-degree phase reversal. These slots would be placed on the common walls at the mid-point between the original columns of slots as shown in Figure 2-8. Although the current intersected by the loaded slots is 180 degrees out of phase with that driving the unloaded slots, the radiated energy will be nearly in-phase because of the unequal electrical lengths of the two types of slots. Each type of slot is nonresonant: one type introduces approximately a 90-degree phase lag into the radiated signal, and the other introduces a similar phase lead. Use of these dielectrically loaded additional slots solves the grating lobe problem because they make the column and row spacings less than one free-space wavelength apart. With very thin common walls, both columns and rows can be spaced as close as 0.707λ.

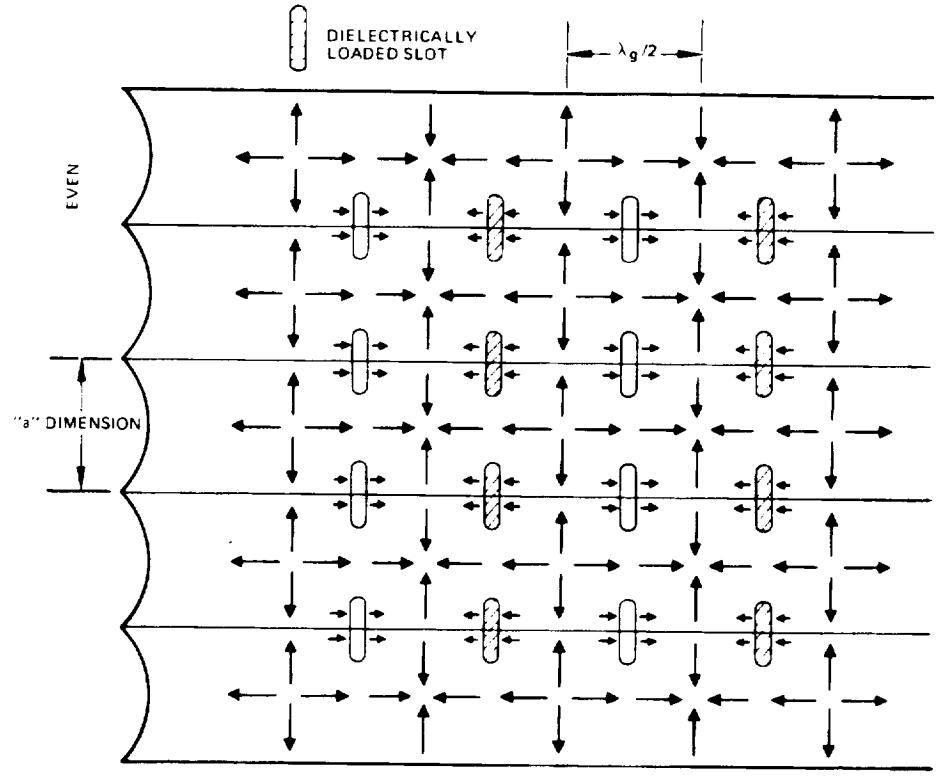

Figure 2-8. Array of transverse common-wall slots coupling to longitudinal current component.

Another possible solution to the grating-lobe problem in large arrays in which the interelement spacing can approach one wavelength is a diagonal deletion of half the elements as shown in Figure 2-8. This approach leaves the remaining slots on a grid of equilateral triangles as seen in Figure 2-9. In this slot arrangement, the distance between successive slots in each of the two principal planes is unchanged, but the distance between successive diagonal rows of slots is too great. It is shown in Appendix A that, if the waveguides are rectangular and unloaded (i.e., contain no dielectric material or periodic structures), if the common walls are negligibly thin, and if the array is designed to produce a broadside beam, the diagonal row spacing, s, is always exactly equal to one free-space wavelength. This result is due to the fact that any change in the "a" dimension of the guide, and hence the cutoff wavelength, λ_c, produces an opposite effect in the guide wavelength, λ_g. The two effects cancel in such a way that the perpendicular distance between diagonal rows is constant.

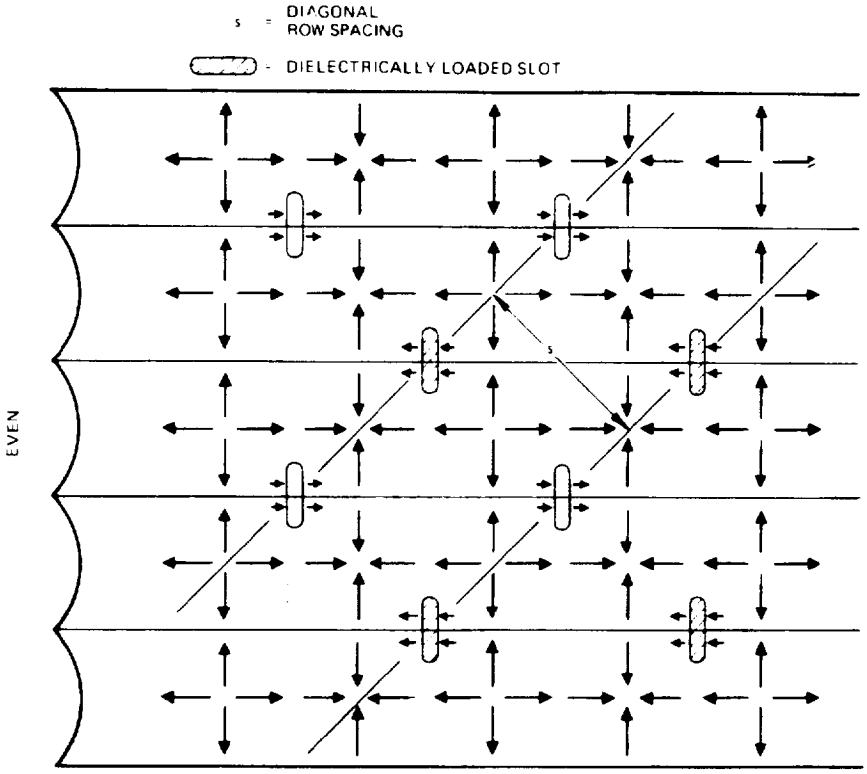

Figure 2-9. Array of slots shown in Figure 2-8 with half the slots removed diagonally.

With a diagonal row spacing of one wavelength, the slot configuration shown in Figure 2-9 will allow the formation of partial grating lobes in the plane of the array in the four quadrants between the principal planes. The peaks of these beams lie exactly in the plane of the array; hence half of each beam is below the plane in "invisible space". In the case of a large array, in which the beamwidth is quite narrow, the inter-row spacing need not be much less than the free-space wavelength, λ_o, to make the entire grating lobe disappear into invisible space. Reduction of the inter-row spacing could probably be accomplished most easily in this array by the use of ridged waveguide rather than rectangular. The "a" dimension of the waveguide would be reduced without a concomitant reduction in λ_c. Hence, λ_g could stay at some desired fixed value while the spacing between common walls was reduced by an amount sufficient to reduce the diagonal row spacing to about $0.9\,\lambda_o$.

The diagonal row spacing for the ridged waveguide case is given by

$$s = \lambda_g \sin\left(\tan^{-1}\frac{2a}{\lambda_g}\right) \qquad (2\text{-}1)$$

where λ_g is related to the cutoff wavelength, λ_c, of the waveguide as follows;

$$\lambda_g = \frac{\lambda_o}{\sqrt{1-\left(\frac{\lambda_o}{\lambda_c}\right)^2}}$$

it is no longer related to the "a" dimension because of the presence of the ridge. If a value of $\sqrt{2}\,\lambda_o$ is selected for λ_g (a value near the center of the recommended operation range for the dominant mode), then a solution of Equation (2-1) for "a" when $s = 0.9\,\lambda_o$ would give the necessary waveguide width. This solution was approximated with the result that

$$s = 0.9006\,\lambda_o$$

when

$$a = 0.5840\,\lambda_o$$

In normal rectangular waveguide, an "a" dimension of 0.707 λ_o would be needed to set $\lambda_g = \sqrt{2}\,\lambda_o$. Hence, the ridges only need to be high enough to allow about an 18-percent reduction in the "a" dimension of the waveguides that make up the array for the grating lobes to be eliminated.

2.3.1.2 Odd-Mode Excitation

For odd-mode excitation of the broad-wall multimode array, the currents in the top wall of the waveguides are as shown in Figure 2-10. It is apparent that longitudinal currents on opposite sides of the common walls are everywhere equal in magnitude and 180 degrees out of phase; hence, the transverse slots discussed previously are not excited.

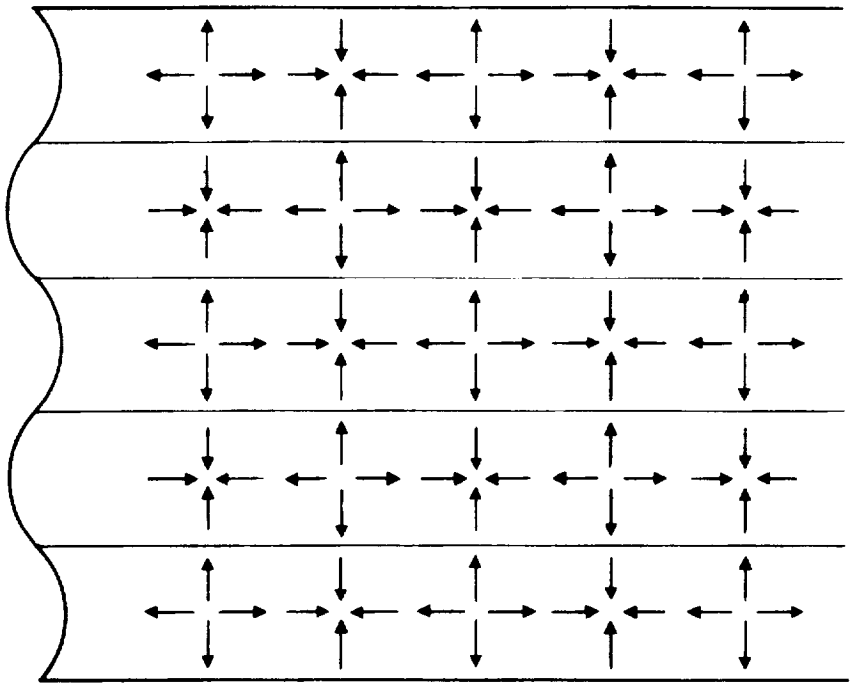

Figure 2-10. Currents in top walls of waveguide for odd-mode excitation of broad-wall array.

For coupling to the odd mode to be accomplished so that the signal radiated is cross-polarized to the one radiated by the transverse slots, longitudinal slots are placed over the common walls to interrupt the transverse currents flowing there. In this case, a choke in the common wall under the slot is not necessary because there is no potential difference between the two ends of the slot (see Figure 2-11). It may be desirable, however, for the slot to be a little wider than usual to compensate for the thickness of the wall.

A slot configuration that will radiate signals in-phase in the broadside direction is shown in Figure 2-12. These slots lie on a grid of equilateral triangles similar to the configuration of transverse slots shown in Figure 2-9; consequently, the results of Appendix B apply, and the spacing between diagonal rows of these slots will also be one wavelength. The grating lobe problem in this configuration could also be solved by the use of ridged waveguide.

Another possible solution for the grating lobe problem with the slot configuration of Figure 2-12 is the use of dielectrically loaded slots between the non-loaded slots as shown in Figure 2-13. The non-loaded slots are shorter than resonance and the loaded slots are electrically longer than resonance; they correct for the out-of-phase current excitation in much the same manner as the transverse slots discussed previously.

2.3.1.3 Dual-Polarized Array

A dual-polarized array can be achieved by combination of common-wall slots into a single configuration in such a way that the array will radiate (or receive) only one linearly polarized component of the signal when excited in the even mode and the orthogonal component when excited in the odd mode. The two types of slots can be combined in several ways.

The most direct method is a combination of the longitudinal and transverse slots into a crossed slot that is centered on the common wall. The slot arrangements of Figures 2-8 and 2-13 could then be combined as shown in Figure 2-14 to form a dual-polarized array. Because of the moderate interelement spacing in both principal planes, there will be no

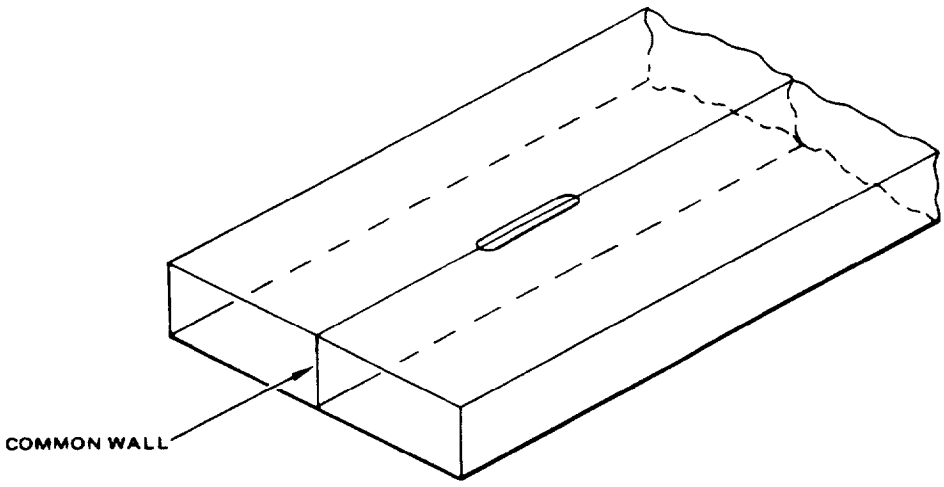

a. PERSPECTIVE VIEW

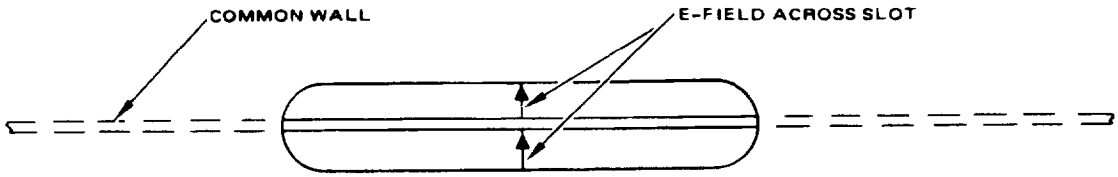

b. PLAN VIEW

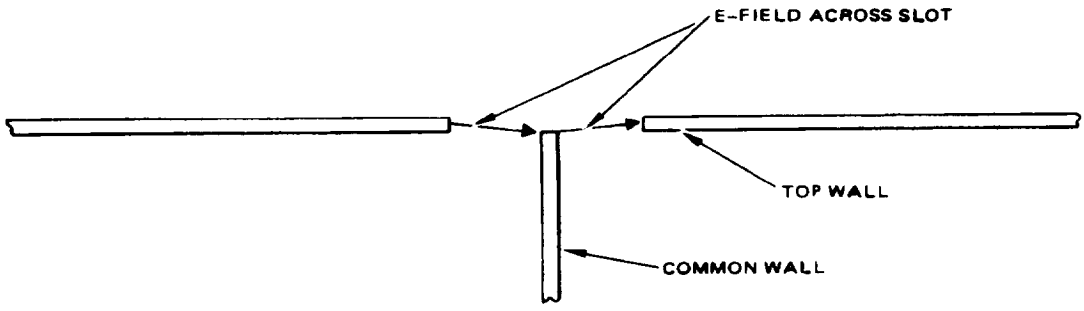

c. CROSS-SECTIONAL VIEW

Figure 2-11. Longitudinal slot centered over the common wall between two adjacent waveguides.

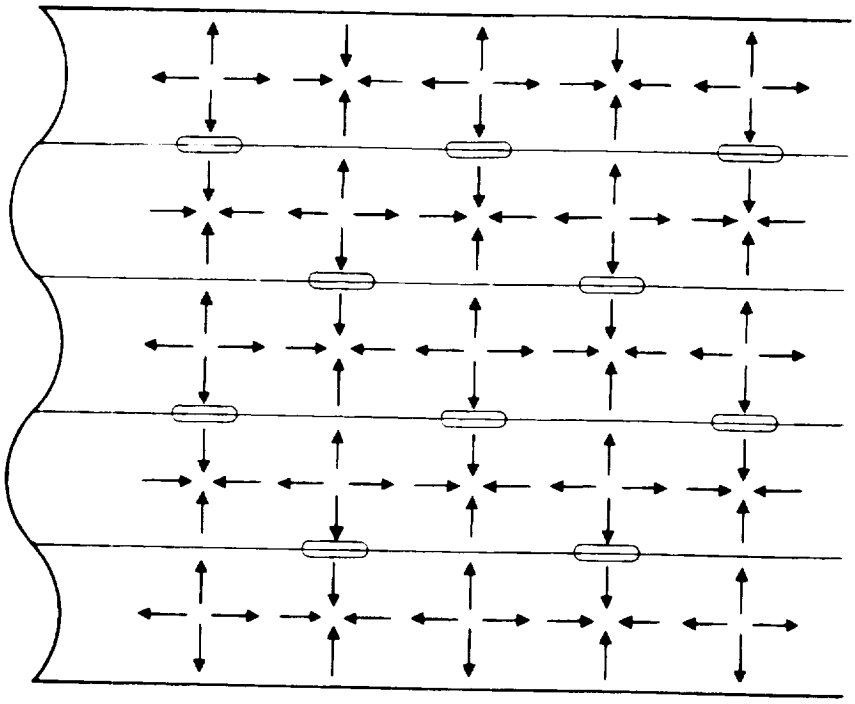

Figure 2-12. Array of longitudinal common-wall slots centered over the common wall in a diagonal grid.

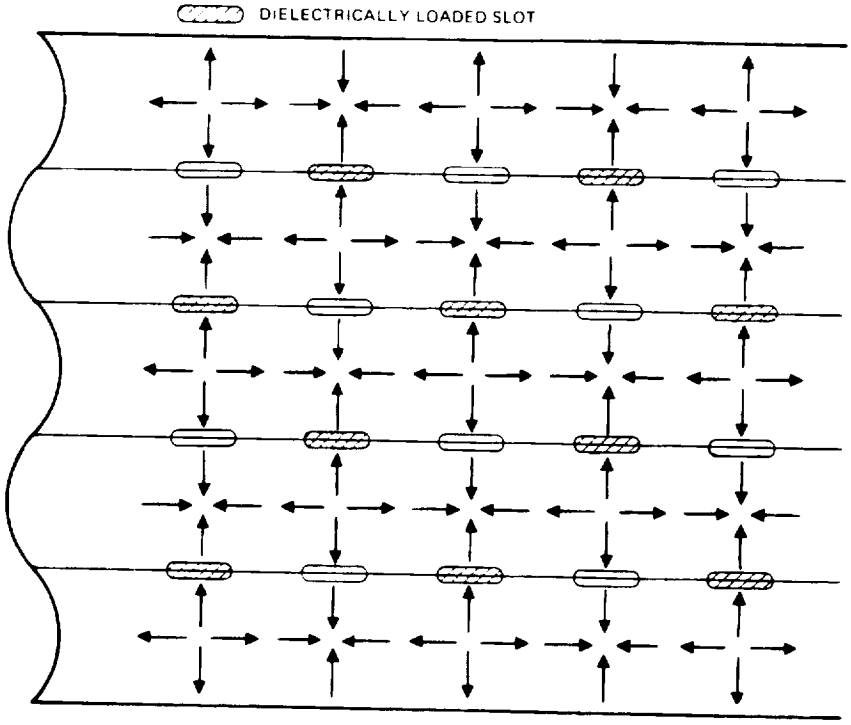

Figure 2-13. Array of longitudinal common-wall slots in a rectangular grid with half the slots dielectrically loaded.

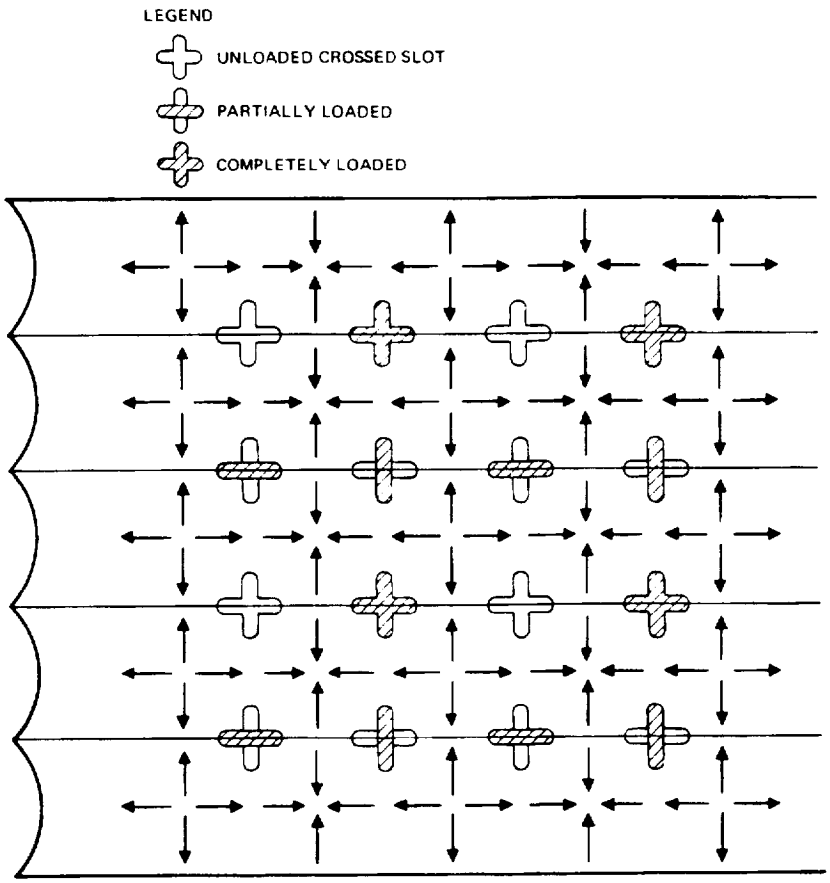

Figure 2-14. Dual-polarized array of crossed common-wall slots.

grating lobes with either component of polarization. The wall currents shown in Figure 2-14 are for even-mode excitation. It can be seen that the longitudinal currents will excite the transverse arms of the crossed slots. The transverse currents, on the other hand, will not excite the longitudinal arms because they are everywhere 180 degrees out of phase on opposite sides of the common walls. If the array were to be driven in the odd mode, however, the opposite would be true: the transverse arms would not couple, but the longitudinal arms would.

The remaining component for the achievement of dual-polarization operation is a properly designed feed network that can drive the array in either the even or the odd mode from two separate input ports. An appropriate feed network might consist of a waveguide magic-tee hybrid at the input of each adjacent pair of waveguides in the array. One port of the

magic-tee would drive the waveguides in-phase for the even mode, and the other port would drive them 180 degrees out of phase for the odd mode. Corporate feeds of appropriate lengths would connect all the even-mode ports to one terminal and all the odd-mode ports to another.

In some of the crossed slots shown in Figure 2-14, one arm is loaded with dielectric and the other arm is unloaded. This arrangement may cause some design problems in a practical array. A composite array can be made without the use of crossed slots in either of the two fashions. In the first, the longitudinal and transverse arms of the slots could be separated by a quarter waveguide wavelength, as illustrated in Figure 2-15; ridged waveguide would still not be needed for the suppression of grating lobes. In the second method, the slot configurations of Figures 2-9 and

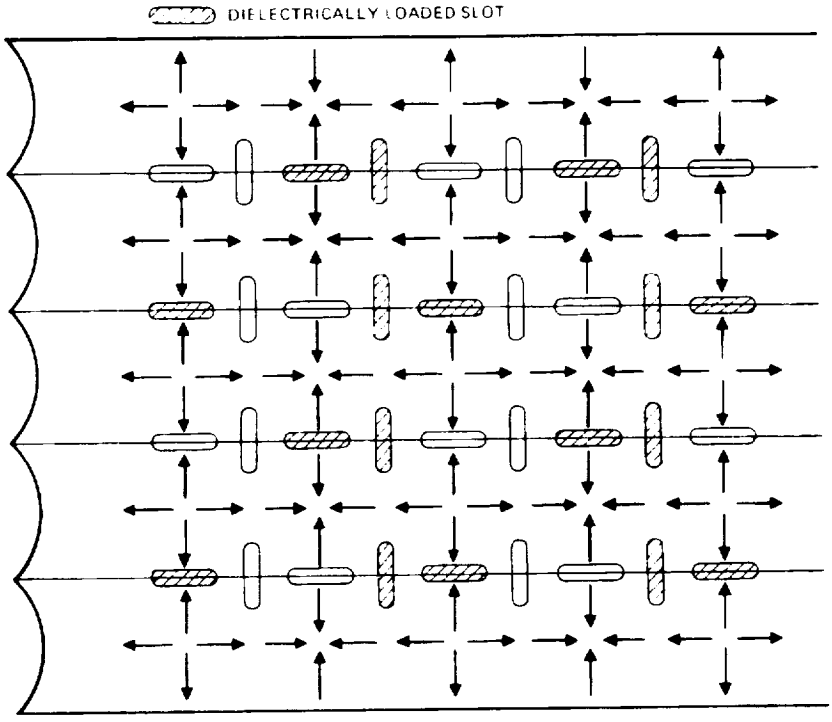

Figure 2-15. Dual-polarized array of longitudinal and transverse common-wall slots separated by a quarter-waveguide wavelength.

2-12 could be combined as shown in Figure 2-16. Both sets of slots have relatively widely spaced slots and, thus, would require the use of some device such as the ridged waveguide discussed above for the suppression of grating lobes. The composite configuration, however, has the advantage that only a fourth of the total number of slots would have to be loaded with dielectric.

2.3.2 Narrow-Wall Multimode Arrays

In the narrow-wall version of the dual-polarized multimode array, the waveguides are laid on edge with common broad walls as shown in Figure 2-17. The dimensions of the waveguides are such that they carry only the dominant TE_{10} mode; hence, as before, there are no problems with spurious modes.

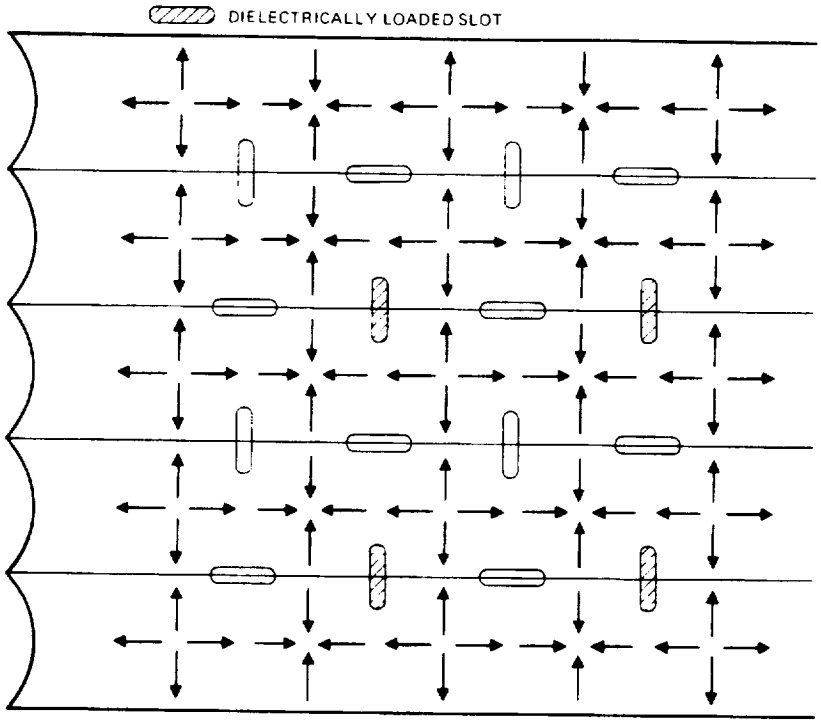

Figure 2-16. Dual-polarized array with transverse and longitudinal common-wall slots with relatively wide separation.

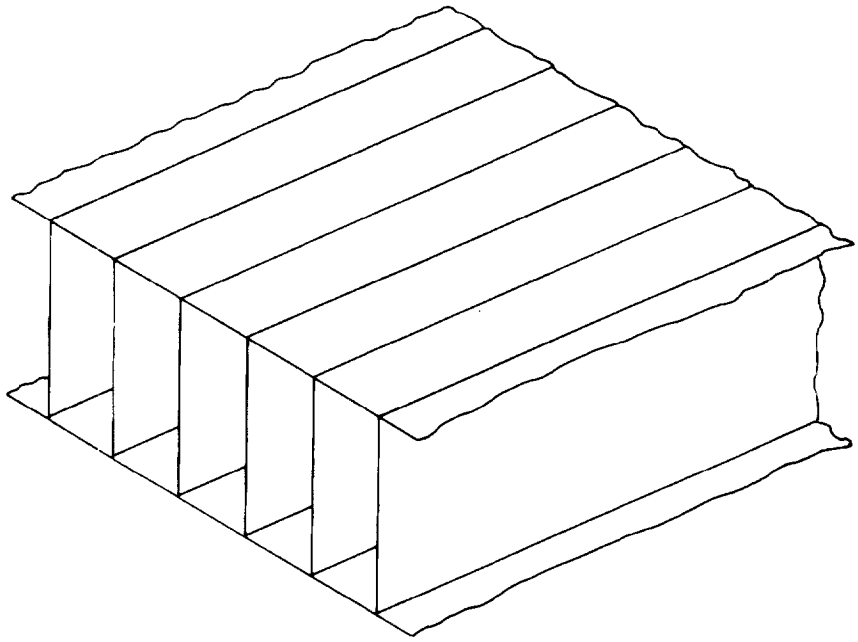

Figure 2-17. Narrow-wall multimode array with common broad walls between adjacent waveguides.

When all the waveguides are driven in phase (even-mode operation), the currents in the narrow walls that make up the aperture plane of the array appear as in Figure 2-18. Longitudinal common-wall slots of the type discussed above and illustrated in Figure 2-11 can be placed over the common broad walls of the waveguides as shown in Figure 2-18. The slots in this configuration are very close together in the transverse plane but a full guide wavelength apart in the longitudinal plane. Thus, for the prevention of grating lobes, slots loaded with a dielectric must be interspersed at a point midway between the existing slots. However, because the narrow dimension of the waveguide is always less than $1/2\ \lambda_o$ for dominant-mode operation, half the unloaded slots can be removed and still leave a slot configuration that has diagonal row spacings on the order of $0.75\ \lambda_o$ (see Figure 2-19); this spacing is sufficient for the suppression of grating lobes in the quadrants. Consequently, ridged waveguide or other means for reduction of λ_g below its nominal value are not required for grating-lobe-free broadside operation.

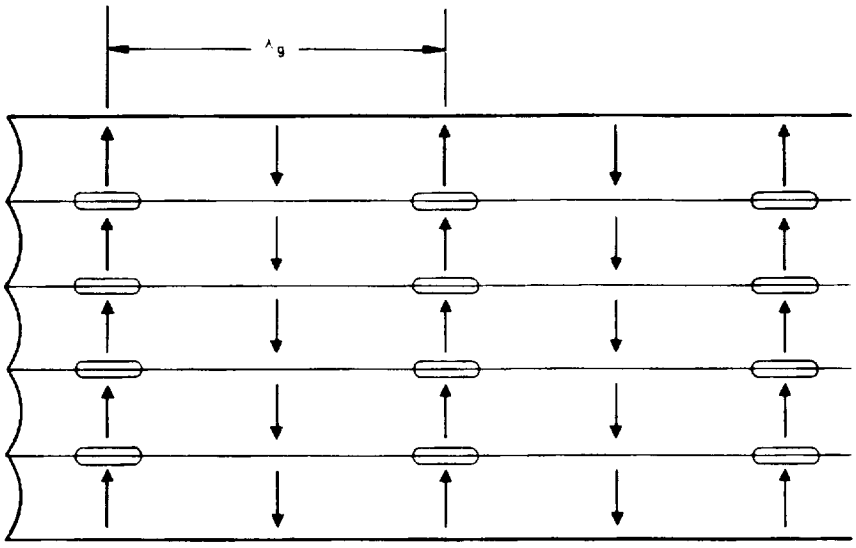

Figure 2-18. Longitudinal common-wall slots placed over the common broad walls in a narrow-wall multimode array.

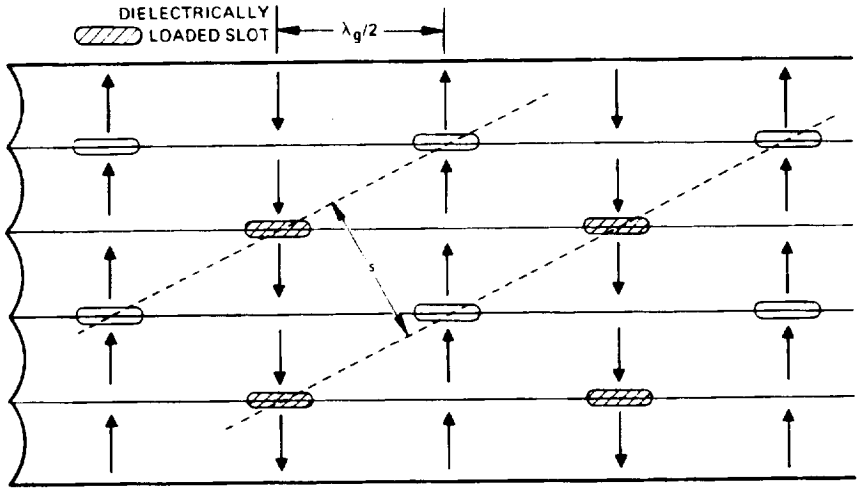

Figure 2-19. Triangular configuration of longitudinal common-wall slots for effective suppression of grating lobes in narrow-wall array.

For odd-mode operation, alternate waveguides are driven 180 degrees out of phase. The narrow-wall currents in the aperture plane will then appear as shown in Figure 2-20. It is apparent that this current configuration will not excite the longitudinal slots on the common walls because the transverse currents that drive them are out of phase. A transverse slot is needed to radiate the orthogonal polarization for this array, but there is no longitudinal component of current in the narrow walls of the waveguides to excite such a slot. However, the choke that must be cut in the common wall below the transverse slot is excited by longitudinal currents in the broad walls of the waveguides when the latter are driven in the odd mode. Because these same currents are 180 degrees out of phase when the waveguides are driven in the even mode, this mode does not excite the choke. In the odd-mode case, the excited choke in turn excites the transverse slot and causes it to radiate. This arrangement is similar to a method used at Hughes for excitation of a crossed slot on the narrow wall of a dual-mode waveguide (Ajioka et al., 1974).

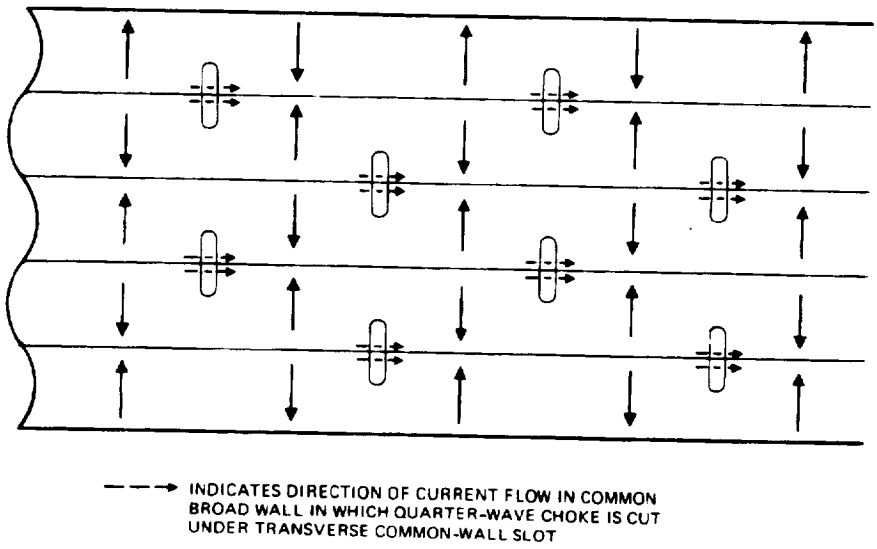

Figure 2-20. Odd-mode excitation of triangular grid of transverse common-wall slots.

The diagonal row spacing for the transverse slot configuration of Figure 2-20 is the same as that of Figure 2-19 so that the grating-lobe problem does not exist and ridged waveguide is not required. Furthermore, none of the slots in this arrangement has to be dielectrically loaded.

A dual-polarized dual-mode array can be made from a combination of the slot configurations of Figures 2-19 and 2-20; the resulting narrow-wall array is shown in Figure 2-21. As with the broad-wall dual-mode array, the array of Figure 2-21 can be fed by magic-tee hybrids that feed adjacent pairs of waveguides. One port of the magic-tee feeds the waveguides in phase for even-mode operation, and the other port feeds them out of phase for odd-mode operation. Also as before, two corporate feeds would be used to drive the two sets of terminals of the magic-tees.

2.3.3 Comparison of Broad- and Narrow-Wall Arrays

Both the broad- and the narrow-wall dual-mode dual-polarized arrays have advantages and disadvantages compared with other types of dual-polarized devices. These are discussed below for each type.

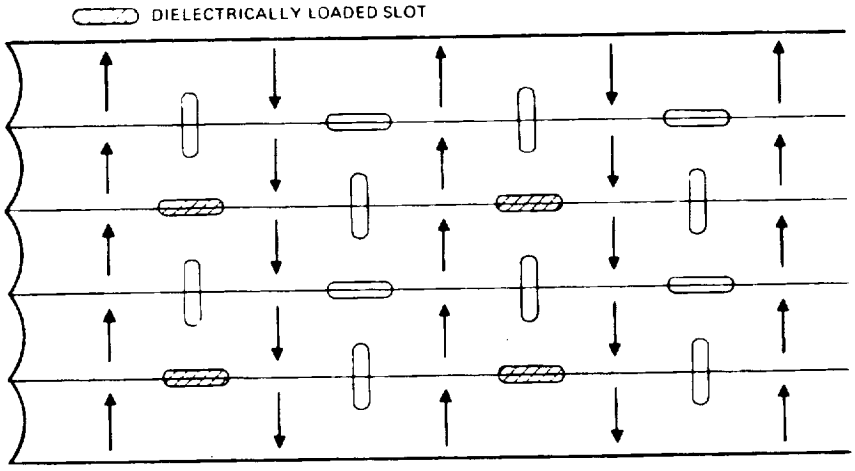

Figure 2-21. Dual-polarized, dual-mode narrow-wall array.

2.3.3.1 Broad-Wall Dual-Mode Dual-Polarized Array

Advantages. Each waveguide in the broad-wall dual-polarized array carries a single mode (TE_{10}) compared with the square waveguide utilized in some dual-polarized arrays which carries many orthogonal modes. The broad-wall dual-polarized array requires a smaller number of waveguides than some dual-polarized arrays, such as the bifurcated-waveguide array reported by Ajioka et al. (1974). In addition, the "b" dimension of the waveguide in the broad-wall array can be near the nominal value for rectangular guide so that losses tend to be lower than in the bifurcated-waveguide array, in whch half-height waveguide is used.

Fewer components are also required in the broad-wall dual-polarized array than in some other dual-polarized arrays: only one magic-tee hybrid is required for each two waveguides in the array. In contrast, in the square-waveguide orthogonal-mode approach, one orthomode transducer is required for each waveguide, and in the dual-mode bifurcated-waveguide array, one half-height short-slot hybrid is required for each bifurcated waveguide. Thus, in the broad-wall array, half as many terminals (or fewer) are needed on the corporate feeds than in most other types of dual-polarized arrays.

Finally, the broad-wall dual-mode array has a greater growth potential than most other types of dual-polarized arrays. The possibility exists that other modes at other frequencies can be incorporated into this array so that it would be a multi-frequency as well as a dual-polarized device.

Disadvantages. The major disadvantage of the broad-wall dual-polarized array is the fact that no techniques have been devised for electronically scanning it; it must be considered only as a mechanically scanned antenna.

The dielectric loading of some of the slots, required to effect the 180-degree phase shift, would make both the design and the fabrication of this array more difficult than more conventional arrays. The use of ridged waveguide for grating-lobe suppression would also raise problems: ridged

waveguide has more attenuation and requires tighter tolerances in the vicinity of the ridge than does rectangular waveguide for the same frequency range.

Finally, the characteristics of the common-wall slot are not well known, and considerable slot data would have to be accumulated before an array design could be undertaken.

2.3.3.2 Narrow-Wall Dual-Mode Dual-Polarized Array

Advantages. With the exception of the smaller number of waveguides utilized and the greater growth potential, the narrow-wall dual-polarized array has the same advantages over other types of dual-polarized arrays as the broad-wall array: single-mode transmission, lower losses, and fewer components. In addition, ridged waveguide is not required in the narrow-wall array because there is no grating-lobe problem.

Disadvantages. As with the broad-wall array, no techniques for electronically scanning the narrow-wall array have been devised, and this type of array also must be considered only as a mechanically scanned antenna. Use of dielectrically loaded slots would add difficulty to the design and fabrication of this array, as before, and there is the same need for data on the characteristics of the common-wall slot. However, in contrast with the broad-wall array, because the narrow walls of the waveguides make up the aperture plane, this array requires approximately twice as many waveguides as an equivalent broad-wall array.

2.3.4 Circular Common-Wall-Slot Array

The characteristics of a circular common-wall slot array with apertures of different diameter were calculated for a particular spacecraft application (SAMSO, 1973). Of particular interest here are the weight values. While the application was different than the radiometric antenna under consideration, the calculations do give an indication of the kinds of weights to be expected with common-wall arrays. Table 2-2 shows the weights for the various apertures.

TABLE 2-2. COMMON-WALL SLOT ARRAY WEIGHT SUMMARY

Diameter (feet)	Array Weight (pounds)
1.5	1.8
2	3.0
3	7.0
4	12.5
5	19.9
6	29.3
7	43.6
8	58.9
9	77.4
10	104.6

The array was intended for operation at 7.9 GHz. However, for a given aperture size, the weight is not too sensitive to changes in frequency. It may actually increase somewhat with increasing frequency because of increased tolerance requirements.

2.4 MULTI-FREQUENCY ARRAYS

A literature survey revealed several new multi-frequency array designs that might be applicable to radiometers. These new designs are discussed below.

2.4.1 Multi-Mode Multi-Frequency Arrays

In one of the new multi-frequency designs reported, a special rectangular waveguide is utilized to carry two orthogonal modes at two different frequencies (X-band and K_u-band). The "a" dimension of the waveguide controls the velocity of propagation of one wave, and the "b" dimension controls that of the other. By proper choice of dimensions, the

waveguide can be made to radiate beams at the two frequencies. The X-band wave is coupled out through transverse slots in the broad wall while the K_u-band wave is coupled out through longitudinal slots in the same wall. These slots correspond to narrow-wall slots in conventional waveguide but appear on the broad wall because the field configuration of the K_u-band wave is oriented at an angle of 90 degrees to the X-band field.

With both the transverse X-band and the longitudinal K_u-band slots, there is no way in which alternate 180-degree phase shifts can be obtained in the coupling of the slots to the waveguide, as is normally done with slot arrays that operate in the neighborhood of broadside. Hence, both sets of slots must be designed as "leaky-wave" arrays; the scan angle of the beam is then limited to the region from about 45 degrees off broadside to near endfire. This limitation is not a problem for radiometric arrays because the design goal specifies a 45-degree scan from broadside so that the proper conical scanning action about the vertical axis can be obtained.

A possible limitation of this scheme is that the two beams are inherently cross polarized. If vertical polarization can be used at one frequency and horizontal at the other, then such an array might be useful for the 10- and 18-GHz bands (or the 18- and 21-GHz bands), at which two polarizations at each frequency may not be required.

Performance data for four dual-band slot arrays designed on this principle have been published by Goebels and Anderson (1970) and are given in Table 2-3. Performance in all four arrays was quite good for all parameters. In particular, the isolation between the two possible modes at K_u-band was never less than 28 dB, which indicates little interference with the X-band array. Thus, it seems possible that each array could be designed for maximum beam efficiency.

TABLE 2-3. PERFORMANCE CHARACTERISTICS OF FOUR DUAL-BAND ARRAYS

Frequency Ratio	X-band Array		K_u-band Array		Measured Isolation Between TE_{01} and TE_{10} Modes at K_u-band (dB)
	Aperture Distribution	Measured Gain	Aperture Distribution	Measured Gain	
1.76:1	Uniform	18.0	Uniform	16.3	≥29.0 (External) 50.0 (Internal)
1.76:1	25-dB Taylor	17.9	Uniform	15.9	≥31.5 (External) 48.0 (Internal)
1.90:1	Uniform	18.0	Uniform	16.4	≥28.5 (External) 42.0 (Internal)
1.90:1	25-dB Taylor	18.0	Uniform	16.0	≥30.5 (External) 42.0 (Internal)

Another multi-mode, multi-frequency array, shown in Figure 2-22, was designed for operation at 9 and 36 GHz. The radiating elements at both frequencies are shunt slots. The waveguide coupling to the slots is accomplished with the TE_{10} mode at 9 GHz and the TE_{40} mode at 36 GHz. The field distribution in the waveguide cavity at 36 GHz is equivalent to that of four virtual waveguides of one-fourth the width operating in the TE_{10} mode. Rows of slots oriented about each of the virtual guide centerlines form linear arrays.* Results indicate the bandwidth to be the same as that for single-mode slot arrays. No second-order beams are generated, and the isolation between 9- and 36-GHz portions is 30 dB.

*A similar array for S- and X-bands is described by Holtzman [1968].

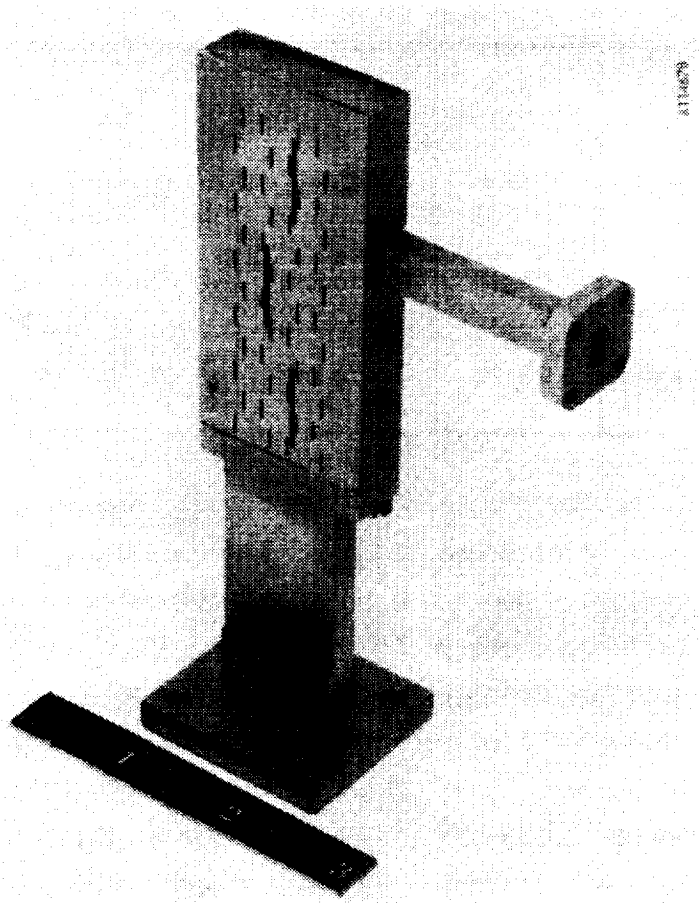

Figure 2-22. Interleaved 9- and 36-GHz array.

Both the arrays are of a standing-wave design with the main beam always broadside. The feedlines can be used as modules to build up the complete aperture. There would be a separate feedline for each frequency. The module size would be determined by the percentage bandwidth at each operating frequency. These arrays radiate only one linear polarization at each frequency. Because the beams are broadside to the array, a one-dimensional scan would only approximate the desired conical scan because the array must be tilted to obtain a 45-degree pointing direction with respect to the local vertical.

2.4.2 Interleaved Multi-Frequency Arrays

A second type of multi-frequency array applicable to the radiometric system consists of interleaved planar arrays. The arrays consist of several separate feeds and radiating systems that are integrated into a common aperture. With modified feeds, these arrays could be used as the radiating structures for phased arrays.

One such array designed for operation at 9 and 34 GHz is shown in Figure 2-23. The 34-GHz portion of the array consists of 108 round holes in six rows of 18 elements each (Figure 23a and b). The 9-GHz portion consists of 20 nonresonant shunt slot elements arranged in two rows of 10 elements each. Each row is fed by a modified ridged waveguide that is U-shaped in cross section. The radiating elements of both portions share a common aperture. Measured radiation patterns are shown in Figures 2-23c and d. The gain of the 34-GHz portion is about 2 dB below the area gain; this lower value is caused by the presence of high level second-order beams that are attributed to the increased diagonal spacing of the round holes necessitated by the interleaving of the 9-GHz portion.

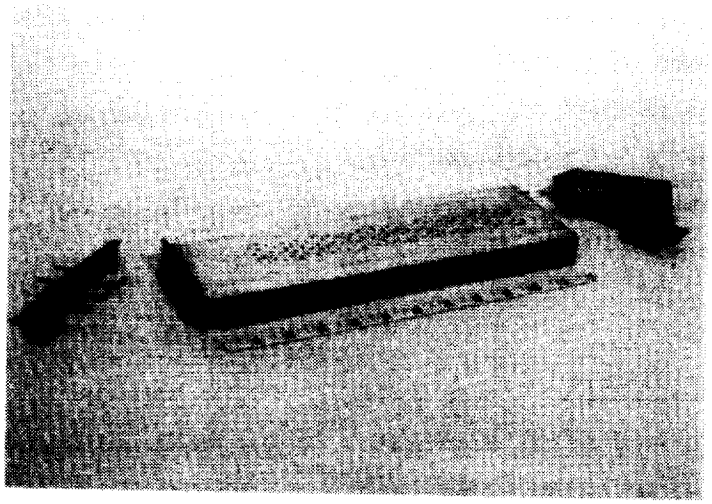

a. Array with round-hole and shunt-slot radiators

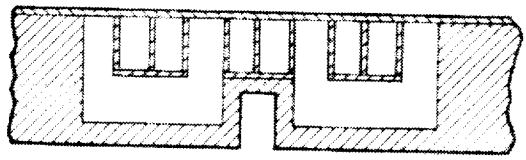

b. Waveguide cross-section

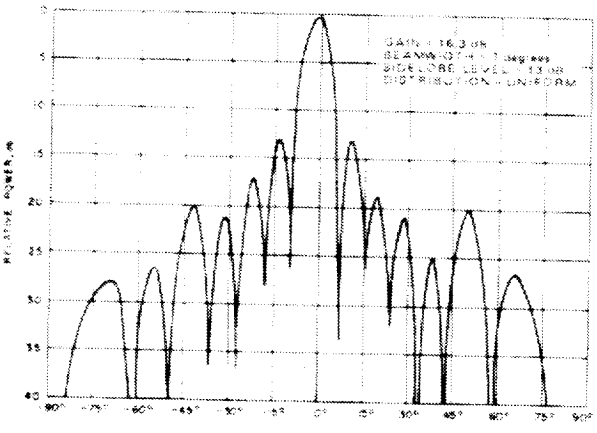

c. Radiation pattern of 9-GHz array.

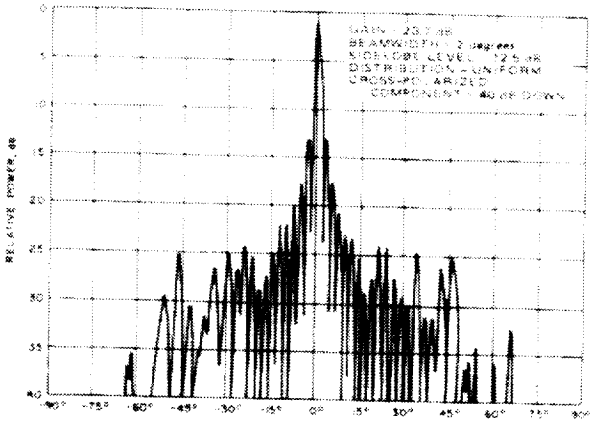

d. Radiation pattern of 34-GHz array.

Figure 2-23. Interleaved 9- and 36-GHz array.

Hsiao (1971) analyzed the case of two different sets of open-ended waveguides occupying the same aperture. Both sets of waveguide radiators are dielectrically loaded so that there is space between the elements of each in which the other can be interleaved. Hsiao's analysis is primarily concerned with the effect that the presence of the low frequency array might have on the performance of the high frequency array. The high frequency waveguides will be below cutoff for the low frequency signal and, hence, should have little effect on it.

An array of this type can be scanned in two dimensions and thus has greater scanning capability than is required for the radiometric application. However, such an analysis would reveal any limitations that might result from the interleaving of any two arrays. Furthermore, concentration on the two principal planes of scan ($\phi = 0°$ and $\phi = 90°$) permits an estimate of the scanning characteristics of either the vertically or horizontally polarized beam of a radiometric phased array that is scanned in one plane only.

Two principal cases were considered by Hsiao: one with the low frequency array polarized perpendicular to the high frequency array and the second with the low frequency array polarized parallel to the high frequency array. For each case, three characteristics of the composite array were computed in degrees off broadside as a function of the scan angle. The behavior of each characteristic was determined for three scan planes (ϕ = 0, 45, and 90 degrees). The ϕ = 0 degrees direction corresponds to scanning in the H-plane, and the ϕ = 90 degrees direction corresponds to the E-plane. The three characteristics studied were transmission coefficient of the high frequency array, proportion of energy coupled from the high frequency array into the low frequency array, and grating-lobe level in the high frequency array pattern.

Two of Hsiao's series of patterns are reproduced in Figure 2-24. They give the results for two particular geometries that are representative of practical situations. These results show that the impedance is fairly constant out to an angle of about 30 degrees; hence, such an array would not be too difficult to match over a limited scan range. They further show that, although some energy is coupled into the low frequency waveguide, it is not severe until a scan angle of 60 degrees is reached. The grating-lobe results (Figure 2-24c) show that the triangular grid is much preferred to the rectangular grid for scanning to angles beyond about 25 degrees. It is thus apparent that Hsiao's analysis does not rule out the use of interleaved arrays that are scanned in either one or two dimensions.

In any practical scheme that would involve the interleaving of elements for a radiometric array, it is very likely that slots cut into waveguides would be used as the radiating elements rather than open-ended waveguides.

Use of slots should result in less mutual coupling amoung elements on the outside surface of the array. However, there would probably be more mutual interaction on the inside of a waveguide among the slots fed from that particular waveguide; therefore, an analysis of the internal effects would be required for each array.

An array that has three sets of interlaced elements was built and tested at the Naval Electronics Laboratory Center, San Diego, California (Boynes and Provencher, 1972). This array is capable of operating simultaneously in L-, S-, and C-bands. It consists of two vertically polarized elements with a 10-percent bandwidth about a center frequency of 1.0 GHz, 64 horizontally polarized elements with a 20-percent bandwidth about a center frequency of 3.2 GHz, and 120 vertically polarized elements with a 20-percent bandwidth about a center frequency of 4.6 GHz. The array was built on a cylindrical surface, 16 feet in diameter, with the axis oriented vertically. All the elements were open-ended waveguides with the L-band elements being double ridged to reduce their size. Figure 2-25 shows the layout of the central portion of the array. The two L-band elements are arrayed in a horizontal plane as shown. The elements of the S-band

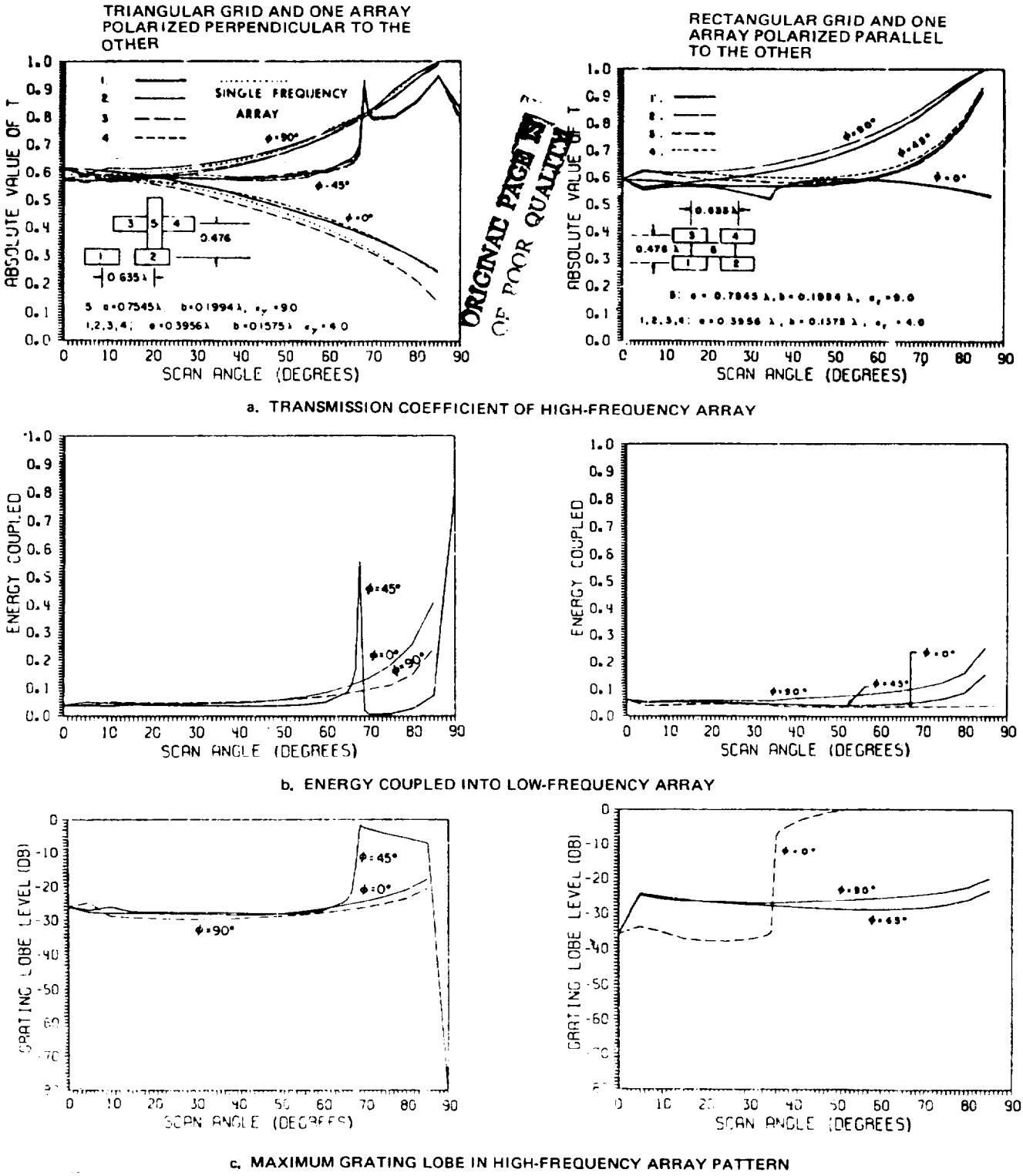

Figure 2-24. Calculated characteristics of interleaved-element dual-frequency arrays of representative geometries. (from Hsiao, 1971)

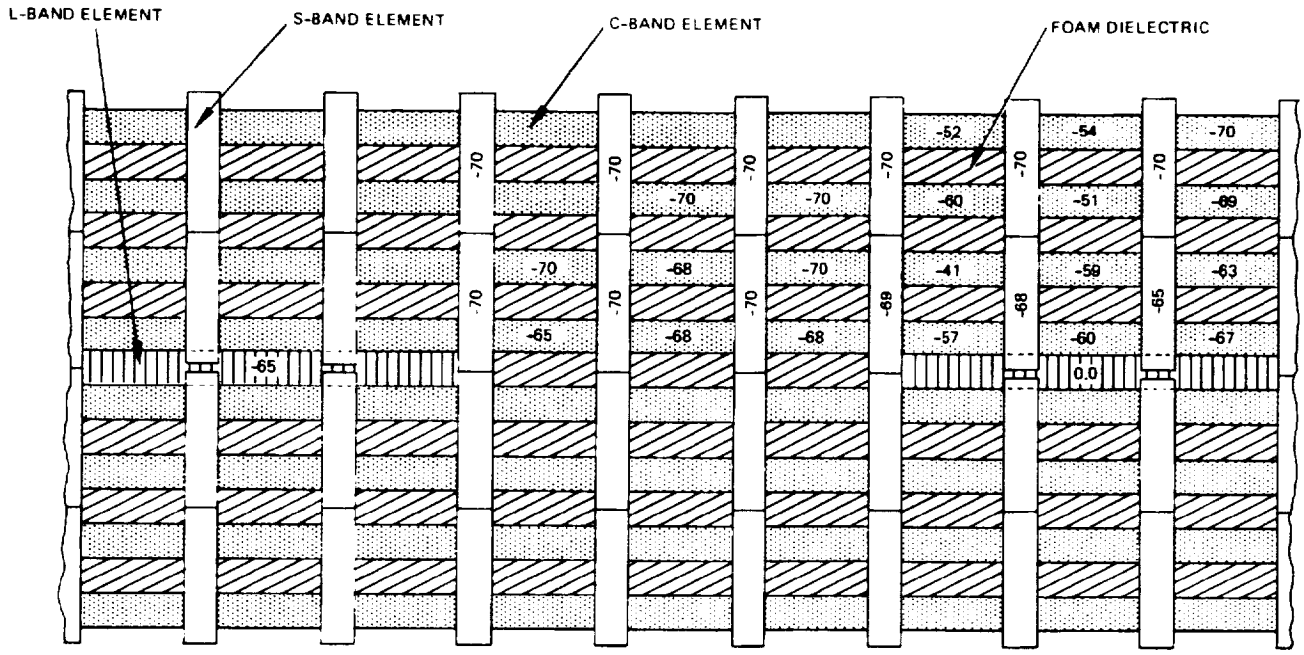

Figure 2-25. Layout of central portion of interleaved-element tri-frequency array.

array were arranged in four rows of 16 elements each, and the elements of the C-band array were arranged in eight rows of 15 elements each.

Horizontal-plane patterns for the three arrays (Figure 2-26) show that the sidelobes of the interlaced arrays tend to be higher than are obtained with comparable single-frequency arrays. In the C-band pattern, rather large grating lobes appear; these may be due to the curvature of the surface, but it is likely that part of the effect is due to the large interelement spacing required to make room for the S-band elements.

The numbers in the various element mouths in Figure 2-25 represent the power in dBm coupled into those elements when the C-band element that is labeled 0.0 was excited with a power level of 0.0 dBm. The numbers show show that mutual coupling is not a severe problem in this design at this frequency even though the elements of the other arrays are capable of carrying the C-band signal quite well. When the S-band elements are excited, energy cannot couple into the C-band elements because the waveguide is below cutoff. For the L-band signal, both the S-band the C-band

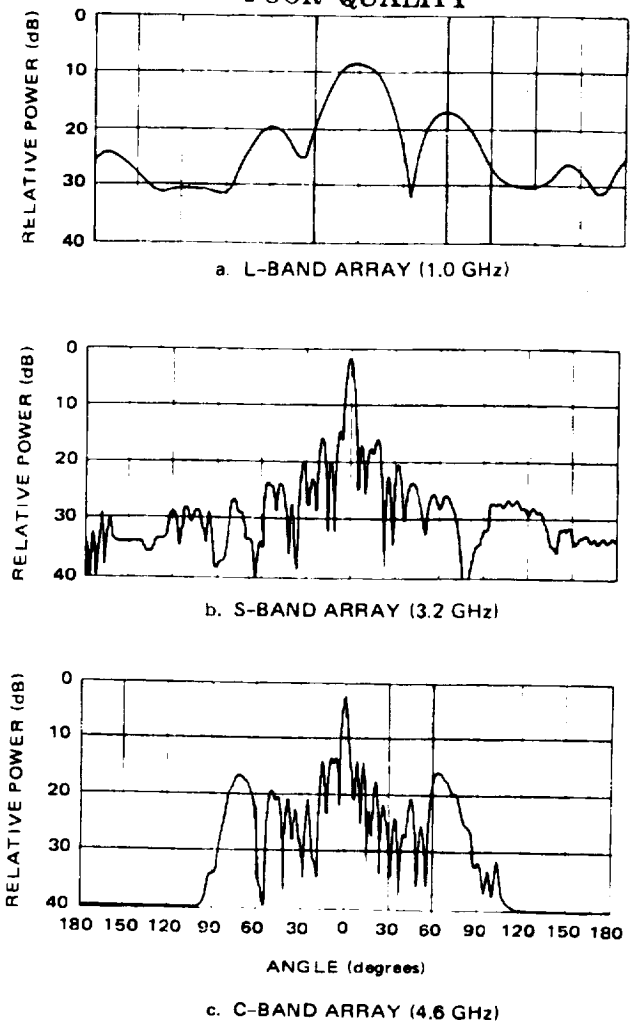

Figure 2-26. Measured horizontal-plane patterns of tri-frequency array. (from Boynes and Provencher, 1972)

elements are below cutoff; hence there is no mutual coupling problem at that frequency. Table 2-4 summarizes the mutual coupling measurements made on the array. The entries marked 0.0 indicate the driven array element.

TABLE 2-4. MUTUAL COUPLING BETWEEN ARRAYS

Frequency of Transmission	Received on L-Band Array (dB)	Received on S-Band Array (dB)	Received on C-Band Array (dB)
750 MHz	0.0	noise	noise
2.9 GHz	-55	0.0	-57
3.2 GHz	noise	0.0	noise
3.5 GHz	-60	0.0	-54
4.6 GHz	-59	-55	0.0
4.9 GHz	-38.1	noise	0.0
5.4 GHz	-39	-60	0.0

The data presented here show that multi-frequency arrays with interleaved elements can, in fact, be made to operate quite well. However, some degradation in performance should be expected over that of a single-frequency array filling the same aperture

2.4.3 High Resolution Radiometry Antenna Study

Two of the reports reviewed in the literature search dealt with the study of high-resolution radiometry at 37 GHz from an earth-orbiting spacecraft (Aerojet, 1971, 1974). The requirements for this 37-GHz system (see Table 2-5) were similar to those of the present study with the exception of the current requirements for multiple-frequency operation. In addition, the earlier system was to be configured for achievement of minimum power, maximum reliability, and a growth potential for higher spatial and thermal resolution.

TABLE 2-5. HIGH-RESOLUTION RADIOMETER REQUIREMENTS

Parameter	Requirement
Polarization	Dual linear
Scan	Constant incidence with ±5° angle variation over scan range
Scan range, degrees	±35 (design goal)
Angular resolution, degree	≤0.5
Weight, pounds	≤200 (design goal)
Size, feet	Baseline package: 7 x 5 x 2
Beam efficiency, percent	≥90 (design goal)
NEΔT, °K	1 (design goal)
Time frame	Engineering model by 1976

Many types of electronically and mechanically scanned antennas were considered during the Aerojet study. Included in the electronically scanned group were RF beam-forming, IF beam-forming, and lens beam-forming types. Some of the systems were capable of generating multiple simultaneous beams, while others were not. However, most of the antennas were capable of simultaneous dual-polarization operation.

Only two of 15 candidate antenna systems met all the requirements of Table 2-5; both were phased arrays, one with IF beam forming and the other with an RF lens. Both are theoretically capable of multiple-beam operation, which was deemed necessary to meet the angular resolution and thermal noise-requirements. Either approach would be applicable to the present study under the phased-array category in which separate arrays are allowed for each frequency.

2.5 PHASE SHIFTERS

In electronically phased arrays, the phase shifters are located outside the calibration loop of the radiometer. Any change in the loss through the phase shifters appears as a calibration error. The following data are extracted from work being performed on X-band diode phase shifters at Hughes.

The characteristics of the phase shifters are:

Frequency	9.5 to 10.5 GHz
Quantization	3-bit
Power handling	10 watts average; (250-watt peak)
Insertion loss	1.5 dB average (0.5 dB rms ripple)
Phase error	<5 degrees rms
Amplitude error	<0.3 dB rms
Switching speed	≈10 microseconds
Mean time between failures	2×10^5 hours
Weight	10 grams
Size	0.4 x 2.0 x 6.3 cm

The temperature was cycled from 100° to -48°C. The parameters were measured within ±3 degrees for phase, 0.3 dB for insertion loss, and 0.06 for VSWR with a HP8542B Automatic Network Analyzer. The results on insertion loss as a function of temperature fall within the measurement tolerances: the change in insertion loss was less than 0.3 dB over the temperature range.

3.0 REFLECTOR SYSTEMS

Exhaustive work has been performed on most aspects of feed and reflector systems, so that the behavior of these systems can be predicted with confidence from theoretically derived results that have been checked against experimental results. In addition, reflector antennas have several definite advantages over arrays (Sletten, 1969):

1. Analysis and, consequently, design procedures based on analysis are simpler than for arrays of comparable performance.
2. Construction is simpler than for arrays of comparable performance. Techniques for the unfurling of large reflectors have been developed and demonstrated.
3. Reflectors are inherently broadband with the bandwidth limited by the feed.
4. For large sizes, the cost per unit area is low.
5. They are lightweight.

However, in comparison with arrays, reflectors also exhibit several shortcomings (Sletten, 1969):

1. Single-reflector systems have fewer degrees of freedom than arrays. Arrays have adjustable feeding coefficients.
2. Aperture blockage may result in loss in beam efficiency and increase in sidelobe levels, especially when multiple feeds are used.
3. In most single-reflector systems, the patterns degrade rapidly for feeds located off the optical axis.

The applicability of various reflector antenna systems to the radiometer requirements was considered. The study included offset-fed paraboloidal reflectors, spherical reflectors, torus reflectors, and parabolic-section reflectors. Several beam-steering methods were also

considered, with particular attention to pattern characteristics. In systems in which the feed and the reflector move together, only the pattern characteristics of on-axis beams are of interest, because the pattern does not change as the antenna is moved. In systems in which the feed moves relative to the reflector, the pattern characteristics of off-axis beams are also of importance. Some reflectors are superior to others in this respect, but few are capable of scanning many beamwidths off the axis.

3.1 SINGLE-FREQUENCY SYSTEMS

The basic reflector system consists of a single symmetrical paraboloidal reflector and a single feed horn (Figure 3-1). Spherical waves emanating from a feed at the focus are converted by the surface into plane waves that travel along the reflector optical axis. The reflected plane waves give rise to a pencil-beam radiation pattern along the axis whose width depends on the ratio of reflector diameter to wavelength and on the details of the field variation across the aperture. These details also affect the sidelobe level of the pattern. The field variation in the aperture, in turn, depends on the characteristics of the primary feed and on the interaction of the feed with the reflected field. Variations of this basic system that are applicable to radiometers are discussed in the following pages.

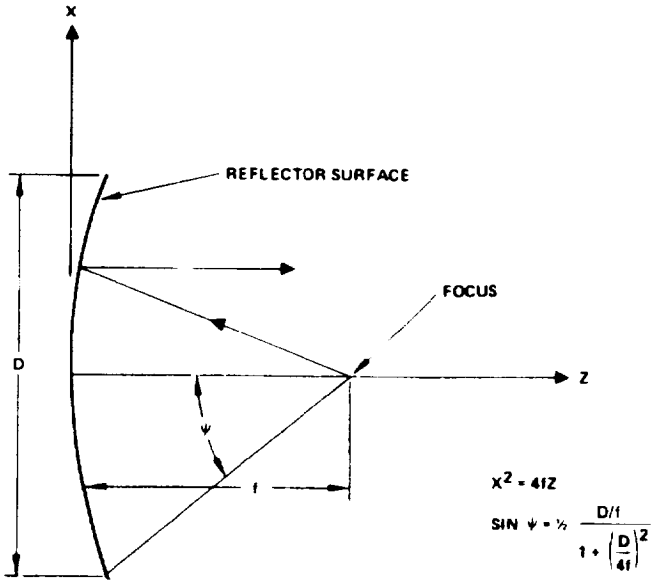

Figure 3-1. Paraboloidal geometry.

3.1.1 Spherical Reflectors

One type of reflector considered was the spherical reflector. Ashmead and Pippard (1946) and Li (1959) have demonstrated that the symmetry of the spherical surface eliminates beam deterioration over wide scan angles, at least when a single movable feed is used to scan the beam. When a cluster of switched feeds is used for electronic beam steering, however, perfect symmetry is not maintained as the various feeds are connected, so that some changes in beam shape might be expected to occur as the beam is stepped throughout the required coverage region. Other factors also affect the applicability of the spherical reflector to scanned antennas.

Figure 3-2 illustrates the geometry and some of the parameters of importance in spherical reflector antennas. The distance a is the radius of the effective aperture which subtends an angle ψ at the primary feed, which is located on the focal locus and is directed at the reflector along a radius from the reflector center. If the beam is to scan to a maximum angle, ζ_m, from the reflector axis, then the following relation must hold if excessive spillover is to be avoided:

$$a = R \sin\left(\frac{\Theta}{2} - \zeta_m\right)$$

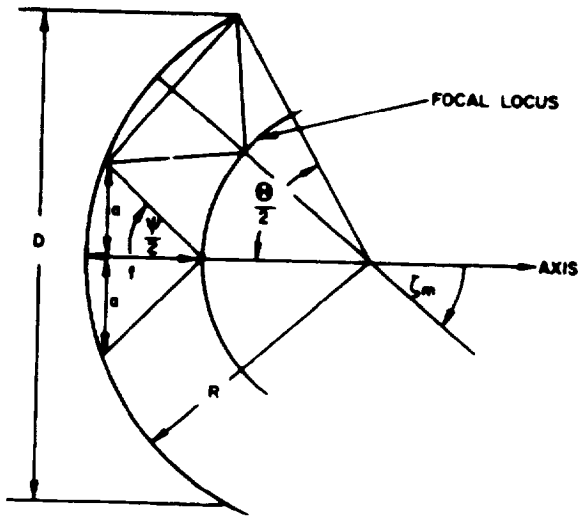

Figure 3-2. Spherical reflector geometry.

The aperture dimension a is determined by system beamwidth requirements and may therefore be considered as a fixed quantity. This expression then gives a relation between R and Ⓗ.

The spherical reflector does not have a well defined focus so that a point source feed gives rise to phase errors over the aperture. According to Li (1959) these are minimized, for a given ratio $\frac{a}{R}$, when f is given by

$$\frac{f_{opt}}{R} = \frac{1}{4}\left(1 + \sqrt{1 - \left(\frac{a}{R}\right)^2}\right)$$

Li also states that, for a given aperture size a, the minimum value of R that may be used to keep the total phase deviation over the aperture within a value $(\Delta/\lambda)_{total}$ is

$$R_{min} = a\left[\frac{(a/\lambda)}{14.7(\Delta/\lambda)_{total}}\right]^{1/3}$$

where Δ is the path length deviation and λ is the wavelength. This value of R also minimizes the total reflector diameter D, given by

$$D_{min} = 2R_{min} \sin\left(\frac{Ⓗ}{2}\right)$$

$$\frac{D_{min}}{2a} = \left[\cos\zeta_m + \sin\zeta_m \sqrt{\left(\frac{(a/\lambda)}{14.7(\Delta/\lambda)_{total}}\right)^{2/3} - 1}\right]$$

If now it is assumed that $(\Delta/\lambda)_{total}$ is restricted to 1/16 and that $a/\lambda = 60$, corresponding to a 0.59-degree beamwidth, the minimum value of D is

$$\frac{D_{min}}{2a} = \cos\zeta_m + 3.90 \sin\zeta_m$$

In the foregoing discussion, scanning in one dimension only was assumed. For conical scan to be provided by motion of the feed, two approaches are possible. In one, the reflector axis is pointed downward to the ground track as discussed in Appendix B. Then, for a ±35-degree conical scan, the antenna beam would have to scan approximately ±2.75 degrees in elevation (in-track) and ±24 degrees in azimuth (cross-track) by motion of the feed or by electronic switching among various feeds. In that case,

$$\frac{D_{min}}{2a} = 2.44 \text{ in azimuth}$$

$$\frac{D_{min}}{2a} = 1.19 \text{ in elevation}$$

The outline of this reflector is not circular but resembles the torus reflector discussed in Section 3.1.3.

The best feed position is given as

$$f_{opt} = 0.99\,(2a)$$

This value is significantly greater than the suggested design values but is required to keep pathlength errors within $\lambda/16$ for a 120-λ aperture. Even this value will not provide low sidelobes with a simple horn feed. Arrays have been investigated as feeds to reduce spherical aberrations (Amitay and Zucker, 1972), but if the system is to be used at multiple frequencies, the design of an array feed may be very difficult.

A second method by which conical scanning can be accomplished involves use of essentially an offset torus reflector with a spherical surface as illustrated in Figure 3-3. In this configuration an offset circular reflector contour is rotated about the vertical axis. The offset contour provides a beam at a cone angle of 45 degrees, and beam scanning is obtained by moving the feed horn on a circular arc concentric with the vertical axis. Several horns may be used to obtain multiple beams, or they may be placed so that,

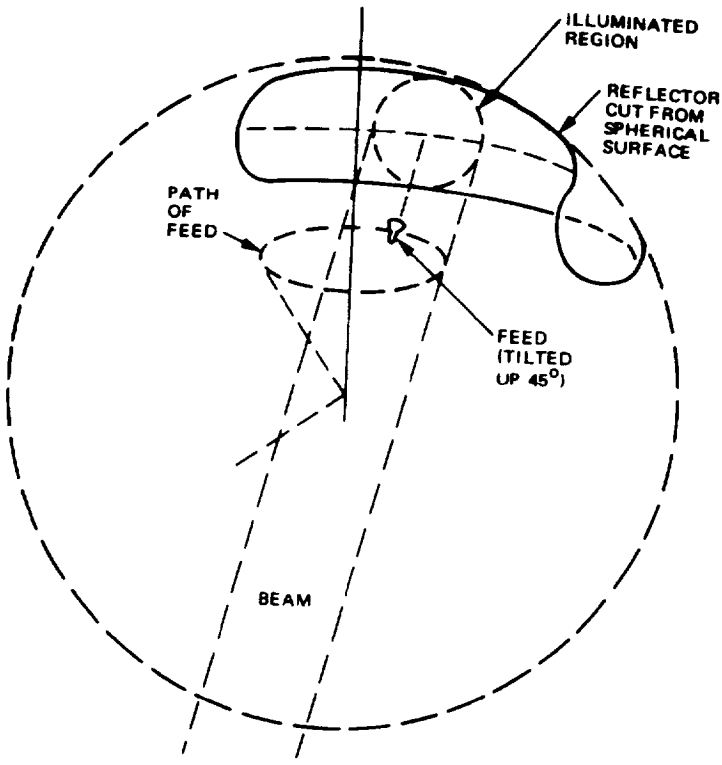

a. Perspective view

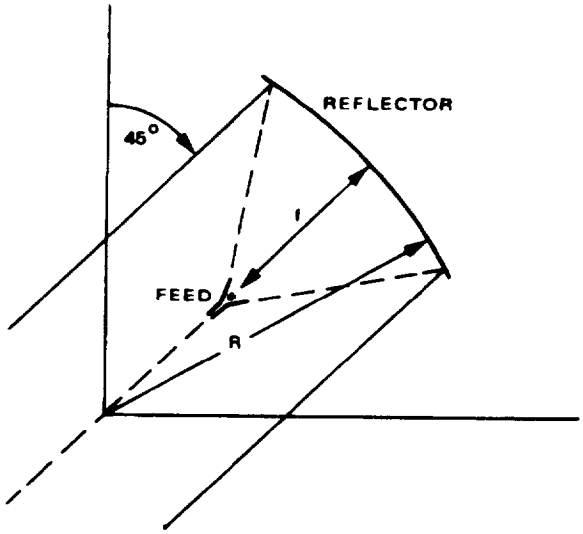

b. Section view

Figure 3-3. Offset torus reflector with spherical surface.

as one moves out of the scan region, it is switched off and a second moves into the scan region at the opposite end and is switched on. In this way, a raster type of scan is produced without any reversal of feed motion or sudden accelerations. If the reflector is a full 360-degree section, the beam can be made to scan the full 360 degrees.

3.1.2 SIMS Reflector Antenna

The spherical reflector has been studied by the Jet Propulsion Laboratory as a potential radiometer antenna for the Shuttle Imaging Microwave System (SIMS). This antenna will have to operate over a very wide range of frequencies and provide beam scanning over a very wide angle (±60°) from a nominal centerline. The frequency bands and associated bandwidths are given in Table 3-1, and the basic configuration is shown in Figure 3-4. The feeds for the various frequencies are depicted as spikes on a wheel, and the wheel is rotated on its axle to scan the beams. With this arrangement the beams will not be coaxial and, in fact, must time-share the reflector because at any one time only about a third of the feeds can illuminate the reflector effectively.

TABLE 3-1. FREQUENCY BANDS AND BANDWIDTHS OF SIMS ANTENNA

Center Frequency (GHz)	Bandwidth (MHz)
118.7	700
94.0	2000
53.0	500
37.0	2000
22.2	1000
20.0	1000
10.69	300
6.6	300
2.695	10
1.413	25
0.610	8

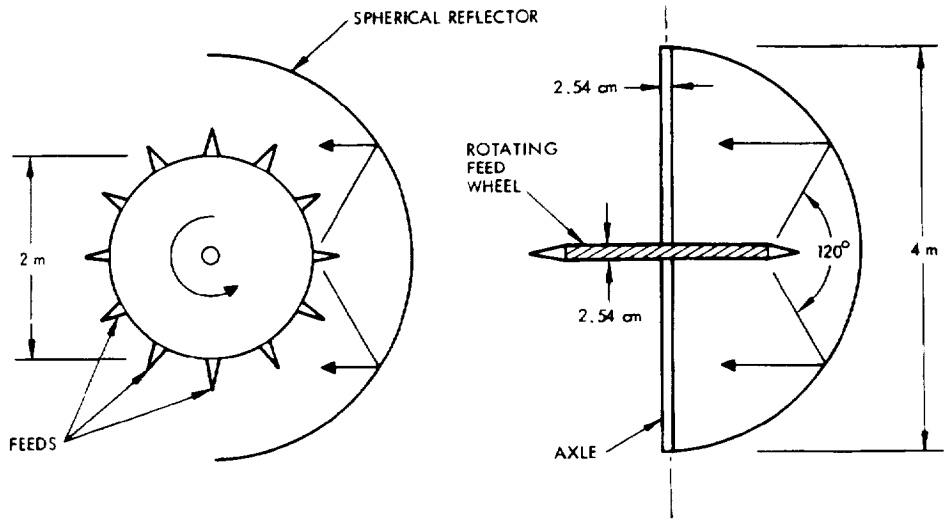

Figure 3-4. Basic configuration of SIMS spherical reflector antenna.

The major problem associated with this concept is correction of the inherent spherical aberration of the reflector by proper design of the various feeds. The problem has been studied in detail for JPL by Hansen (1974) and Gustincic (1974). Both studies conclude that error-correcting line-source feeds would be good solutions to the design problem for frequencies equal to or above 10.69 GHz. In these ranges, line-source feeds are long enough to produce well-shaped patterns with low back lobes, and the effective area of the feeds is small enough to make feed blockage negligible.

For frequencies equal to or lower than 6.6 GHz a different kind of feed would be required, and blockage may be a problem. The wheel that supports the feeds as well as the axle causes a considerable amount of blockage at all frequencies; but at low frequencies, the problem is aggravated because the beamwidth is so wide that the wheel presents an electrical obstacle larger than its physical shadow.

Spherical as well as paraboloidal reflector antennas tend to produce cross-polarized components that result in cross-polarized sidelobes that lie principally in or close to the main beam. The cross-polarized energy represents a loss in main beam power. In some applications, such as in

radiometer work in which measurements of both components of a received signal is desirable, loss in power due to cross polarization limits the ability of the system to isolate the two components. Calculation of the total power that may be lost in the cross-polarized component of such antennas is thus very important.

Gustincic also addressed the cross-polarization problem for the spherical reflector. He reports a cross-polarized component that is 18.8 dB below the principal component for the geometry shown in Figure 3-4 when the aperture is uniformly illuminated. This figure drops off to -24.5 dB for a highly tapered illumination. During the present study, Gustincic's 18.8-dB figure was checked by a coarse numerical integration of a set of curves published by Hyde (1968) for the three field components of a spherical reflector in the neighborhood of the circle of least confusion. These field components resulted from Hyde's assumption of a uniform plane wave incident upon the reflector. The surface over which he computed the three components was spherical and intercepted only waves reflected from that portion of the reflector that subtended an angle of approximately ±30 degrees at the center of the sphere. This portion of the sphere is almost exactly the same as that used by Gustincic for his study; hence, the cross-polarized component should correspond to that for Gustincic's uniformly illuminated aperture case.

The integration of Hyde's curves gives a total cross-polarized energy 19.0 dB below the total principal polarized energy. This figure is in very good agreement with Gustincic's 18.8 dB for the similar case and lends support to the credibility of both methods, because in Gustincic's work the fields were integrated across the aperture of the reflector while Hyde's fields were computed for a region near the paraxial focus of the reflector. The recent results also tend to support Gustincic's figure of -24.5 dB for a highly tapered illumination.

However, because one of the goals of this spherical reflector study was determination of the feasibility of obtaining a -25 dB cross-polarized component, these results indicate only marginal success. For -25 dB to be achieved in practice with an imperfect reflector and simple linearly

polarized feeds, a sphere whose diameter is less than half that assumed for the study would probably have to be used or the illumination across the existing aperture would have to be highly tapered. In either case, the beam-width would increase and resolution would suffer.

An alternative solution to the cross-polarization problem would be the use of specially designed feeds that tend to counteract the depolarizing effect of the reflector. One such alternative would be the use of Huygen's sources instead of simple waveguide slots in the design of the aberration-correcting line source feed; however, there are many practical problems in achievement of such a feed. Another alternative is the feed for the spherical Arecibo reflector, in which circular waveguide carrying the TE_{11} mode and circular fins on the outside of the waveguide are utilized for reduction of the cross-polarized component and achievement of high aperture efficiency (Love and Gustincic, 1968; Love, 1973). However, this feed is quite complex and would be difficult to duplicate at higher frequencies.

3.1.3 Parabolic Torus Reflector

The parabolic torus is a surface of revolution as shown in Figure 3-5. In azimuth, a portion of the circle approximates a parabolic sector with a focal length of R/2 where R is the radius of the circle; this sector collimates the beam from a point source feed as shown in the lower part of Figure 3-6. Because the antenna is a surface of revolution, the beam is independent of scan as the feed is moved along the feed circle (R/2 circle) or with fixed feeds along the circle. The polarization can be controlled by the feed.

Figure 3-7 is a photograph of such an antenna with multiple feeds that operates from 7 to 11 GHz. Patterns for this antenna, measured at 7 and 12 GHz, are shown in Figure 3-8. The sidelobe levels are higher than desired; the feed arrangement could be modified to make possible lower sidelobes, but at the expense of greater complexity. Modification of the elevation contour can also improve performance through a reduction of the phase error across the aperture (Wolff, 1966).

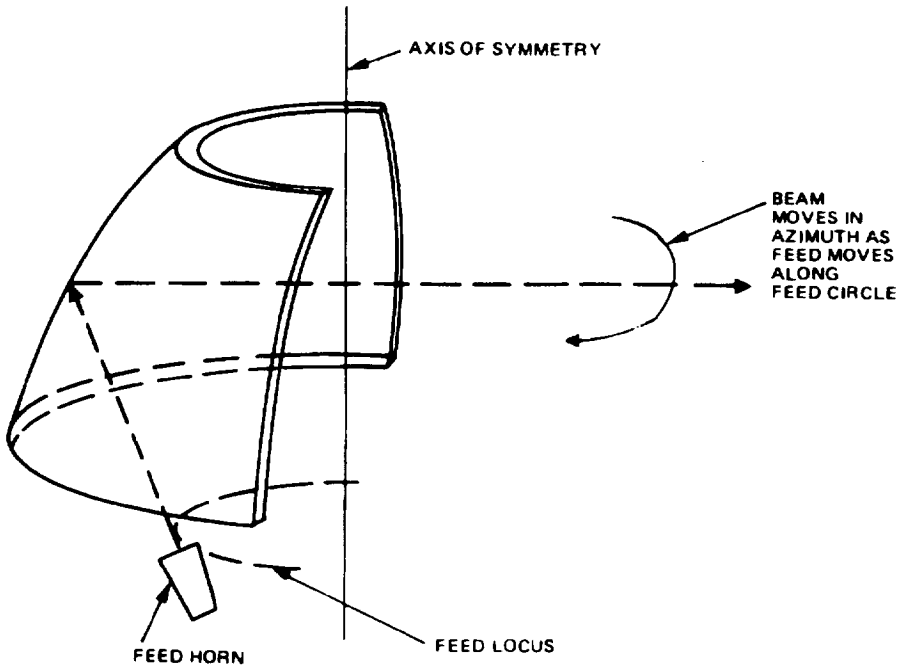

Figure 3-5. Parabolic torus antenna for quadrant sector coverage.

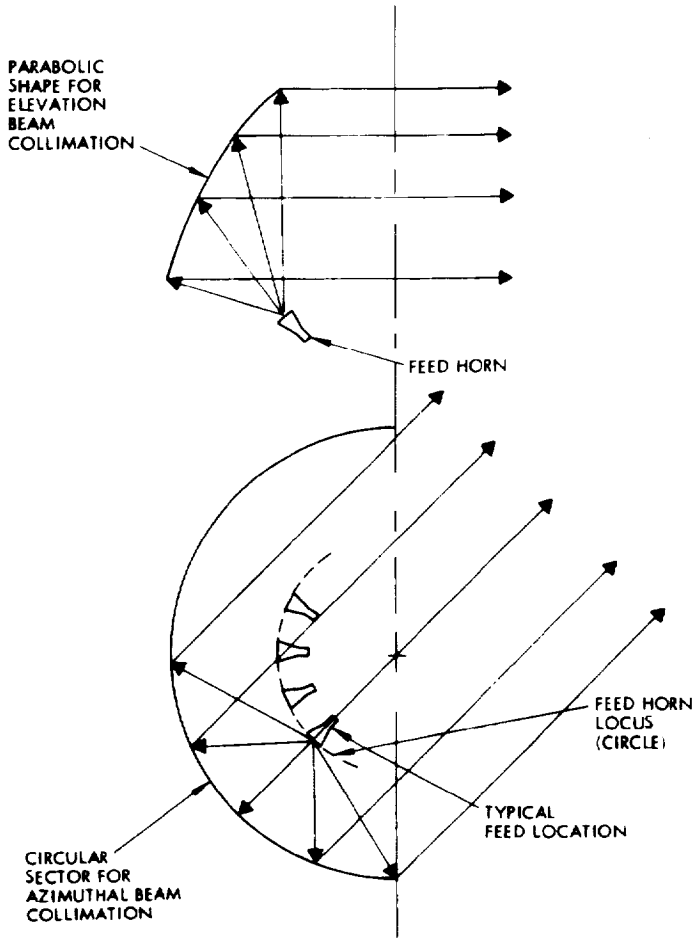

Figure 3-6. Beam collimation in parabolic torus antenna.

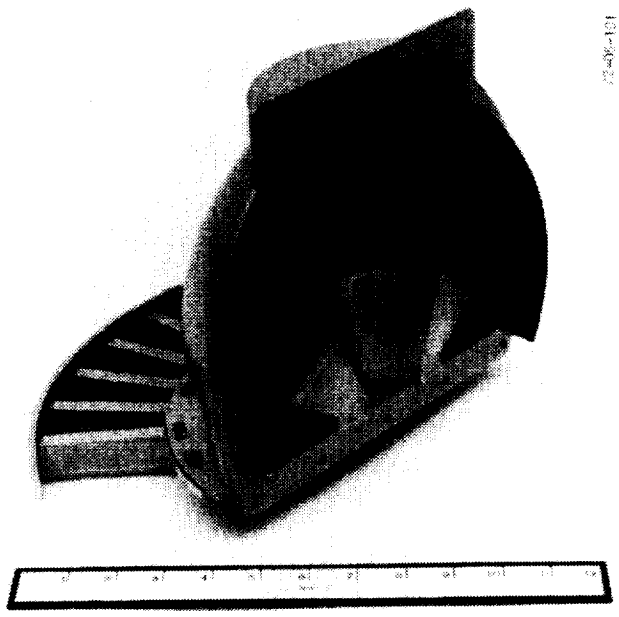

Figure 3-7. Multiple-beam parabolic torus antenna.

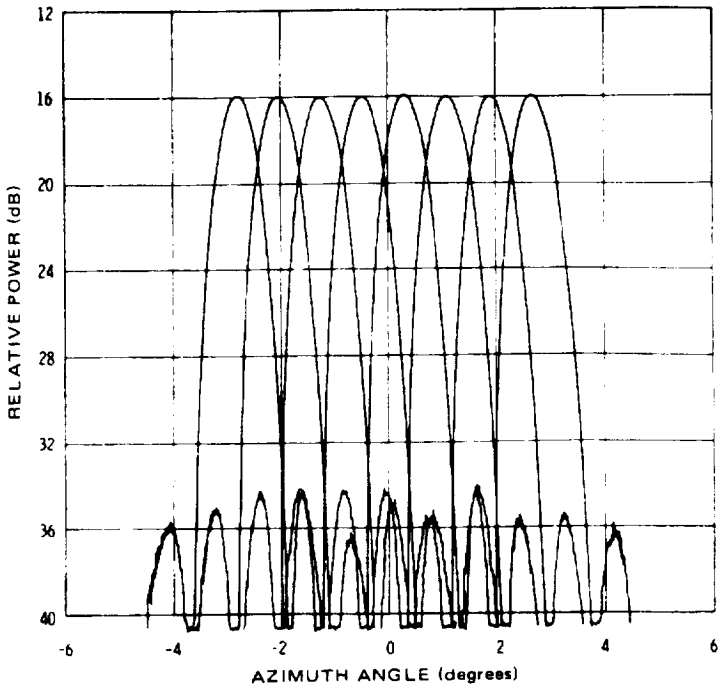

a. At 7 GHz

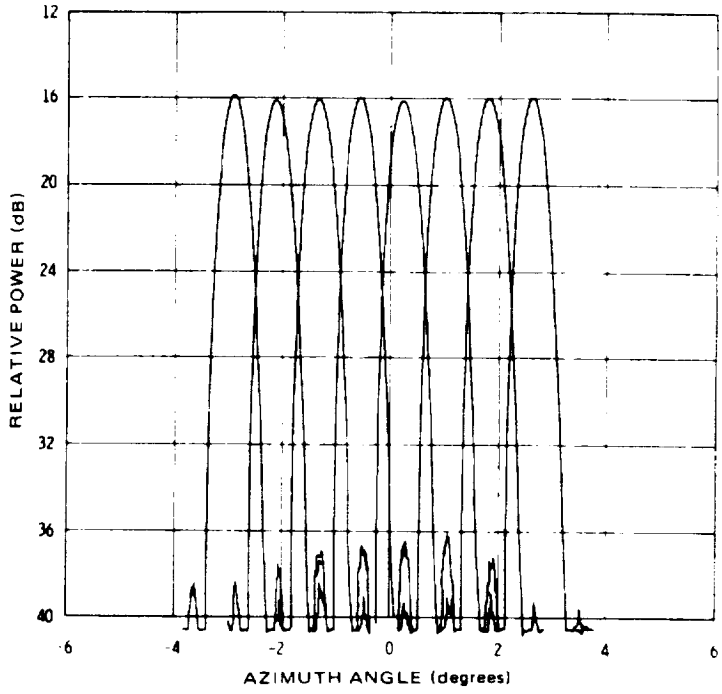

b. At 12 GHz

Figure 3-8. Radiation patterns of multiple-beam parabolic torus antenna.

The parabolic torus has the significant advantage of circular symmetry about one of its axes. If this axis is aligned with the local vertical, the torus can be used as a fixed reflector that can collimate a beam with reasonable efficiency at the desired angle of 45 degrees off axis. The beam is scanned by scanning the feed alone. This approach has been studied in depth at General Electric (Meier and Thomas, 1972) for radiometer use. Their system used separate feed horns for each of the frequency bands considered; hence, the beams were not coaxial. As such, it is not directly applicable to this study.

An offset arrangement of the parabolic torus reflector might possibly permit the beam to be scanned down 45 degrees so that the conical scan desired for the present application could be achieved. However, it is not clear whether the parabolic contour would remain desirable in elevation; this problem needs further study. Coverage of the five frequency bands might be achieved through use of two corrugated feed horns of sufficiently wide bandwidth, but integration of the antenna into a total spacecraft package would be extremely difficult. A five frequency feed system has been developed using a set of coaxial horns for the required bands (Frey, 1976).

3.2 FEED HORNS FOR RADIOMETRIC ANTENNAS

The corrugated conical horn (Clarricoats and Saha, 1971; Love, 1976; Bokurka, 1975) has previously been studied as a potential feed horn for radiometric antennas that are required to operate over a bandwidth of 2:1. Most of the feed horns investigated to date have a bandwidth limitation of about 1.6:1 (Roberts, 1973) and, thus, may not be adequate.*

An alternative to the corrugated horn that may provide a broader bandwidth is the use of an artificial dielectric with an index of refraction less than unity in a region near the walls of an uncorrugated horn, as shown in Figure 3-9. Such dielectrics can be referred to as fast-wave artificial dielectrics because waves passing through them have phase velocities greater than the speed of light. It has been shown that loading a horn along its walls with conventional dielectric materials (which have an index of

*Recently a corrugated horn with tapered grooves has provided greater bandwidths (Zvic, F., 1975).

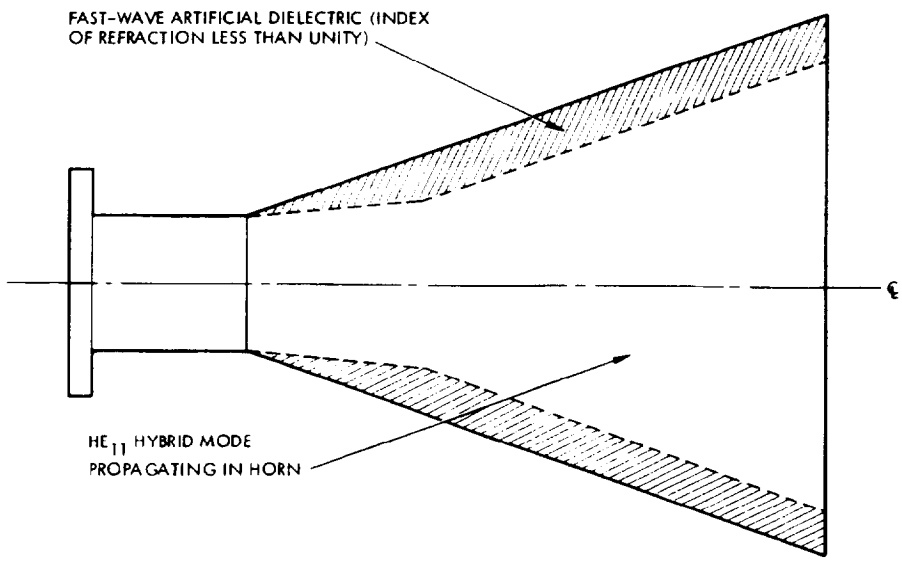

Figure 3-9. Fast-wave artificial dielectric-loaded horn.

near the throat produced equal E- and H-plane patterns with low sidelobes (Satoh, 1972); however, the bandwidth reported for this technique was only 25 percent.

Because loading a horn over a large region of its walls with a dielectric whose index of refraction is greater than unity tends to pull the fields towards the walls, it seems logical to assume that loading a horn similarly with an artificial dielectric with an index of refraction less than unity would tend to force the fields away from the walls. The latter result is desirable and is the same effect obtained with the corrugated horn. The corrugations, however, must be limited to certain ranges in depth, i.e., between $\lambda/4$ and $\lambda/2$ deep or between some similar multiple such as $3\lambda/4$ and λ. It is this limitation that restricts the bandwidth of such horns.

The corrugations in a corrugated horn appear anisotropic to the mode propagating in the horn. As a result, they operate primarily on the fields in the E-plane and leave the H-plane undisturbed. This phenomenon is beneficial because, in conventional horns, the E-plane pattern is the one

with high sidelobes and a low beam efficiency due to the uniform field distribution in that plane. In the design of fast-wave, artificial dielectrically loaded conical horns, use of an anisotropic-loading structure would also probably be desirable to achieve the same results. Such a structure can be most easily accomplished by the etching of a configuration of thin radially directed conducting strips on thin dielectric sheets. Numerous such sheets would be arrayed to form a periodic structure extending from near the throat out to the aperture of the horn. The conducting strips would be positioned on each sheet in such a way that they would start at the wall and extend part way in toward the axis of the horn.

In the corrugated conical horn, the principal mode generated is the HE_{11} hybrid mode. Hence, for the performance of the corrugated horn to be duplicated in a dielectrically loaded configuration, the fast-wave dielectric in conjunction with the normal modes in the new horn must tend to generate the same hybrid mode. An analysis of the modal relationships within a loaded horn is needed before the presence of the hybrid mode can be confirmed.

Detailed design of the fast-wave artificial dielectric can follow previous work along this line. Three-dimensional grids of parallel conductors have been analyzed and reported extensively in the literature (Rotman, 1962; Brown, 1953; Carne and Brown, 1958; Skwirzynski and Thackray, 1959; Goodall and Jackson, 1959). In the case of interest, in which the conductors have very good conductivity and the E-vector is parallel to the conductors, it is shown that the propagation characteristics of such a medium are very similar to those of a waveguide. The structure has a cutoff wavelength below which no propagation takes place. Just above cutoff, the phase velocity of the wave is much greater than the free-space velocity of propagation; as the frequency increases, the phase velocity decreases and approaches the free-space velocity asymptotically as the frequency approaches infinity. At some relatively high frequency the structure is capable of carrying higher-order modes, and thus, its bandwidth for waves incident normal to the surface is from some point not too close to cutoff to quite close to the higher-order mode region. If the spacing between conductors is on the order of

0.1λ at the lowest operating frequency, the higher-order modes cannot be generated until that spacing equals 0.5λ at the higher frequency. Hence, the bandwidth is 5 to 1. However, it should be noted that the index of refraction would be changing throughout this band in proportion to the ratio λ_o / λ_g, where λ_g is the wavelength in the gridded medium. This large change in dielectric constant may be detrimental for some applications but should not affect its use in conical horns, as proposed here, provided that the loaded region of wall is sufficiently long in terms of wavelengths to make the wave lift off the surface in the E-plane.

A factor that may limit the bandwidth more severely than the generation of higher order modes is the fact that the medium starts to become anisotropic in the plane perpendicular to the conductors as the conductor spacing becomes greater than about $0.2\lambda_o$. This characteristic may be seriously detrimental to the operation of the conical horn and requires investigation.

3.3 OFFSET PARABOLOIDAL ANTENNAS

Because initial review suggested that a reflector antenna was superior to both array and lens systems for the multi-frequency dual-polarized radiometer application, an intensive computer study was performed of a promising offset paraboloidal reflector fed by corrugated conical horns. Two different feed horns were used: one horn covered two X-band frequencies, 6.6 and 10.7 GHz, and the second covered three higher frequencies (18, 21, and 36 GHz). The reflector had a diameter, D, of 1.25 meters and a focal length, f, of 0.946 meter. The bottom was offset a distance, h, of 0.178 meter, as illustrated in Figure 3-10. The horns were tilted up at an angle ψ of 44.18 degrees

3.3.1 Horn Design

Both horns had half-angles of 30 degrees and the same angle of flare. The X-band horn had an aperture diameter of 6.075 inches and a corrugation groove depth of 0.47 inch. The higher frequency horn had an aperture diameter of 2.228 inches and a groove depth of 0.25 inch. The feed horns were designed to provide a taper of approximately 18 dB at the edge of the reflector. Such a taper provides low sidelobes and low spillover and should result

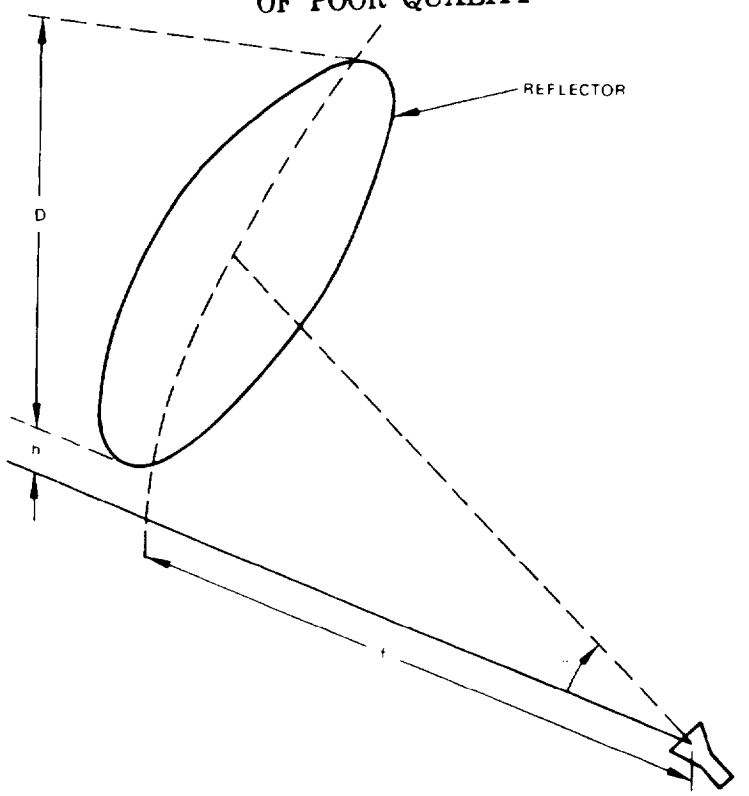

Figure 3-10. Geometry of offset paraboloid with feed.

in relatively high beam efficiencies. The relatively large flare angle is required to make the feed beamwidth insensitive to frequency. The corrugation depth was selected so that the wall reactance was not inductive at the operating frequencies. Patterns were computed for each horn by use of a modification of a program supplied by P. D. Potter (1973).

The primary patterns of the X-band horn at each of the coverage frequencies are shown in Figure 3-11. Because of the wide flare angle, the patterns are very similar at both frequencies. The presence of the corrugations also tends to make the E- and H-plane patterns very similar. These characteristics, i.e., frequency insensitivity and equal E- and H-plane patterns, are desirable to obtain satisfactory secondary patterns.

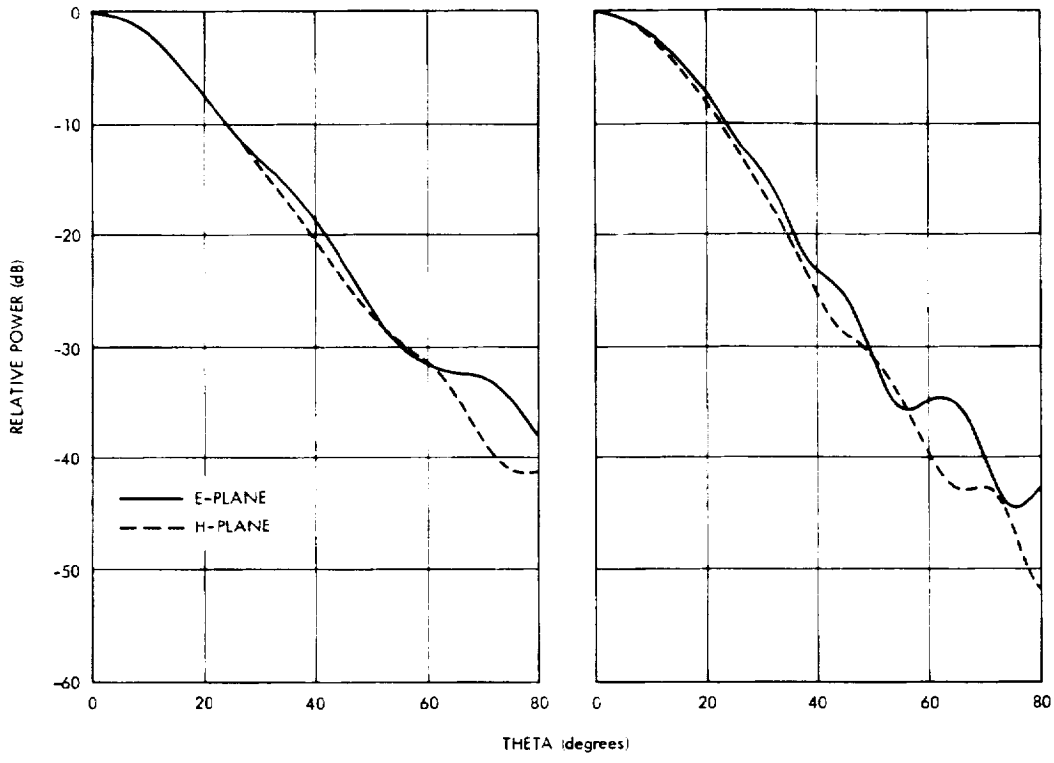

a. At 6.6 GHz

b. At 10.7 GHz

Figure 3-11. Calculated primary radiation patterns for X-band corrugated conical horn.

At the higher operating frequencies (18, 21, and 36 GHz) the corrugation depth had to satisfy approximately the following conditions;

$$1/2 > \frac{d}{\lambda_{18}} > 1/4$$

$$1 > \frac{d}{\lambda_{36}} > 3/4$$

$$1/2 > \frac{d}{\lambda_{21}} > 1/4$$

where d is the depth of the corrugations and λ is the wavelength. These inequalities are satisfied in the region of the horn mouth for d = 0.25 inch. However, for frequencies between about 23.6 and 35.4 GHz, the reactance is positive and can support surface waves that could degrade the primary pattern. Patterns of the smaller horn, computed at 18, 21, and 36 GHz, are presented in Figure 3-12. As was seen for the X-band horn, the patterns are relatively independent of frequency and have very similar E- and H-plane patterns.

Ideally, the horns should be positioned so that their phase centers are at the reflector focus. However, they do not have a precise phase center, and in fact, E-plane patterns may have somewhat different phase centers than H-plane patterns. Thus, only approximate phase centers can be determined, and the positions of these vary as a function of frequency. When the horns are used at several frequencies, they must thus be positioned at some compromise location. A selection technique used was location of the horn at a weighted mean between the approximate phase centers of the highest and lowest frequency. This position was selected so that the electrical shift from the correct phase center was equal at the two frequencies. The position of the horn is established by specification of the location of the point in the center of the horn aperture. For the lower frequency horn, the position relative to the focus was 7.24 cm along the axis toward the reflector and up 7.03 cm. For the higher frequency horn, the position relative to the focus was 2.73 cm toward the reflector and up 2.67 cm.

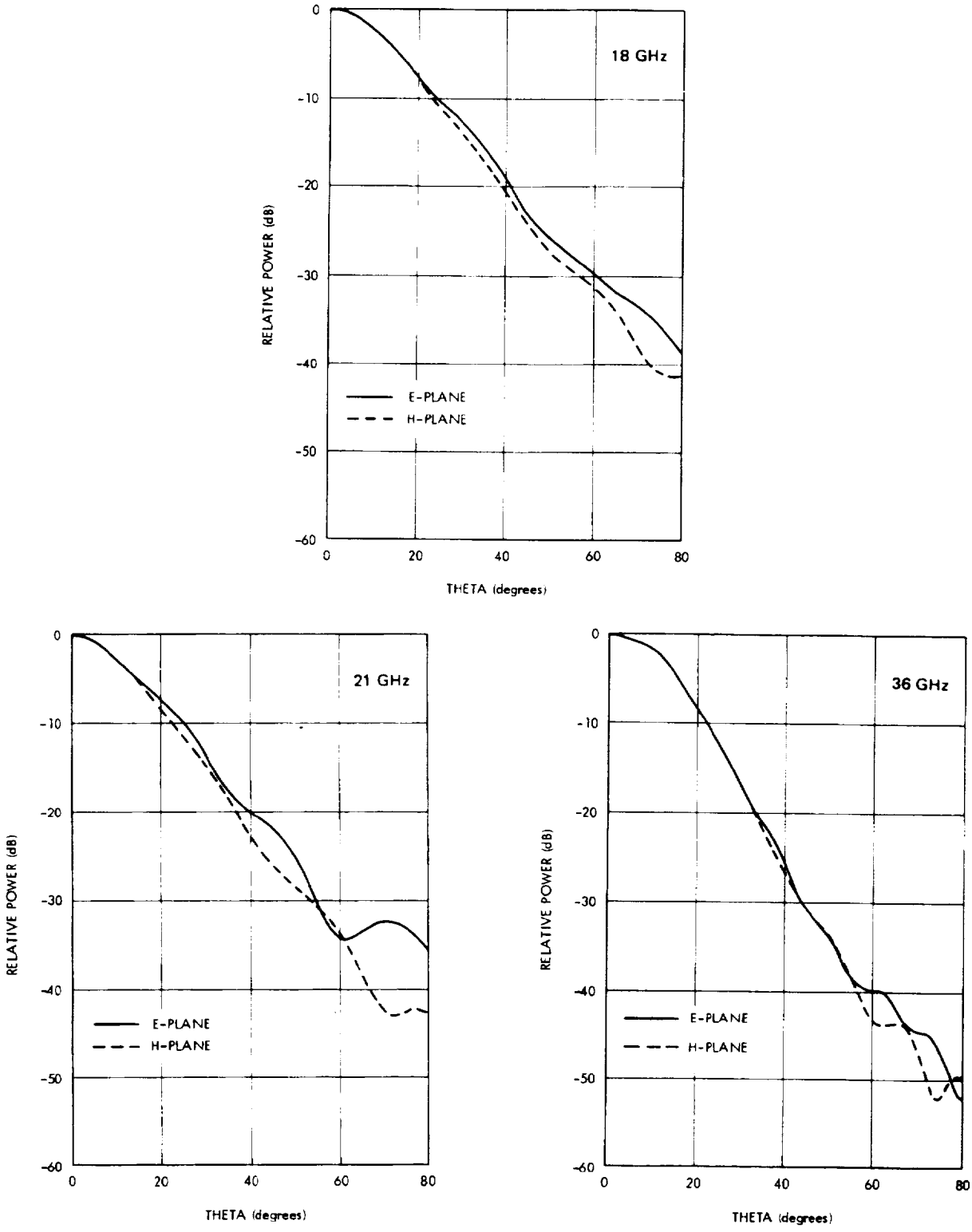

Figure 3-12. Calculated primary radiation patterns for 18-, 21-, and 36-GHz corrugated conical horn.

3.3.2 Secondary Patterns

Radiation patterns of the reflector feed combination were computed at the five frequencies of interest for both vertical and horizontal polarization. The desired polarization and the cross-polarized component of the radiation field are shown over a region near the main beam and first few sidelobes in Figures 3-13 through 3-17. The patterns were computed with a vector physical optics program that suggested excellent results for this angular region. Because of the symmetry of the antenna, the patterns are symmetrical in azimuth so that only half of each azimuth pattern is shown. The symmetry is not preserved in the elevation plane, and patterns are illustrated both above and below the boresight direction. The effect of positioning the feed horns at some point other than the phase center is evident in the null filling and skewing of the skirts of the beams, but the major portion of the main beams are preserved down to nearly the -20 dB level. Nearly all remaining sidelobes are more than 30 dB below the peak. The cross-polarization vanishes in the elevation cuts. In the azimuth cuts it rises to a peak value slightly off the beam axis, but still within the main beam. All cross-polarized principal maxima are greater than 23.3 dB below the peak of the main beam and appear to fall off rapidly beyond the maximum.

3.3.3 Beam Efficiency

Beam efficiency, η_B, is the fraction of total power supplied by the horn that is contained within the main beam and has the correct polarization. In terms of the gain function of the desired polarization, $G_d(\theta, \phi)$, it is given by the following expression.

$$\eta_B = \frac{1}{4\pi} \iint_{\text{main beam}} G_d(\theta, \phi)\, d\Omega$$

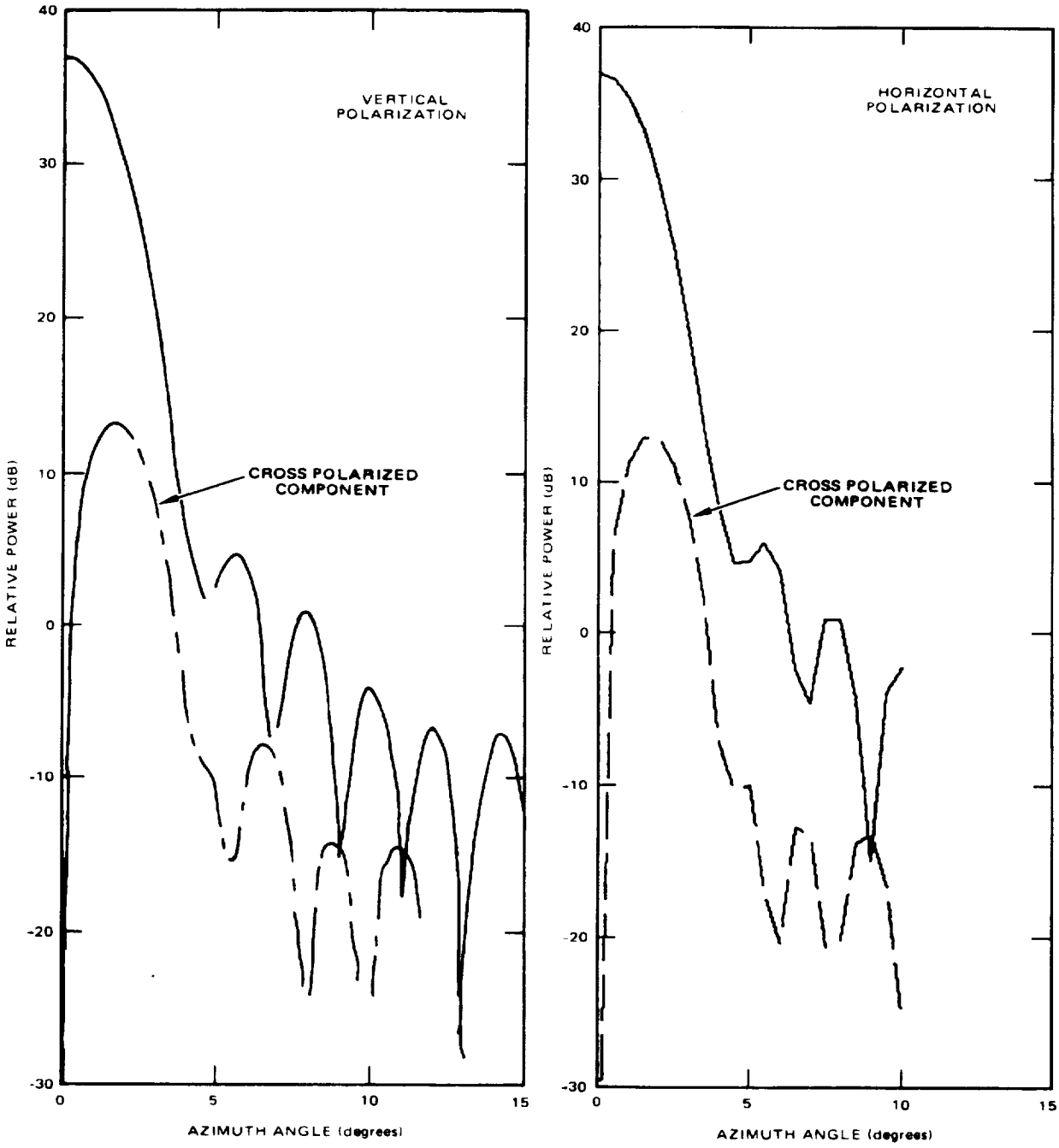

Figure 3-13. Calculated radiation patterns at 6.6 GHz of offset reflector with corrugated horn feed.

ORIGINAL PAGE IS
OF POOR QUALITY

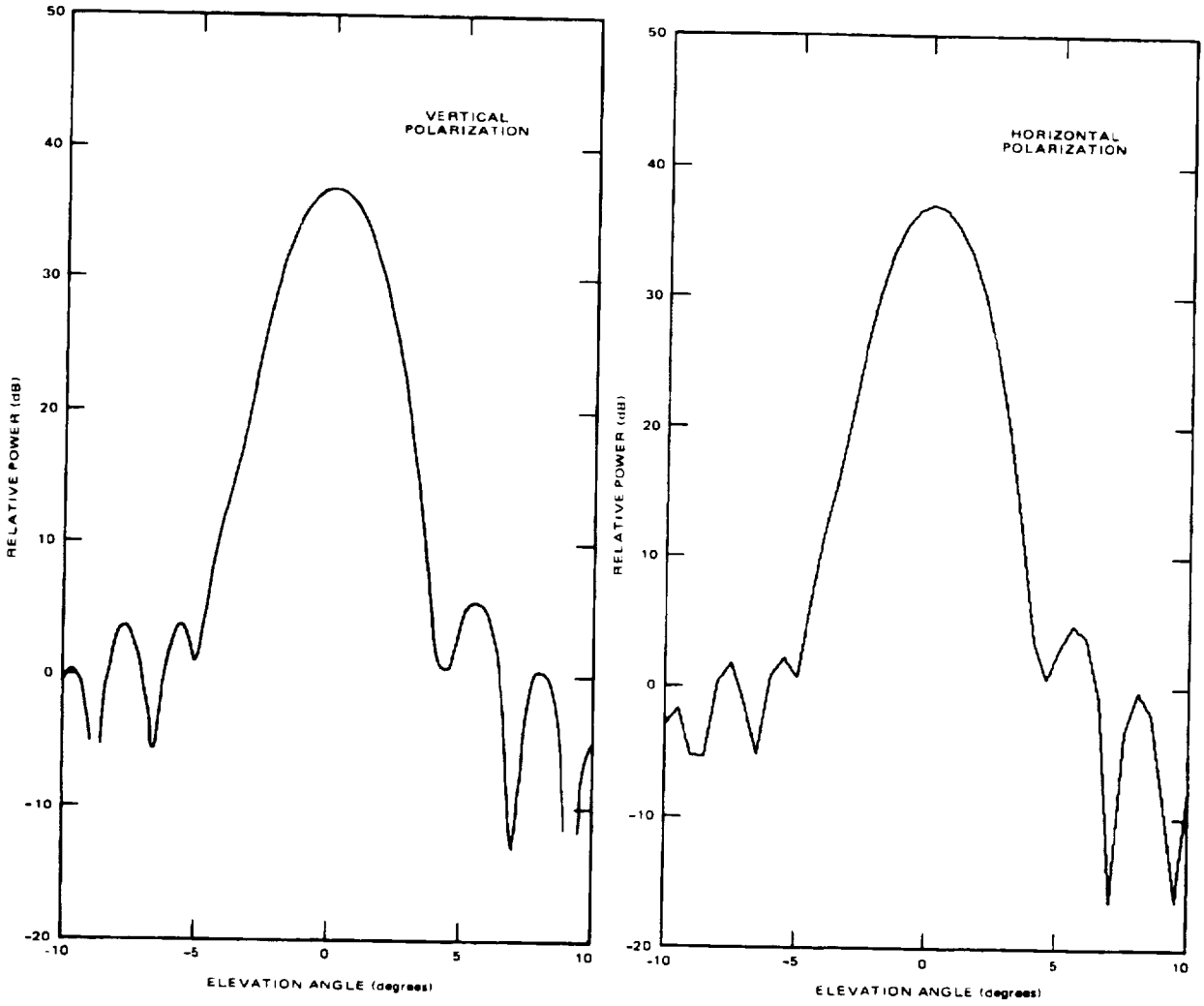

Figure 3-13 (Concluded)
(Cross-polarized component vanishes)

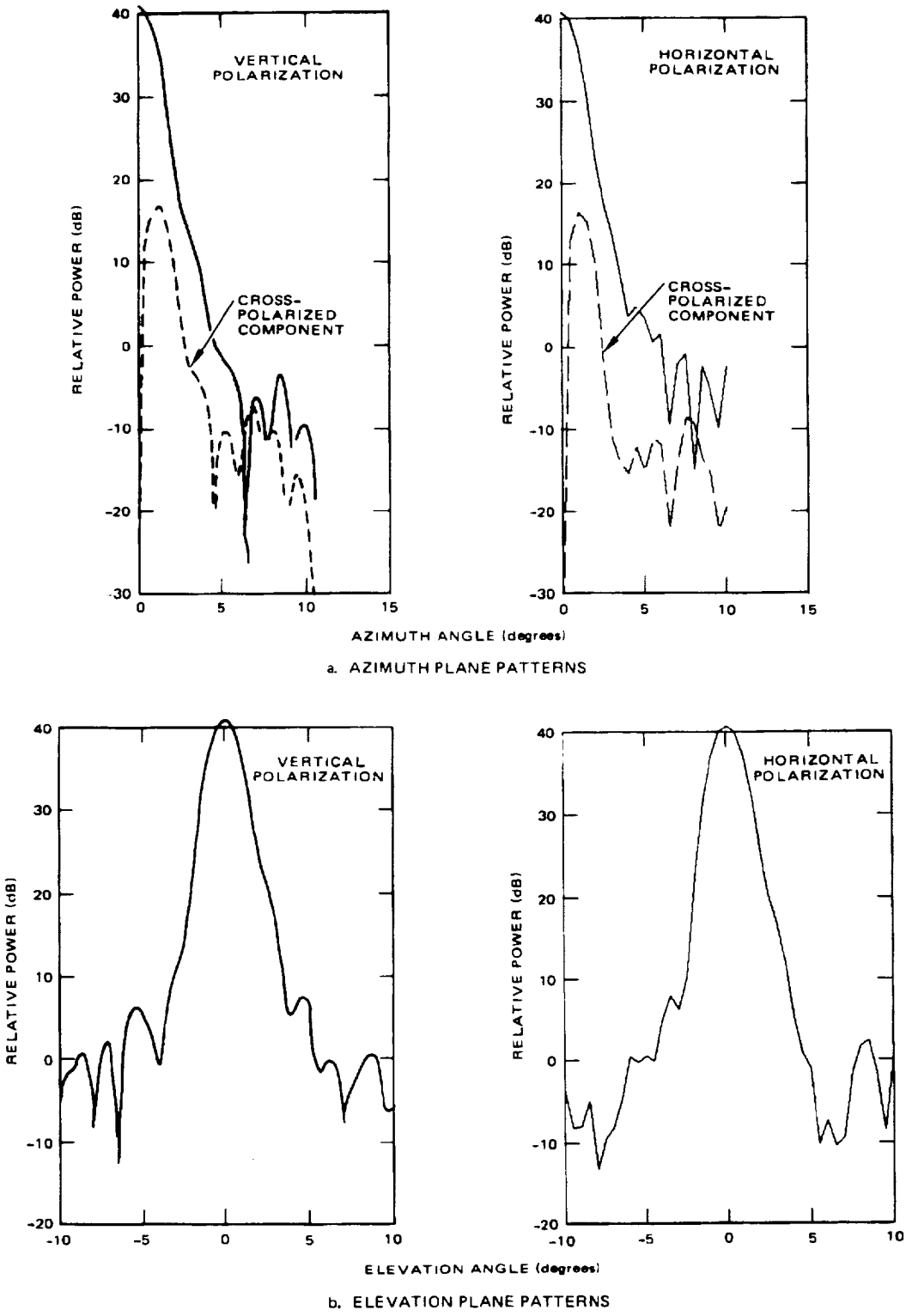

Figure 3-14. Calculated radiation patterns at 10.7 GHz for offset reflector with corrugated horn feed. Cross-polarized component vanishes in elevation plane.

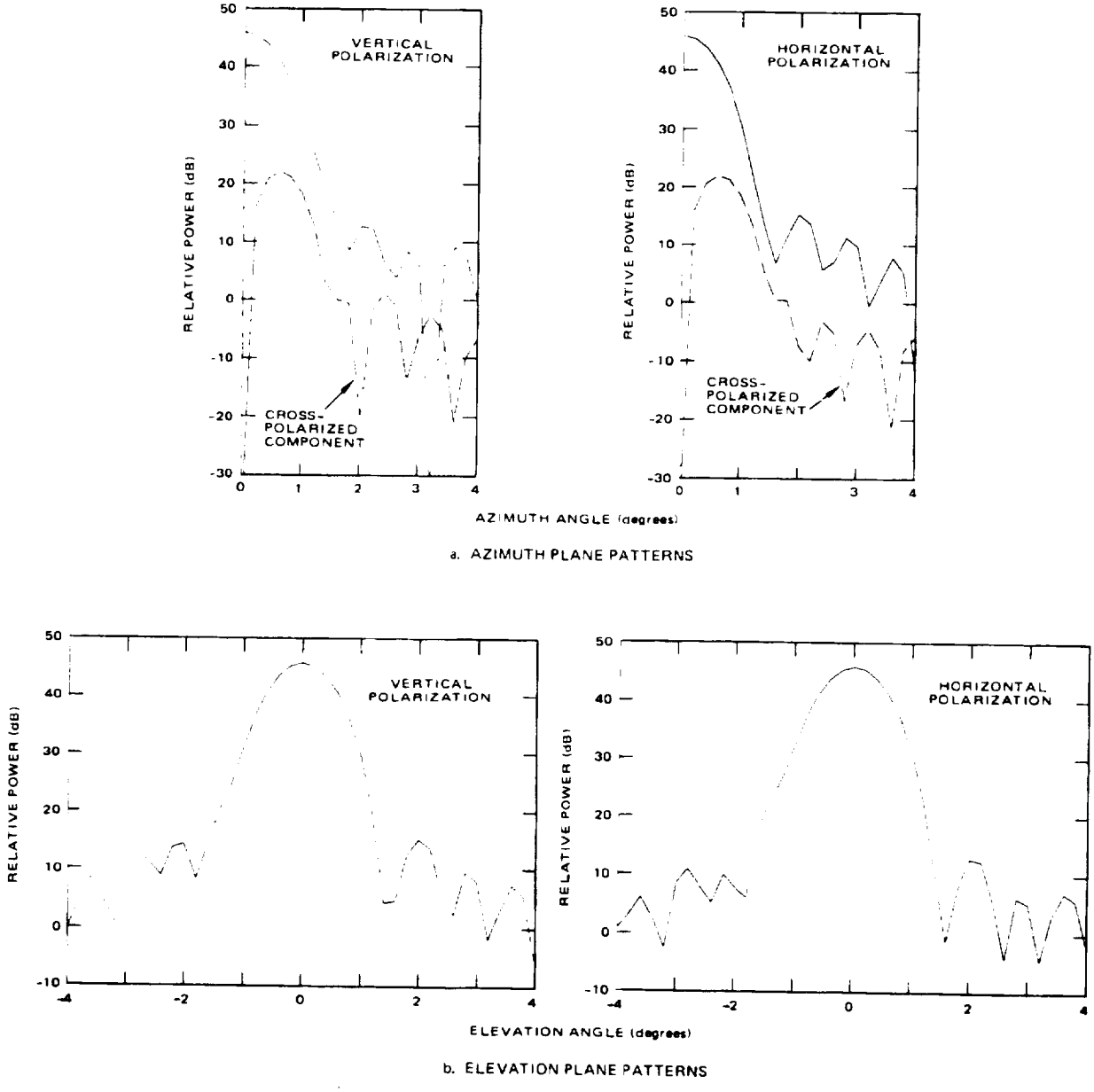

Figure 3-15. Calculated radiation patterns at 18 GHz of offset reflector with corrugated horn feed. Cross-polarized component vanishes in elevation plane.

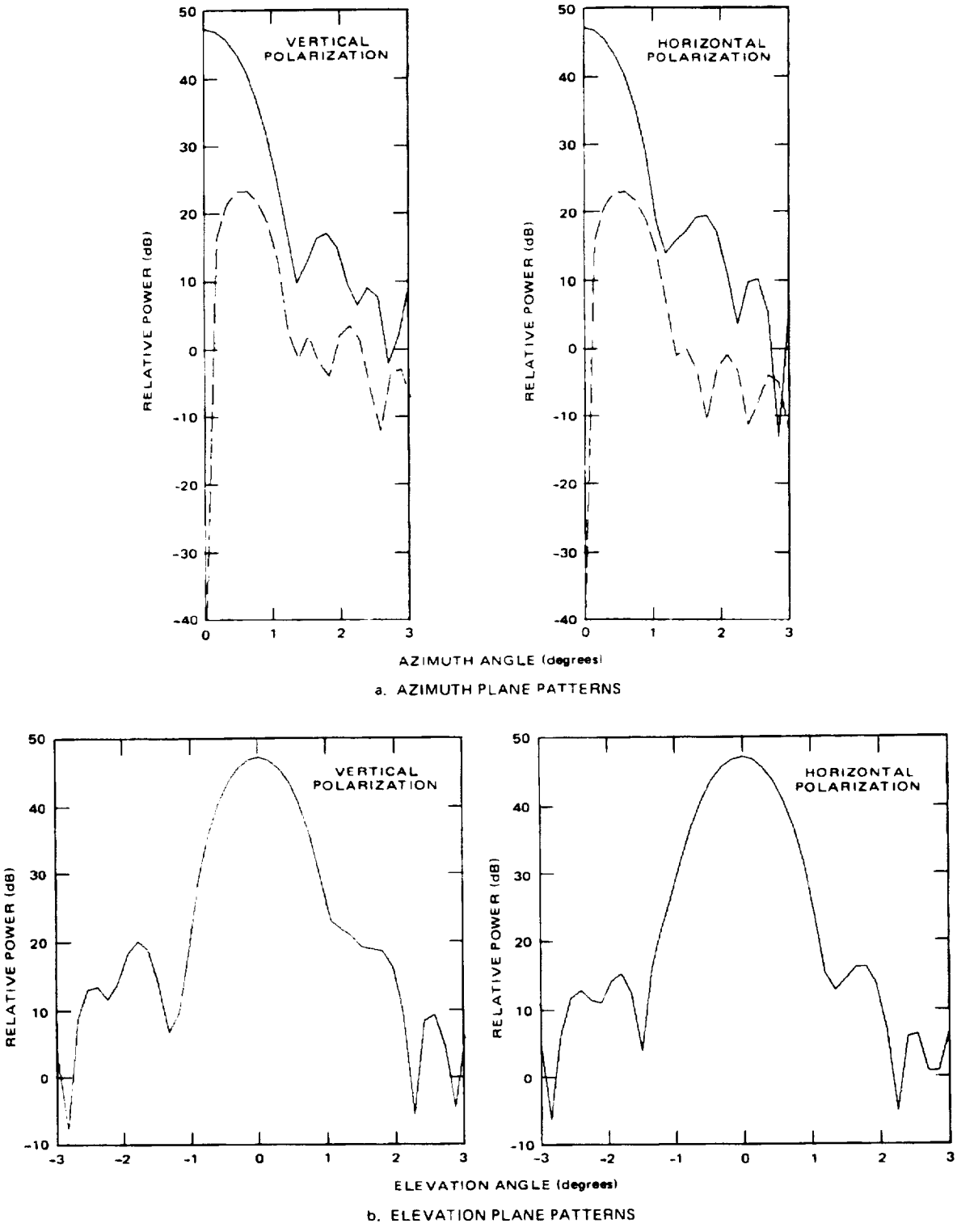

Figure 3-16. Calculated radiation patterns at 21 GHz for offset reflector with corrugated horn feed. Cross-polarized component vanishes in elevation plane.

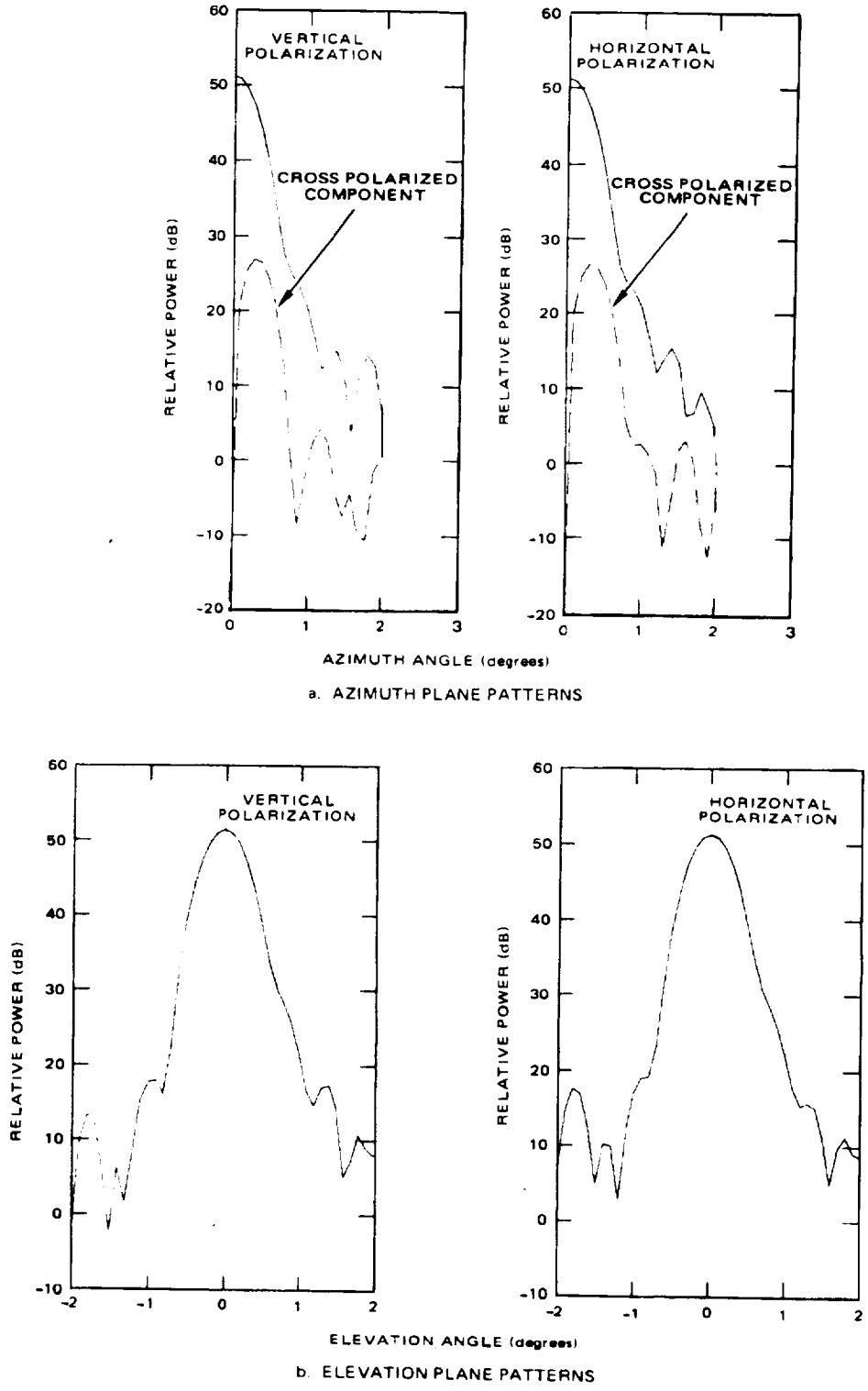

Figure 3-17. Calculated radiation patterns at 36 GHz of offset reflector with corrugated horn feed. Cross-polarized component vanishes in elevation plane.

where the integral is taken over the main beam. The gain, G_d, is defined relative to the total power radiated by the feed horn and thus includes the effects of cross polarization and spillover. Losses due to dissipation, fabrication tolerances, and other errors are not included.

Determination of the exact extent of the main beam from the calculated patterns is somewhat arbitrary: because of phase errors, the first null tends to fill in and, in some cases, coalesces into a shoulder on the main beam. The values used in the calculations were those that would be expected if there were no full filling and were selected by extrapolation of the undistorted portion of the main beam down toward a null. The corresponding beamwidths and beam efficiencies are included in Tables 3-2 and 3-3, which is a summary of the characteristics of the antennas at each frequency.

3.3.4 Cross-Polarization Isolation

Direct calculation of cross-polarization isolation requires calculation of the secondary pattern of the reflector over a half-space and integration of the power in the resulting cross-polarized component of the field. For antennas of the size considered in this study, such a procedure would require excessive computer time and is impractical. However, an estimation of the relative level of the cross-polarized signal from the patterns already calculated is possible and was accomplished.

When the power in the main beam with the desired polarization and the spillover have been accounted for, the remaining power must be in sidelobes and in cross-polarized fields. In nearly all the azimuth patterns, the cross-polarized component appears to be at least 10 dB below the sidelobe level, on the average. In the elevation patterns the cross-polarized component is negligible. It was assumed that the cross-polarized components decrease smoothly from a value 10 dB below the sidelobe level down to a negligible value. With this assumption, the integrated value should be an additional 3 dB below the integrated value of the sidelobe energy. This result may be expressed by the following relation.

$$\frac{P_{cp}}{P_o} = \frac{\alpha}{\alpha+1}\left(1 - \frac{P_B}{P_o} - \frac{P_{sp}}{P_o}\right)$$

TABLE 3-2. COMPUTED CHARACTERISTICS OF VERTICALLY POLARIZED OFFSET PARABOLOID WITH CORRUGATED HORN FEEDS

Frequency (GHz)	Peak Gain (dB)	Sidelobe Level (dB below peak gain)		Maximum Cross-Polarization (dB below peak gain)	3-dB Beamwidth (degrees)		Full Beamwidth (degrees)	Beam Efficiency (percent)	Area Gain (dB)	Antenna Efficiency (percent)	Spillover Loss (dB) ±0.05	Estimated Cross-Polarization Isolation (dB)
		Azimuth	Elevation		Azimuth	Elevation						
6.6	36.99	32.2	22 (shoulder)	23.3	2.6	2.7	9.0	93	38.74	67	0.23	-30
10.7	40.77	24 (shoulder)	19 (shoulder)	23.8	1.6	1.7	5.0	93	42.93	61	0.10	-26.5
18	45.79	33	23 (shoulder)	23.6	0.94	0.92	3.0	90	47.45	68	0.30	-28
21	47.17	30	22 (shoulder)	23.6	0.82	0.82	2.6	91	48.79	69	0.25	-28
36	51.34	26 (shoulder)	19 (shoulder)	24.1	0.52	0.52	1.4	93	53.47	61	0.08	-26

TABLE 3-3. COMPUTED CHARACTERISTICS OF HORIZONTALLY POLARIZED OFFSET PARABOLOID WITH CORRUGATED HORN FEEDS

Frequency (GHz)	Peak Gain (dBi)	Sidelobe Level (dB below peak gain)		Maximum Cross-Polarization (dB below peak gain)	3-dB Beamwidth (degrees)		Full Beamwidth (degrees)	Beam Efficiency (percent)	Area Gain (dBi)	Antenna Efficiency (percent)	Spillover Loss (dBi) ±0.05	Estimated Cross-Polarization Isolation (dB)
		Azimuth	Elevation		Azimuth	Elevation						
6.6	37.01	30.8	23 (shoulder)	23.9	2.6	2.7	9.0	93	38.74	67	0.25	-30
10.7	40.81	24 (shoulder)	22 (shoulder)	23.8	1.6	1.7	5.0	94	42.93	61	0.19	-27.5
18	45.80	30	20 (shoulder)	24.0	0.94	0.92	3.0	90	47.45	58	0.30	-28
21	47.18	27.5	25 (shoulder)	24.0	0.82	0.82	2.6	91	48.79	59	0.25	-28
30	51.33	26 (shoulder)	20 (shoulder)	24.5	0.52	0.52	1.4	93	53.43	61	0.15	-26

where α is the estimated ratio of integrated cross-polarized power to integrated sidelobe power, P_{cp} is the integrated cross-polarized power, P_B is the main-beam power in the desired polarization, P_{sp} is the spillover power, and P_o is the total radiated power. For the estimate made in this study, α was taken to be 1/20. Then, with values of beam efficiency and spillover from Tables 3-2 and 3-3, the worst case gives a value of cross-polarization isolation of -26 dB.

3.3.5 Accuracy of Calculations

The patterns were calculated by means of various theoretical approaches that inherently involve approximations. For example, the primary horn patterns were computed under the assumption that a single HE_{11} conical waveguide mode exists on the spherical cap at the horn aperture and concentric with the horn vertex. In addition, any fringing fields over the remainder of the spherical surface were neglected. This latter approximation is equivalent to the assumption that the horn is located in a conducting spherical surface as illustrated in Figure 3-18. These assumptions are

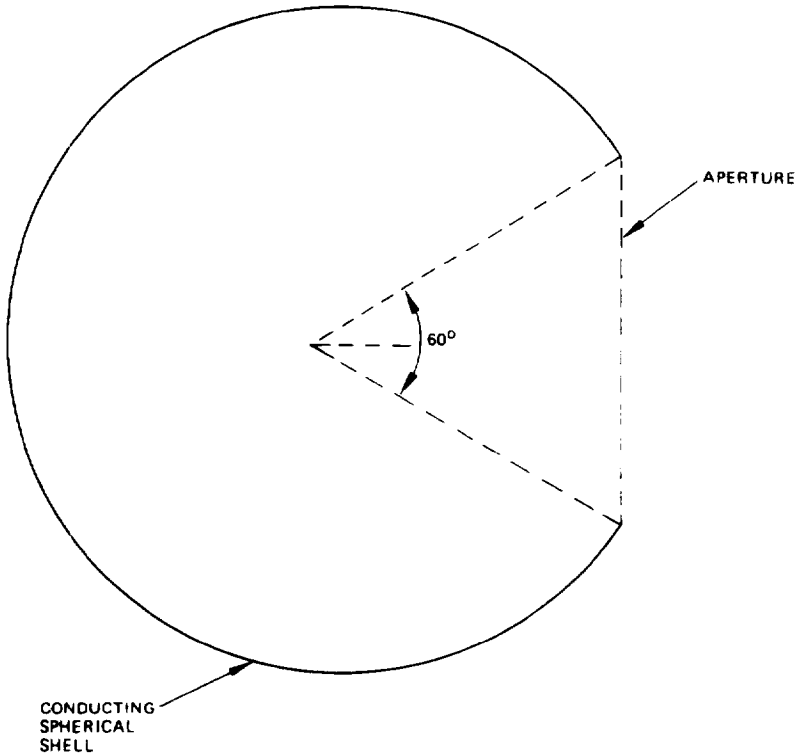

Figure 3-18. Equivalent corrugated conical horn geometry.

reasonable when the HE_{11} mode is balanced, because then the fields all vanish at the aperture edge and the presence or absence of the conducting shell makes little difference. If the mode balance is poor, then the fields are not all small at the aperture edge and the calculated patterns will depart somewhat from those predicted by the mathematical model. The degree of departure will depend on the mode imbalance. Checks against measurements over a fairly wide frequency range indicate that the errors in the calculated patterns remain quite small, at least over most of the main region of the horn pattern (Clarricoats and Saha 1971). In addition, the computer program, as written, only approximates the conical waveguide HE_{11} mode by curving the mode for a cylindrical guide over spherical surfaces within the horn. This approximation is good for small to moderate flare angles but can be expected to be in error for large flare angles. It was checked against the results of Clarricoats and Saha for a 30-degree half-angle flare, and agreement is good.

The secondary patterns of the horn reflector combinations were computed by use of physical optics. This method yields excellent results, especially around the main beam and near-in sidelobes, for reflectors that are large in wavelengths, as are the ones considered in this study. In addition to the inherent approximations in the method of physical optics, the accuracy of the results depends on the precision with which the integration over the reflector is performed. By adjustment of the integration step size to a 41-by-41 grid, the accuracy of the gains of the main beam are estimated to be within four to five hundredths of a dB, and the first sidelobes to be within a few tenths of a dB, of the values that would be obtained from a perfect integration.

The calculation of beam efficiency requires an integration of the gain function over the main beam. It has been found that a 10-by-10 grid with quadratic interpolation over the beam or, as in the cases of azimuthal symmetry in this study, a 10-by-5 grid is adequate to obtain the beam efficiency to within a few tenths of a percent.

After the pattern and beam efficiency calculations had been performed, a misprint was discovered in one statement of the computer program. This

statement was corrected, and several cases were rerun to determine the extent of change from the previously computed patterns. These new patterns are shown in Figure 3-19. There is essentially no difference in the main beam regions between these patterns and those previously computed. The levels and details of the sidelobe structures are slightly different, but not enough to affect the calculations of beam efficiency significantly. Consequently, recomputation of all the cases was not considered necessary.

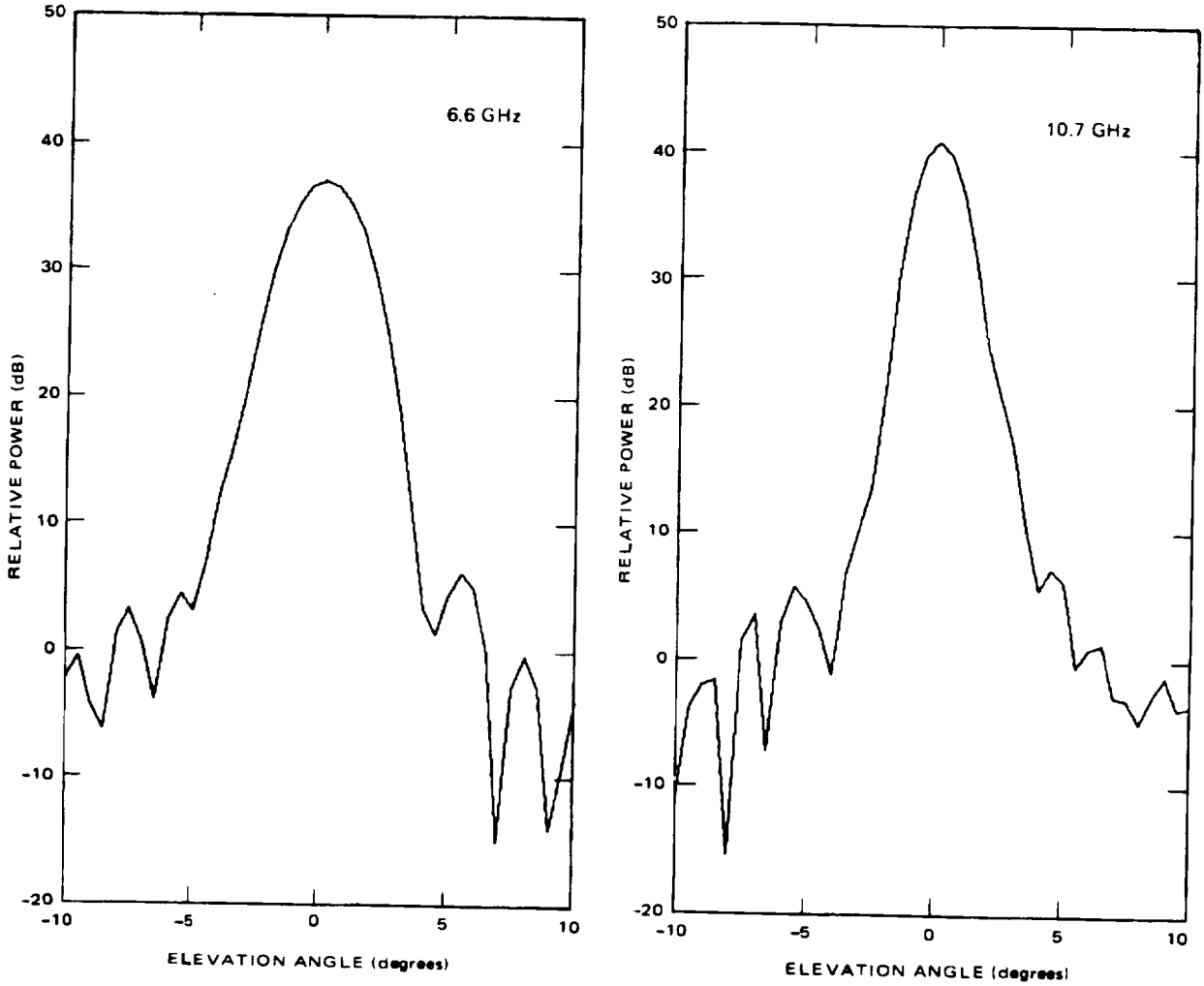

Figure 3-19. Corrected radiation patterns of offset reflector with corrugated horn feed. (Vertical polarization). Cross-polarized component vanishes in elevation plane.

3.3.6 Integration for Spillover Calculation

The spillover loss was obtained by integration of the power pattern of the feed horn over the angular region subtended by the reflector as seen from the horn location. Because of the complicated relationships expressing the angular coordinates of the horn in its coordinate system in terms of the reflector angular coordinates in its coordinate system, determination of an exact expression for the limits on the angle of integration was impractical; consequently, the following scheme was used.

The horn coordinate θ_h was subdivided into sufficiently small increments so that integration over θ_h from 0 to π by use of Simpson's rule with m=2 gave an accuracy of at least 3 parts in 10^{-5}. The resulting step size in θ_h was 1.18 degrees. The theta integration out to the reflector's edge for each value of ϕ was then carried out by a test of each point to see if it lay inside or outside the reflector limits. If it lay outside, the value of the integrand was set equal to zero and the integration on theta was terminated.

Such a procedure results in some error, because the exact edge of the reflector may be missed by up to the width of one increment. For the increment size used, the maximum error is estimated at somewhat less than about ±0.05 dB. However, because both positive and negative errors can be expected to occur for different values of ϕ_h, the actual error will be less than that value. Since actual horn patterns will vary from the theoretical ones used, it is not considered necessary to attempt to improve the accuracy of the calculations at this time.

The results of the θ_h integration were then integrated over ϕ_h. Because the horn power patterns are nearly independent of ϕ_h, fewer subdivisions were required in ϕ_h. The step size used was 4.74 degrees, which introduced negligible error into the ϕ integration.

3.3.7 Tolerances in Reflector Antennas

The effects of surface irregularities in reflectors are increased sidelobe levels and reduced beam efficiencies. Ruze (1966) discusses these effects for large pencil beam antennas; his results are pertinent to

the radiometer study. In terms of an rms effective surface error, ϵ, the mean gain pattern is given by the following equation;

$$G(\theta,\phi) = G_0(\theta,\phi)e^{-\delta^2} + \left(\frac{2\pi C}{\lambda}\right)^2 e^{-\delta^2} \sum_{1}^{\infty} \frac{\delta^{2n}}{n \cdot n!} e^{-(\pi cu/\lambda)^2/n} \qquad (3\text{-}1)$$

where

$u = \sin\theta$

c = correlation distance on surface ($c \ll$ diameter)

$\delta = 4\pi\epsilon/\lambda$

The first term on the right-hand side is the unperturbed pattern multiplied by a factor $e^{-\delta^2}$ that reduces the gain. The second term is a rather broad pattern that affects the peak gain somewhat but affects mainly the sidelobe level. For a given design peak sidelobe level, this term must be sufficiently below the design level that the latter is not changed significantly.

As an example of the magnitude of this term relative to the beam peak, the expression was evaluated for a 120-λ aperture for two values of ϵ/λ, 1/16 and 1/32, which at 36-GHz represent rms errors of approximately 20 and 10 mils, respectively, over a 1-meter aperture. A correlation distance of 50ϵ was assumed in the calculations. For the case of ϵ/λ = 1/32, the term near the beam axis is down about -38 dB from the peak or about 13 dB below the desired -25 dB sidelobe level. This value can cause the sidelobe level to increase approximately 0.2 dB on the average but could result in individual sidelobes significantly higher. An rms error of 1/16 provides much more significant degradation because the error term is now only about -25 dB below the beam peak, i.e., equal to the design sidelobe level.

The beam efficiency may be obtained by integration of Equation (3-1) over the main beam and comparison of the result with an integration over all angles. The resulting expression is as follows.

$$E(\theta_1) = e^{-\delta^2}\left[E_0(\theta_1) + \sum_{n=1}^{\infty} \frac{\delta^{2n}}{n!}\left(1 - e^{-\frac{(\pi c \sin\theta_1/\lambda)^2}{n}}\right)\right]$$

where θ_1 represents the beam edge and the term $E_0(\theta_1)$ is the beam efficiency without any errors. The summation represents power in the main beam due to scattering by surface irregularities and is generally much smaller than E_0. It is seen that the beam efficiency is essentially reduced by the factor $e^{-\delta^2}$; therefore, for a high beam efficiency, the rms phase error δ must be kept small.

Two examples were worked out. In the first, θ_1, the angle from the beam axis to the first null, is 0.383 degree. This value corresponds to a 0.29 degree half-power beamwidth (a 2-meter aperture at 36 GHz and a 25-dB design sidelobe level). The results are shown in Table 3-4. A value of $c = 50\epsilon$ was used in these calculations, where c is the correlation distance.

TABLE 3-4. EFFECT OF TOLERANCES ON BEAM EFFICIENCIES FOR FIRST EXAMPLE

ϵ/λ	$E(0.383^\circ)$
0.020	$0.939\ E_o(0.383^\circ)$
0.03125	$0.857\ E_o(0.383^\circ)$
0.0625	$0.540\ (E_o(0.383^\circ) + 0.003)$

At 36 GHz, $\lambda = 0.328$ inch, and an rms variation of 0.02λ corresponds to about 6 mils. Thus, for the beam efficiency not to degrade significantly from its zero-error value, fairly tight tolerances are required at the high frequency end of the band.

In the second example, θ is 5.636 degrees. This angle corresponds to a half-power beamwidth of 4.27 degrees (1-meter aperture at 5 GHz and 25-dB design sidelobes). The results are shown in Table 3-5.

TABLE 3-5. EFFECT OF TOLERANCES ON BEAM EFFICIENCIES FOR SECOND EXAMPLE

ϵ/λ	$E(5.636^{\circ})$
0.020	$0.939\,(E_o(5.656^{\circ}) + 0.00585)$
0.03125	$0.857\,(E_o(5.636^{\circ}) + 0.03343)$

At 5 Ghz, $\lambda = 2.362$ inches, so that an rms variation of 0.02 corresponds to about 50 mils, a much more easily realized value than 6 mils for the 2-meter aperture at 36 GHz.

For deep reflectors, the surface error is not exactly equal to the effective error, ϵ, since the rays do not all strike the surface normally but at varying angles across the reflector. Ruze (1966) relates ϵ to the actual surface errors. In actuality, ϵ is somewhat less than the rms surface error. For example, if Δn represents the surface error measured normal to a paraboloidal surface at a radius ρ from the paraboloidal axis, then the effective error $\epsilon(\rho)$ at that radius is

$$\epsilon(\rho) = \frac{\Delta n}{\sqrt{1 + (\rho/2f)^2}}$$

If this effective error is averaged over the aperture, the resulting average value of ϵ is given by

$$\epsilon_{av} = \Delta n \, 32\left(\frac{f}{D}\right)^2 \left[\sqrt{1 + \left(\frac{D}{4f}\right)^2} - 1\right]$$

For an f/D of 1/4, this expression gives $\epsilon_{av} = 0.818 \, \Delta n$ or $\Delta n = 1.22 \, \epsilon_{av}$.

For an rms error of 0.03125λ, the actual error will be about 0.3 mm for a two-meter aperture for a reduction of beam efficiency to a value of 85 percent. Thus even for a 100-percent efficient error-free aperture, the 85-percent efficiency means that only 0.7 dB can be lost due to energy in the sidelobe levels, including all factors. For the aperture mentioned, the 0.3 mm corresponds to a phase error of about 22 degrees.

The required tolerance limits will affect the construction methods utilized in the formation of the reflectors and will thereby influence weight and cost. A more detailed analysis of tolerance requirements needs to be made.

The results of these tolerance calculations for a particular set of parameters are presented in Figure 3-20. The following assumptions have been made.

1. Rms tolerances are uniform across the aperture.
2. Beam efficiency is 95 percent for a perfect reflector.

From Figure 3-20, a 1-meter dish would require a 0.2-mm surface tolerance when operated at 36 GHz.

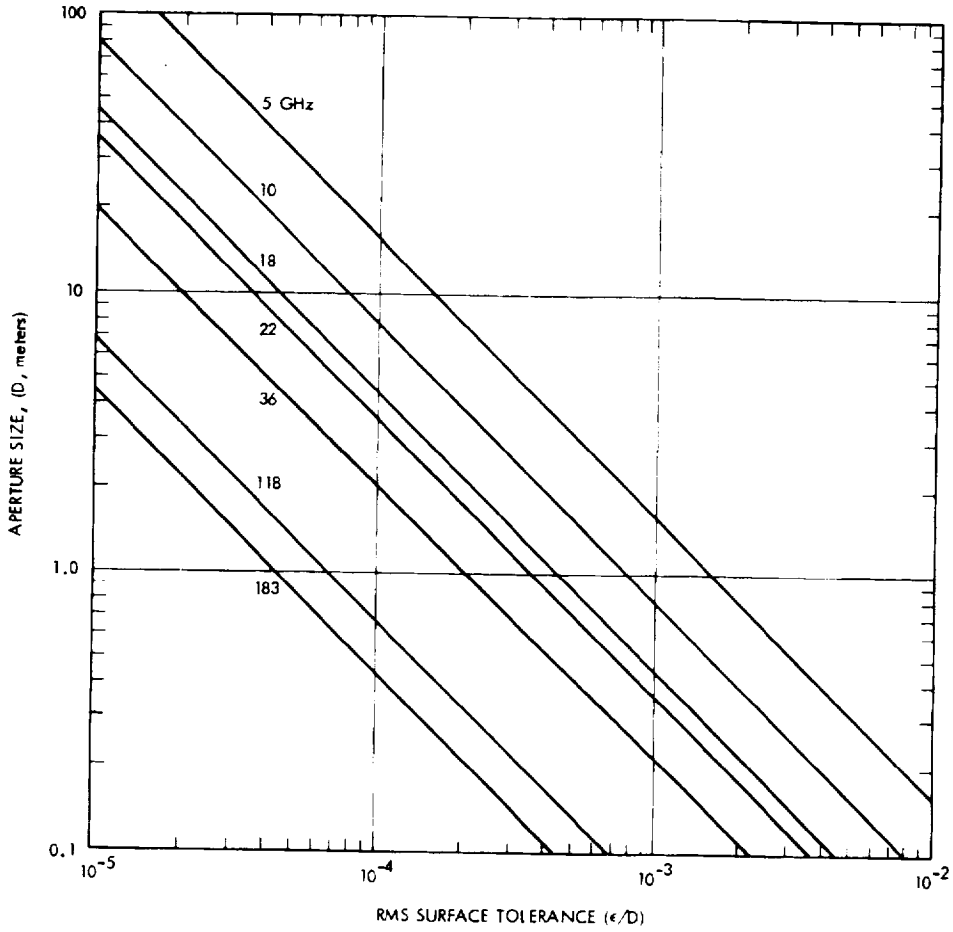

Figure 3-20. Maximum aperture diameter as a function of rms surface roughness for an overall beam efficiency of 85 percent (95-percent efficiency assumed for perfectly smooth reflector).

3.4 MULTIPLE REFLECTOR SYSTEM

A multiple reflector system consisting of two offset paraboloids mounted one above the other (Figure 3-21) is a possible approach for obtaining coaxial beams at all five frequency bands. In this scheme, two corrugated conical horns would be used to feed both reflectors. The horn feeding the lower reflector would cover the 18-, 21-, and 36-GHz bands, and the horn feeding the upper reflector would cover the 6.6- and 10.7 GHz bands. The whole assembly — reflectors, feed lines, and feeds — would scan as a unit over the desired azimuth angle.

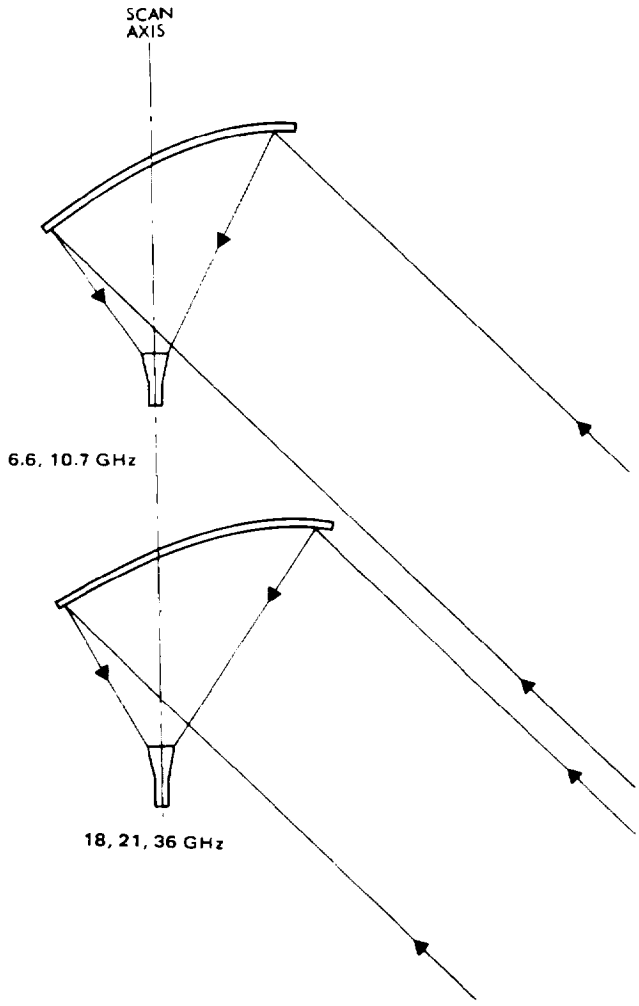

Figure 3-21. Dual offset paraboloid system.

This concept has the advantage of being quite simple from an electrical design point of view. However, it poses a considerable mechanical problem in that both reflectors must maintain nearly perfect alignment while being scanned at a rate fast enough to cover the swath at 36 GHz. It has the further disadvantage of being awkward, from both a packaging and a driving standpoint.

3.5 SINGLE REFLECTOR WITH DICHROIC MIRROR

A modification of the two-reflector system that would allow the two horns to feed a single reflector to provide five coaxial beams is a viable candidate for the radiometer antenna. In this approach, a frequency-selective flat surface, perforated with crossed slots, is placed in the path of the rays converging on the normal focus of the paraboloid, so that some of the incoming waves are thereby reflected to a virtual focus at a point removed from the normal focus (point F in Figure 3-22). This approach is analogous to one of the techniques disclosed in a Hughes patent application covering methods by which broadband performance can be obtained from waveguide lenses (Kummer and Seaton, 1973). The range of frequencies is most conveniently split at a point approximately midway between the 10- and 18-GHz bands.

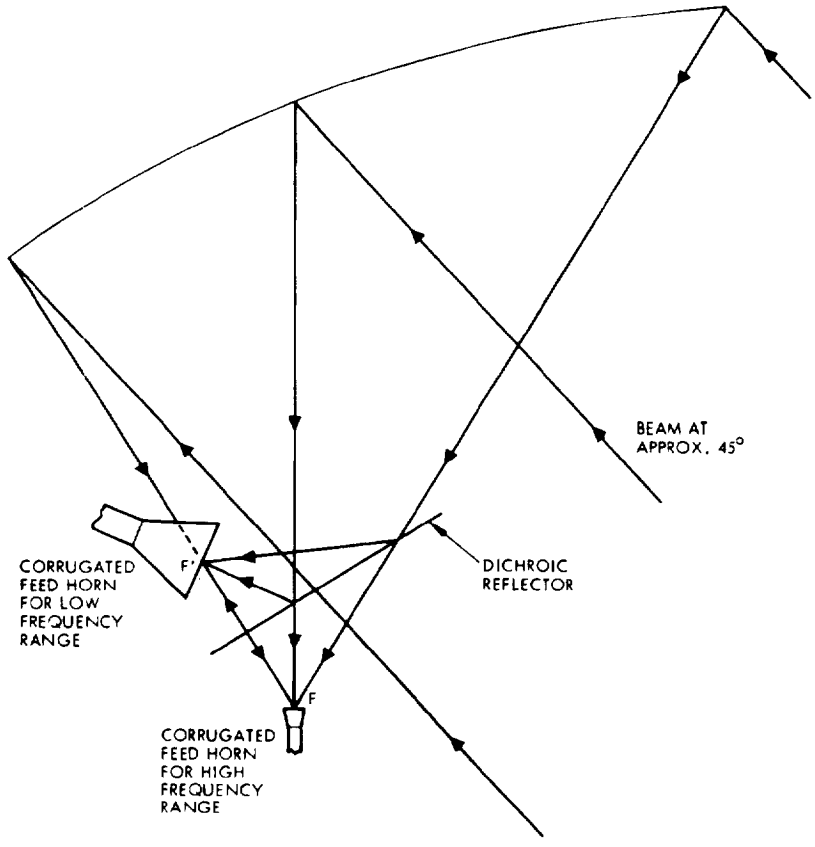

Figure 3-22. Multi-band dichroic reflector system.

As presently conceived, the 6.6- and 10.7-GHz bands would be reflected to F', while the 18-, 21-, and 36-GHz bands would pass through the dichroic surface to the normal focus at F. Thus, the dichroic surface would act as a spatial high-pass filter.

Studies conducted at Hughes indicate that such a filter can be constructed in either of two ways. The first way, which involves the use of two perforated plates, is an extension of earlier work at Hughes on perforated plates (Chen, 1971; Chen, 1973). The second way involves the use of a number of layers of reactive screens; by the proper choice of shunt inductance (or capacitance) in the screens and the spacing between them, a high-pass (or low-pass) filter can be obtained with a cutoff frequency between the 10- and 18-GHz bands.

As in the two-reflector system, the feeds for this all-band system would be two corrugated conical horns.

The complete antenna assembly, consisting of main reflector, dichroic surface, and feed horns, would have to be scanned as a unit. The scan axis would be oriented at 45 degrees to the main beam as shown in Figure 3-22 and would be positioned so that the total mass would be approximately balanced. The different polarizations received by each horn would be separated by an orthomode junction behind the horn, and the frequencies would be separated by a multiplexer. It can be shown that, when the feed horns scan with the reflectors about an axis parallel to the local vertical, as proposed here, polarization purity will be maintained at both the "vertical" and "horizontal" terminals of the feed horns at all frequencies.

3.5.1 Dichroic Surface Design

The dichroic surface must be designed to pass one set of frequencies and to reflect the other set. (Arnaud and Pelow, 1975; Saleh and Semplak, 1976). The most logical breakpoint between the pass band and the stop band is between the 10.7- and 18.0-GHz frequencies. The surface can be designed to pass the high frequencies (18.0, 21.0, and 36.0 GHz) and to reflect the low frequencies (6.6 and 10.7 GHz), or vice versa. The dichroic sheet could also be designed with either a flat or a curved surface. If a curved surface were

used, it would have to be hyperboloidal in shape to focus the reflected waves properly at a new focus (Agrawal and Imbriale, 1976). That portion of the antenna system would then become an offset Cassegrainian antenna.

There are three possible approaches to the electrical design of the dichroic surface (Schennum, 1973), all variations of filter theory. The first and simplest is the use of two identical sheets of conducting material that are rather widely spaced and perforated with slots that are resonant in the pass band; the second is an extension of Chebyshev and Butterworth filter theory to spatial configurations; and the third is an application of the theory of periodically loaded lines to arrays of gratings or screens in free space. The first approach, the two-layer bandpass design, is considered as a baseline configuration and is discussed in detail below.

3.5.2 Baseline Electrical Design*

The basic building block of the bandpass filter is a flat sheet of metal pierced by a set of identical holes (Pelton and Munk, 1974). The holes may be in the form of electrically small round holes or slots resonant in the upper half of the 6.6- to 36-GHz frequency band. The resonant frequency occurs when the wavelength is approximately equal to the circumference. At the resonance of the slots, the incident energy is transmitted without loss. The transmission characteristics for one design are shown in Figure 3-23. The design is for a bandpass filter with the passband being at the high end of the band. Below resonance, the slots become reactive, and the complete sheet becomes reflective. The reflection and transmission bands can be interchanged by use of a shorted dipole imprinted on an electrically transparent sheet as the dual to the slot. There is limited control over the slope between reflection and transmission bands so that transmission at frequencies close to the slope is lossy.

The data shown in Figure 3-23 are for transmission normal to the surface. It is evident that the rays enter from a normal direction up to an angle of 63 degrees for the design considered. The changes in both amplitude and phase as a function of angle for each transmission frequency are important because these changes will cause a degradation in the beam efficiency

*The design is due to N.C. Olsen

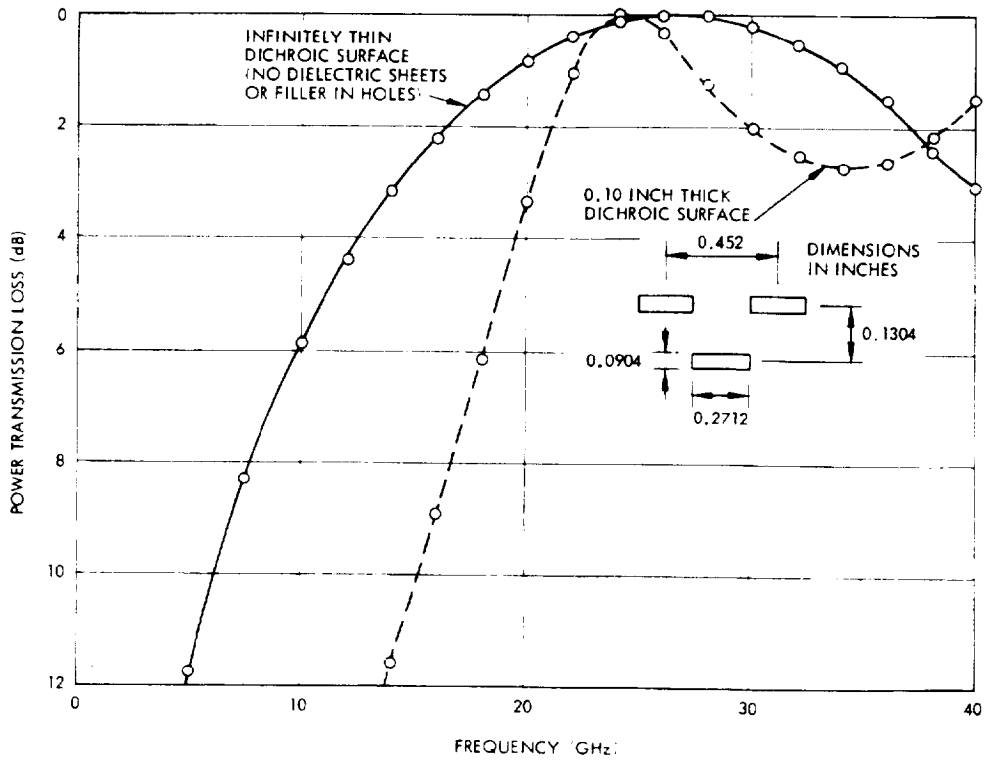

Figure 3-23. Transmission characteristics at normal incidence of one-plate bandpass filter.

due to the phase and amplitude errors across the aperture. Another effect occurs as the angle of incidence departs from the normal. The spacing of the slots becomes larger when measured normal to the direction of propagation. Thus, electrical spacing for all angles of incidence must be such that grating lobes are not formed. The use of non-uniform spacing that is adjusted to angle of incidence complicates construction but obviates most of these problems.

A second sheet of identical design placed a suitable distance behind the first one will increase the steepness of the slope between transmission and reception bands. Because the resonant frequency is the same for two sheets, all the energy will be transmitted irrespective of the spacing between the two sheets at the resonant frequency. For another frequency, say 36 GHz, the spacing can be adjusted for complete transmission also. The reflections from the second sheet cancel those of the first one to form a resonant cavity as sketched in Figure 3-24. The incident wave E_{INC} is

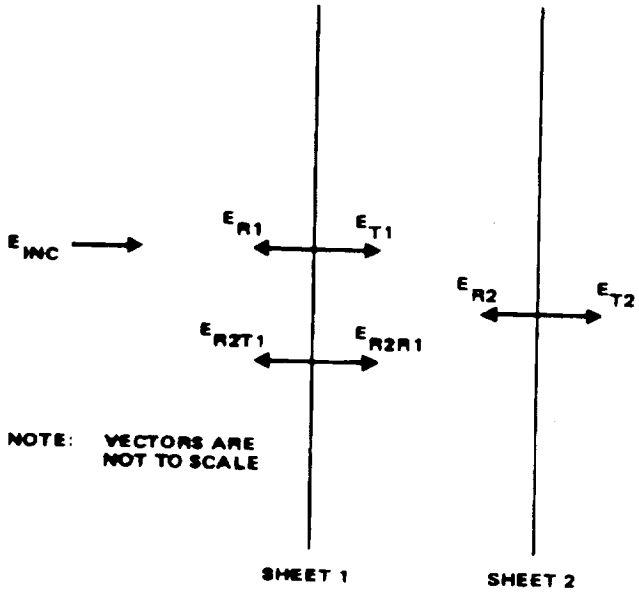

Figure 3-24. Energy around dichroic surface.

partially transmitted (E_{T1}) and partially reflected (E_{R1}) by sheet 1. E_{T1} is partially transmitted by sheet 2 (E_{T2}) and partially reflected (E_{R2}). The latter is partially transmitted by sheet 1 toward the source (E_{R2T1}) and so forth. It is possible for the spacing to be adjusted so that the summation of all the waves transmitted toward the source is equal to zero. The summation of these partially transmitted amplitudes ($E_{R2T1}\ldots$) is equal but 180 degrees out of phase with E_{R1}. Because the system is lossless, all the energy must be transmitted to the right. The losses for a one-sheet and a corresponding two-sheet design for two variations of the basic design are shown in Table 3-6. It will be noted that the reflection coefficient is less at 10 GHz because of the proper phasing of the reflected energy.

For an effective design of two flat conducting plates perforated with holes to be achieved, their combined performance characteristics must be predicted before actual fabrication. Although an exact solution of the problem is not available, the problem can be reduced to the mathematical model of a doubly periodic grid of identical holes and infinite extent, and a very good approximation can be achieved. The model is designed to include slots with

TABLE 3-6. TRANSMISSION AND REFLECTION LOSSES OF VARIATIONS OF BASIC DESIGN

a. Design A: Spacing = 0.215 inch

Frequency (GHz)	Loss for Normal Incidence (dB)			
	Single Sheet		Two Sheets	
	Reflection	Transmission	Reflection	Transmission
5	0.3	—	0.009	—
10	1.3	—	0.13	—
18	—	1.43	—	0.01
22	—	0.40	—	0.47
36	—	1.56	—	0.0

b. Design B: Spacing = 0.180 inch

Frequency (GHz)	Loss for Normal Incidence (dB)			
	Single Sheet		Two Sheets	
	Reflection	Transmission	Reflection	Transmission
5	0.54	—	0.03	—
10	2.40	—	0.36	—
18	—	0.14	—	0.004
22	—	0.12	—	0.21
36	—	10.43	—	0.06

arbitrarily linear polarized amplitudes at arbitrary angles of incidence. The higher mode coupling between the two sheets is neglected. Effects are significant only when the spacing between the sheets is small in terms of the wavelength of the impinging signal. Effects become noticeable for spacings less than

three-eighths of a wavelength. For design variation A shown in Table 3-6, a 0.215-inch spacing is 0.66λ at 36 GHz but only 0.1λ at 5 GHz. The computer programs are based on this model, and their accuracy has been verified by comparisons of the computed results with those available in the literature and by the use of the computed data in the successful design of a metallic X-band conical radome.

The types of slots that should be considered in the design of the sheets include crossed, folded, and reentrant slots (Luebbers and Munk, 1975; Munk and Luebbers, 1974). The computer program can be modified to include the type of slot selected for the final design.

The angle of incidence as a function of frequency is another important parameter to be evaluated. An example, the results for a third variation of the basic design, based on the use of two sheets separated by 0.2623 inch, are shown in Table 3-7. These values shown are losses versus scan angle

TABLE 3-7. TRANSMISSION AND REFLECTION LOSSES OF DESIGN C

Frequency (GHz)	Incidence Angle	Loss (dB)	
		Vertical Polarization	
		Reflect	Transmit
5	0	0.01	
	15	0.01	
	30	0.01	
	45	0.03	
10	0	0.11	
	15	0.12	
	30	0.15	
	45	0.25	
18	0		1.14
	15		0.75
	30		0.07
	45		0.23
22	0		1.33
	15		1.18
	30		0.70
	45		0.13

from 0 to 45 degrees. The lattice is triangular, the slot size is 0.2712 by 0.0904 inch, and the slot spacing is 0.1304 inch vertical and 0.452 inch horizontal. The somewhat large spacing in the horizontal plane led to grating lobes at the highest frequency for angles different than normal incidence. For the 36-GHz band to be included, more closely spaced slots must be used.

The predicted results for a smaller lattice are shown in Table 3-8. The design was intended for incidence angles up to 45 degrees, but results

TABLE 3-8. TRANSMISSION AND REFLECTION LOSSES OF DESIGN D*

Frequency (GHz)	Incidence Angle	Loss (dB) Vertical Polarization		Loss (dB) Horizontal Polarization	
		Reflect	Transmit	Reflect	Transmit
5	0	0.04		0.02	
	15	0.05		0.02	
	30	0.05		0.01	
	45	0.09		0.01	
	60	0.24		0.01	
10.7	0	0.43		0.24	
	15	0.44		0.20	
	30	0.50		0.13	
	45	0.71		0.07	
	60	1.39		0.02	
18	0		0.00		0.05
	15		0.04		0.29
	30		0.46		2.02
	45		1.10		6.41
	60		1.25		12.21
21	0		0.92		0.97
	15		0.60		0.59
	30		0.08		0.00
	45		0.11		1.74
	60		0.49		7.47
36	0		0.28		0.00
	15		0.31		0.01
	30		0.30		0.49
	45		0.13		5.80
	60		0.01		21.8

*The original frequency of 5 GHz rather than the modified value of 6.6 GHz was used in these calculations.

are shown for angles to 60 degrees. Some improvement in design for the larger incidence angles is possible, but it must be anticipated that such improvement will be accompanied by a degradation in performance at other incidence angles. The slot dimensions are such (0.192 by 0.166 inch in a triangular lattice of 0.360 inch by 0.104 inch) that crossed slots are not necessary; the design is adequate for both senses of linear polarization, although the results for horizontal polarization are less than desired for the transmission band at the larger incidence angles. The data shown are for the vertical plane in which the incidence angles are as large as 63.4 degrees. For the horizontal plane, the incidence angles are less than approximately 31.7 degrees. Although no data are shown for the horizontal plane, the results would be approximately the same as those for the vertical plane at comparable incidence angles.

Several design conclusions can be drawn from these results:

1. The single sheet should be designed to have the optimal performance at the angle of incidence that will have the maximum incident energy.
2. The separation of the pair of sheets should be optimized for the same angle.
3. This optimization may not be adequate to cover a 0 to 63-degree scan for all five of the frequencies.

The sheet can be designed into several zones. The shapes of the zones will be determined by the angle of incidence between the rays from the horn and the surface.

3.5.3 Tolerances

The effects of tolerances on the dichroic surface can be examined separately for the reflection and transmission bands. Because the mirror is a good reflector at the low frequencies, the primary design goal is as flat a sheet as is necessary. Thus, a tolerance value close to that specified for the reflector should be adequate.

In the transmission band, the absolute flatness is not so important as the spacing and uniformity of the dielectric constant. A motion of the entire sheet will cause little or no distortion of the wavefront. Figure 3-25 shows

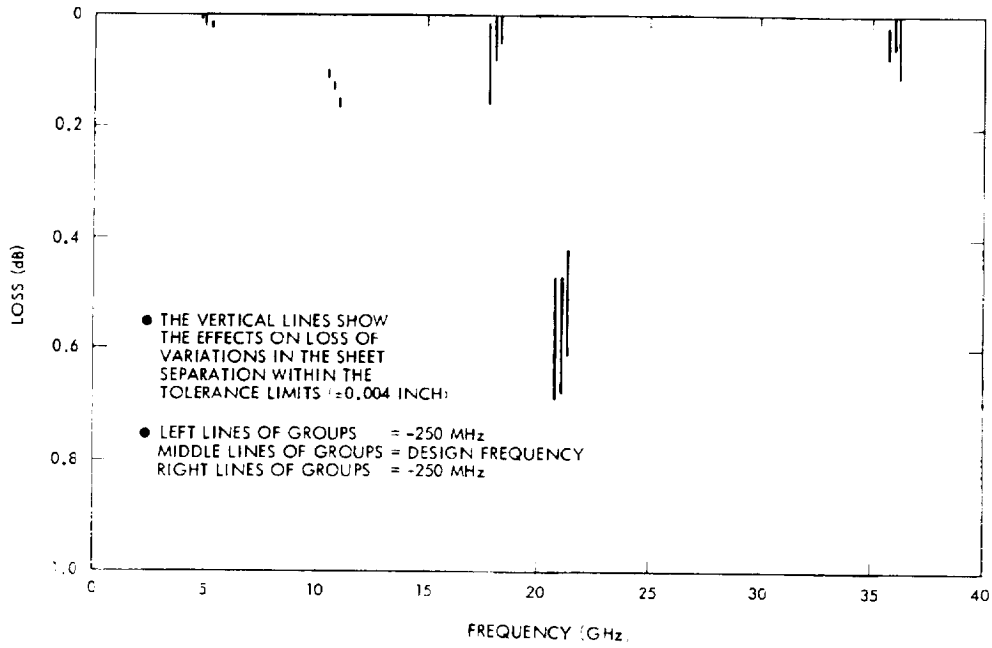

Figure 3-25. Computed losses at normal incidence for two-plate bandpass filter with 0.215±0.004-inch separation between plates.

the computed losses at normal incidence of a two-plate bandpass filter for a tolerance of ±0.004 inch. Data at ±250 MHz are also shown. This particular design is not very sensitive to tolerances; however, it also does not give the lowest possible transmission loss in the 21-GHz band (see Table 3-6). It is expected that an alignment of better than 0.001 inch would be maintained in the mechanical design chosen.

3.6 WEIGHTS OF REFLECTORS

The weights of several reflectors that have been constructed for space applications are summarized in Table 3-9. For a given type of construction, the weights may be scaled approximately as the square of the diameter over about a 2-to-1 variation in diameters (TDRSS Users Guide, 1976).

TABLE 3-9. WEIGHTS OF SPACECRAFT REFLECTORS

Vehicle	Size	Construction	Reflector Weight (pounds)	Surface Deviation, ϵ/R*
Hughes Aircraft Company				
INTELSAT IV	Parabolic, 50-inch diameter	Fiberglass honeycomb solid	3.8	0.001
	Offset paraboloid, 60-inch projected diameter	Graphite-fiber-reinforced plastic (GFRP) Mesh (gold on nickel chromium)	8.5	0.0004
INTELSAT IVA	Parabolic section, 53-inch square, with offset feed	Fiberglass honeycomb and mesh (gold-NiCr)	3.0	0.0004
COMSTAR	Parabolic section, 50 x 70 inches, with offset feed	GFRP honeycomb and mesh (gold-NiCr)	8.0	0.0004
Lockheed Missile and Space Company	Paraboloidal, 84-inch diameter	Unfurlable, 36 titanium ribs and mesh gores	13.7	0.0006 (est.)

*RMS deviation from true paraboloidal surface = ϵ
R = Radius of reflector

PRECEDING PAGE BLANK NOT FILMED

4.0 LENSES

In addition to reflectors and arrays, lens antennas were considered for systems to be scanned by motion of the feed relative to the aperture. Lenses have an additional degree of freedom over reflectors in that both surfaces of the lens are available for pattern control. As a result, it is possible to obtain wide-angle beam scan by proper positioning of feeds in the focal region, without significant pattern deterioration. Because lenses do not suffer from the problem of aperture blockage, they can be used in symmetrically-fed arrangements. With such arrangements, patterns are more easily maintained as the beam is scanned. Lenses are also amenable to multiple-beam operation. The beam scans required for the radiometer application are primarily in one dimension as discussed in Appendix A. Therefore, the lenses need not be rotationally symmetric about their boresight direction. Several types of lenses are discussed in this section.

4.1 WIDE-ANGLE SCANNED CONSTRAINED LENS

Constrained lenses, which do not obey Snell's law, may be designed to scan over fairly broad angular regions. These lenses use transmission lines or parallel metal plates that constrain the waves to follow prescribed paths. If the metal plates are arranged in an egg-crate fashion so that they form square dominant mode waveguides, then waves of any polarization will be accepted and constrained to follow these waveguides. By adjustment of the input and output surfaces of these lenses, desirable radiation characteristics may be obtained over relatively wide scan angles. Such lenses are discussed by Ruze (1950), and the example considered here is illustrated in Figure 4-1.

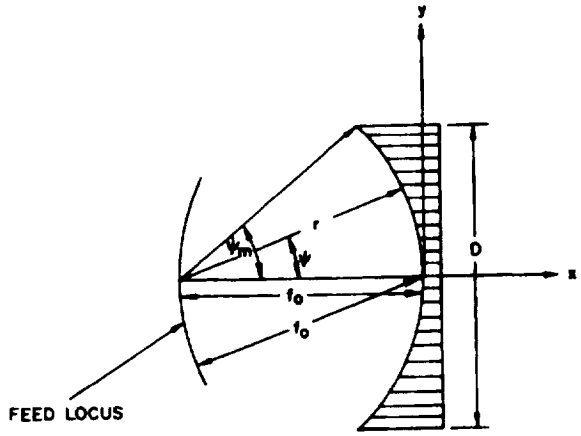

Figure 4-1. Constrained lens.

The lens considered is two-dimensional; however, the general technique applies approximately to three-dimensional lenses, although the actual numbers obtained for that case would be different. The lens aperture, D, is 72 wavelengths and $f_0/D = 1.5$. It is so designed that, with the feed located on a feed locus of radius f_0, there are no phase errors in the aperture for feeds positioned at angles of ±45 degrees with the axis. With the feed on axis at $-f_0$, there is no quadratic phase error over the aperture. Under these conditions the antenna is capable of scanning a 1 degree (half-power beamwidth) beam over a ±50-degree range. Ruze also gives a relation between the f/D ratios, the half-power beamwidth, and θ_s, the total scan angle, for this type of lens as

$$\theta_s = 93^\circ \left[BW^\circ_{1/2} \left(\frac{f_0}{D} \right)^2 \right]^{1/3}$$

For the particular antenna considered, it can be found that $BW_{1/2} = 65^\circ \lambda/D$ so that

$$\theta_s = 374^\circ \left[\lambda/D \left(\frac{f_0}{D} \right)^2 \right]^{1/3}$$

For $D = 75\lambda$ and $f_0/D = 1.50$, this relation gives $\theta_s = 113$ degrees, in substantial agreement with the experimental results.

ORIGINAL PAGE IS
OF POOR QUALITY

4.2 ZONED WAVEGUIDE LENSES

Hughes has undertaken a program to theoretically and experimentally investigate the zoned waveguide lens. Electrical and mechanical designs have been studied and a 5-foot diameter X-band lens fabricated on the basis of these studies. The waveguide lens was designed for a constant index of refraction and a single focus on axis following the equations of Dion and Ricardi (1971). It was fabricated from a large number of square waveguide cells, bonded together, and exhibited excellent electrical characteristics at the design frequency over a ±10-degree scan angle. Typical patterns are shown in Figure 4-2.

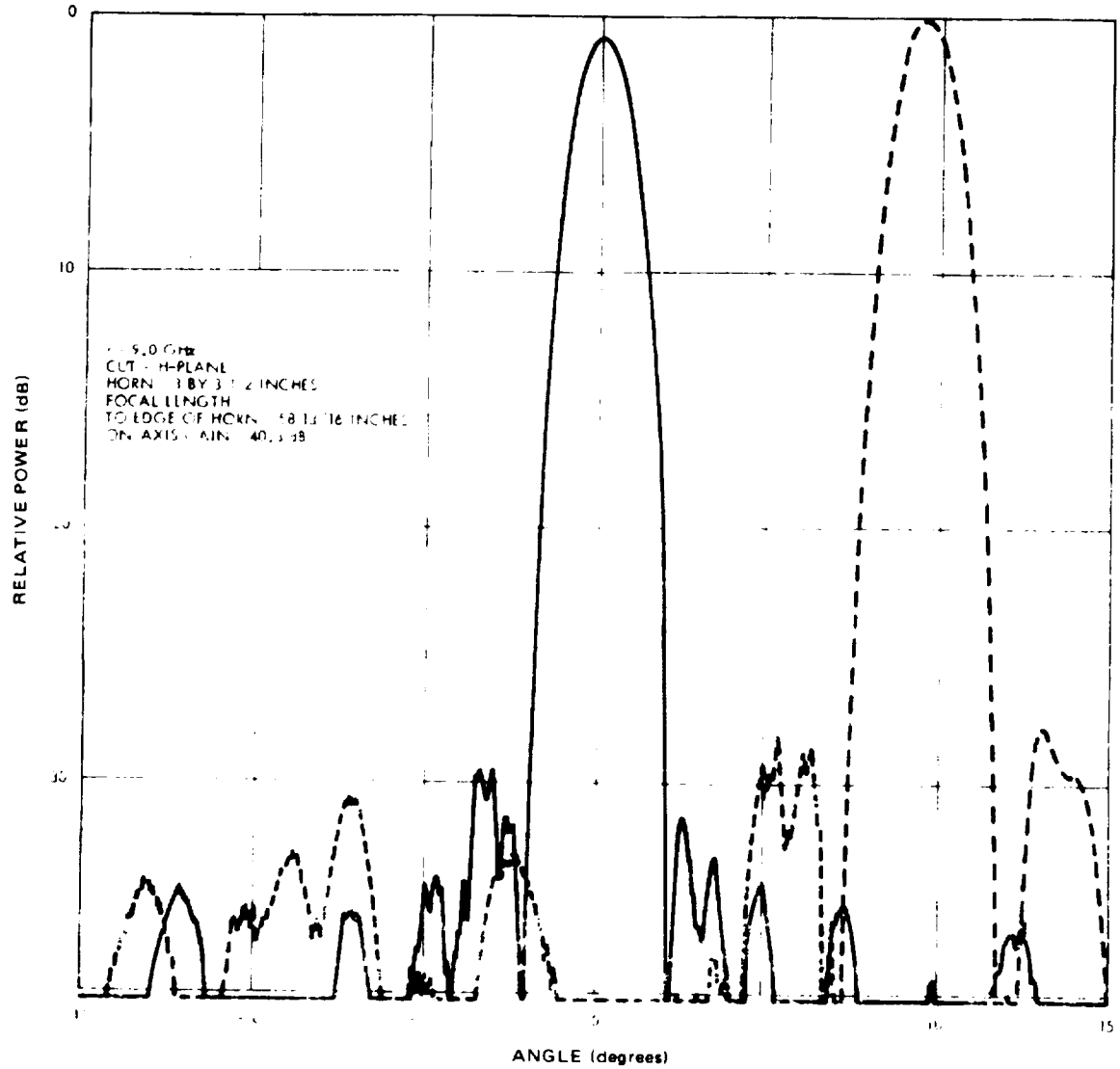

Figure 4-2. Measured patterns of Hughes 5-foot-diameter waveguide lens antenna for two beam scan angles.

The experimental investigation of waveguide lenses was continued theoretically with lenses ranging in size from 3 to 10 feet in diameter (Samso 1973). The computer program developed by Dion (1969) was extended for use in these calculations. The feed position was optimized for lowest sidelobe level at the design frequency for every beam position within the field of view. Patterns were computed for several design sidelobe levels, frequencies, and scan angles for 3-, 5-, 7-1/2-, and 10-foot lenses. The beam positions are described in Figure 4-3.

Because there are so many variables in the design of waveguide lenses, a summary of the characteristics of lenses of various diameters has been prepared in Table 4-1. It can be seen that the waveguide lens has application over a limited bandwidth and that sidelobes deteriorate increasingly as a function of size of lens, scan angle, and bandwidth. The weights of waveguide lenses of various diameters and wall thicknesses were also calculated and are provided in Table 4-2. The lens model used in these calculations is an assembly of square waveguide elements bonded together with epoxy adhesive: structural ribs divide the lens into modules small enough so that the waveguide elements can withstand the applied loads.

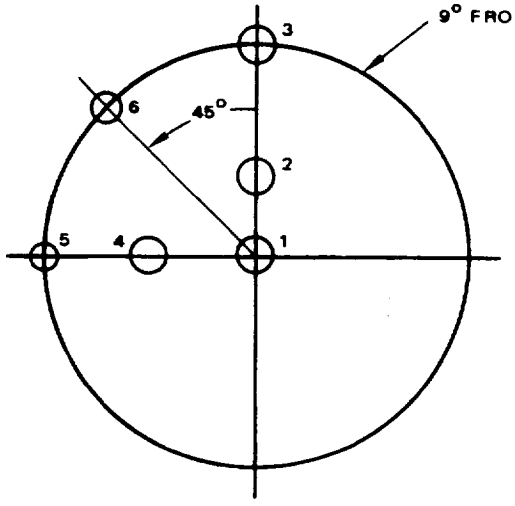

BEAM POSITION	ANGLE (degrees)	
	AZIMUTH	ELEVATION
1	0	0
2	0	4-1/2
3	0	9
4	4-1/2	0
5	9	0
6	6.4	6.4

Figure 4-3. Beam positions.

TABLE 4-1. SUMMARY OF CHARACTERISTICS OF WAVEGUIDE LENSES
(CENTER FREQUENCY 7.9 GHz)

Lens Diameter (Feet)	Feed Horn* Diameter (Inches)	SLL Design (dB)	Highest Sidelobe Levels off Axis, off Frequency			Minimum Directivity Over Frequency Band Shown (Including Spillover Losses)
			Frequency (MHz)	SLL (dB)	Bandwidth (MHz)	
3	2.6	25	-250 +250	18.2 18.2	500	32-1/2
	3.7	35	-250 +250	18.6 21.2	500	
5	2.6	25	-75 +75	16.5 19.6	150	36-1/2
	3.7	35	-75 +75	20.9 25.5	150	
7-1/2	2.6	25	-75 +75	17.0 17.7	150	39-1/2
	3.7	35	-75 +75	17.4 25.0	150	
10	2.6	25	-75 +75	11.5 15.7	150	42
	3.7	35	-75 +75	13.5 21.0	150	

*TE_{11} mode conical horns

TABLE 4-2. WEIGHTS OF WAVEGUIDE LENS ASSEMBLIES

Diameter (feet)	Weight at Various Wall Thicknesses (pounds)				
	At 0.002 in	At 0.004 in	At 0.006 in	At 0.008 in	At 0.010 in
1.5	1.3	2.1	3.0	3.9	4.8
2	2.5	3.8	5.4	7.0	8.6
3	5.8	9.3	12.6	16.2	20.0
4	11.1	17.5	24.2	30.4	36.2
5	18.8	29.5	39.8	50.7	60.7
6	29.2	45.0	60.5	76.3	92.4
7	42.9	65.4	87.6	108.0	131.0
8	60.4	90.7	119.9	149.7	176.7
9	81.9	122.0	160.4	198.9	235.4
10	108.0	159.4	205.8	255.4	305.1

4.3 BOOTLACE LENSES

Bootlace lenses are a class of lens antennas in which two arrays of radiators are connected by TEM cables as illustrated in Figure 4-4. Because the basic phasing network is inherently broadband, the bootlace lens antenna tends to have radiation patterns that vary only slightly over bandwidths as large as 20 percent. The bandwidth is limited by the bandwidth of the elements comprising the input and output surfaces. Furthermore the availability of two surfaces allows the designer the opportunity to optimize pattern performance over a field of view.

If beam steering is to be used the choice of the shapes of the two surfaces is determined by a well known theorem in optics, the Abbé Sine Condition (Born and Wolf, 1959). The Abbé Sine Condition refers to a general optical system with an axis of symmetry and a perfect focus. It provides a condition that results in no first-order phase errors even when the feed is located off-axis.

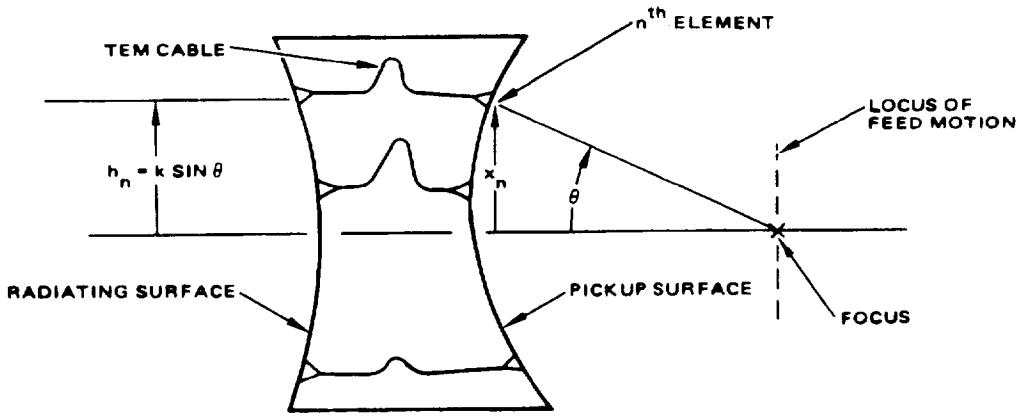

Figure 4-4. Bootlace lens illustrating geometry for Abbé Sine Condition.

The Abbé Sine Condition provides a tool for determining which bootlace lens configurations are suitable for further analyses. For example, as shown in Figure 4-4, assume that the n^{th} element in the pickup surface is located a distance x_n from the axis and is connected through a cable to an element in the radiating surface. If that element is also located a distance x_n off-axis, then the Sine Condition implies that the pickup surface of the lens must be spherical with its center on the focus. The analysis also indicates that the radiating surface should be flat. The cables connecting the two surfaces should be of equal length for perfect focusing.

Hughes has studied bootlace lens antennas operating at 7.9 GHz (SAMSO, 1973). Performance and weight calculations were made for lenses with diameters from 1.5 to 10 feet. The lens utilized in the calculations was considered to be made up of cylindrical elements closely stacked in a triangular arrangement that maximized the number of elements on each lens surface. Two semi-rigid coaxial cables joined the operating pairs of lens elements on opposite faces of the lens. The elements were enclosed in a structural cylinder and then foamed in place to fill all regions not occupied by elements and coaxial cable. Fiberglass plates of the various lens diameters were bonded in place on both lens surfaces. Three different radiating element sizes and two different types of coaxial lines were included in the weight calculations; the results of these calculations for each case are

summarized in Table 4-3. Dissipative loss estimates, made for three different coaxial lines and the three different element sizes, are shown in Figure 4-5.

Wesley and Tomita (1971) designed an experimental bootlace lens for operation from 8.6 to 10.2 GHz. The diameter of this lens was 3 feet, and the f/D was 0.35. The lens elements were linearly polarized slot radiators connected by stripline. An 8-element horn, designed for 40-dB sidelobes, was used to feed the lens. Measurements showed this experimental lens to

TABLE 4-3. WEIGHTS OF BOOTLACE LENSES WITH COAXIAL CABLE CONNECTORS

Diameter of Bootlace Lens (feet)	Weight with UT-141 Coaxial Cable and Elements of Various Size* (pounds)			Weight with UT-701 Coaxial Cable and Elements of Various Size* (pounds)		
	Case I	Case II	Case III	Case I	Case II	Case III
1.5	10	9	13	8	9	12
2	18	16	22	15	15	21
3	46	38	48	36	35	46
4	90	71	86	68	65	82
5	156	117	138	116	106	132
6	246	179	205	180	161	196
7	364	258	290	262	231	276
8	513	356	393	366	317	374
9	700	476	517	494	421	490
10	924	618	662	646	545	626

*Lens Element Sizes (inches)

Case	Diameter	Length
I	1.3	2.0
II	3.0	4.5
III	4.5	10.0

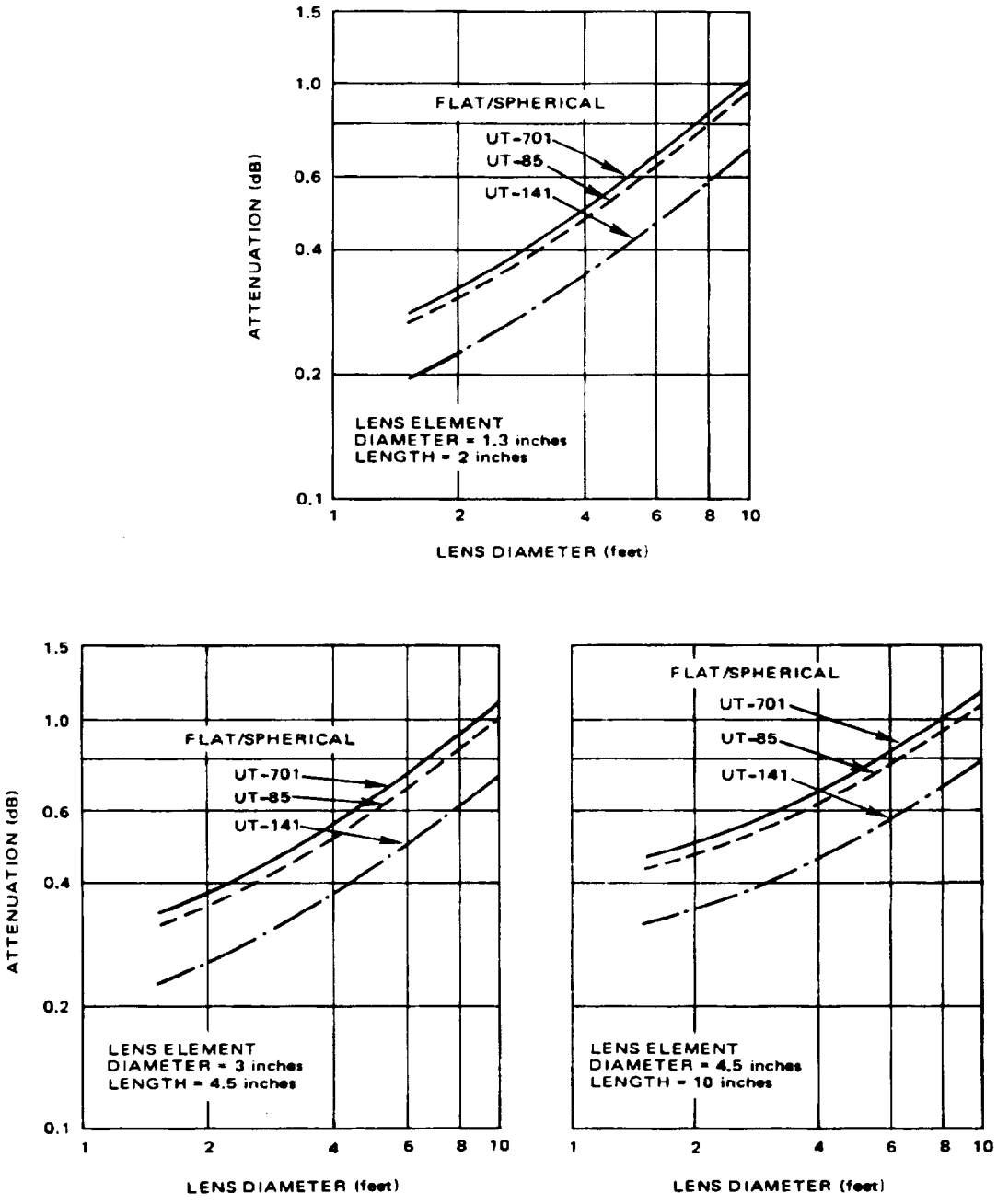

Figure 4-5. Resistive losses in bootlace lenses.

have a maximum gain of 34 dB with a 30-dB minimum, sidelobe levels in the principal planes of 27 dB minimum, an average beamwidth of 3.3 degrees, and a maximum VSWR of 2:1. The experimental lens structure weighed 29 pounds, but it was estimated that a lightweight version would weigh 18 pounds.

Because off-axis scanning was not required with this bootlace lens, it did not have to have small feeds or an f/D ratio close to unity. Furthermore, use of linear polarization results in a lens element and connecting structure that are less complex than ones that must carry both senses of circular polarization. A direct comparison with the lenses discussed above is thus difficult, but general agreement is apparent. The weight estimates for lens antennas given in this report (Tables 4-2 and 4-3) are reasonably conservative.

5.0 CONCLUSIONS

Various types of antennas were considered in this study for application to a multi-frequency microwave radiometer. Of those considered, array antennas offer the most flexibility in aperture control. In some configurations, they are compatible with electronic scanning techniques. Electronic scanning, however, adds significant weight and complexity to such antennas. Operation at multiple frequencies simultaneously from a single aperture also adds weight and complexity. Achievement of both multiple-frequency operation and dual polarization simultaneously from the same aperture involves extreme complexity and difficulty. Consequently, it appears that at least four apertures would be required to obtain the desired coverage with arrays.

Lens antennas offer the possibility of either mechanical scan or, with the addition of multiple feeds, electronic beam steering. These antennas are essentially dual-polarization devices. However, relatively lightweight lenses such as waveguide or bootlace lenses are not sufficiently broadband to cover the frequency range of interest. Consequently, at least four, and possibly five, lenses would be required to obtain the desired coverage.

Reflectors and feeds appear to offer the lightest weight configurations. Reflectors are inherently broadband with the bandwidth limited primarily by the feed. They also have dual-polarization capability and can be steered in several ways: by motion of the entire antenna, by motion of the feed relative to the reflector, or by switching among several feeds. Certain reflector surfaces, for example, the spherical surface or the parabolic torus surface, permit wide-angle beam steering by the latter two methods. The paraboloidal reflector and, in particular, the offset paraboloidal reflector are not suited to wide angle steering by mechanical or

electronic motion of the feed. The offset paraboloid does, however, offer the possibility of a simple lightweight configuration with no aperture blockage. It appears that two such reflectors with corrugated feed horns can cover the entire frequency range and provide both vertical and horizontal polarization. Use of a dichroic reflector may permit the incorporation of both feed horns into a single aperture. The general characteristics of the various types of antennas are summarized in Table 5-1.

Based on the trade-offs summarized in Table 5-1, it appears that offset reflectors using corrugated feeds and mechanically rotated as a single unit are the most promising candidates for the radiometer applications considered in this study.

The scanning of the paroboloids involves the use of gimbals and moment compensating schemes. The cost of these parts of the system can be expensive due to the severe thermal environment and required long life.

TABLE 5-1. GENERAL CHARACTERISTICS OF CANDIDATE ANTENNAS FOR MICROWAVE RADIOMETER

Scan ues	Multiple-Frequency Capability	Dual-Polarization Capability	Beam Efficiency	Sidelobe Levels	Cross-Polarization Isolation	Multiple-Beam Capability	Feeding Techniques	Reliability in Operation	Complexity	Weight	Relative Cost
by mov- r and feed	Yes: two to three bands from one corrugated conical horn	Yes: determined by feed design	Computed at 90% for geometry given in Section 3.3	Computed at -19 to -23 dB in elevation; -24 to -33 dB in azimuth	Estimated below -21 dB for geometry given in Section 3.3	No	Horns, waveguide transmission lines, and rotary joints	Determined mainly by bearings and rotary joint	Relatively simple	Lightest	Relatively inexpensive ($60 K$/channel)
by f feed; by eds	Yes: two to three bands by use of corrugated conical horns	Yes: determined by feed design	Needs special feed pattern in scan plane to achieve high efficiency	Needs special feed in scan plane to achieve low sidelobes	Unknown	Yes: by the use of several feed horns on the scan circle	Spherical-abberation-correcting horns or line source feeds; rotary joints or waveguide switches	Determined mainly by bearings and rotary joint or by waveguide switches	Relatively complex	Heavier than offset paraboloid because larger area required for scanning	
by f feed by eds	Yes: two to three bands by use of corrugated conical horns	Yes: determined by feed design	Needs special feed pattern in both planes to achieve high efficiency	Needs special feed pattern in both planes to achieve low sidelobes	Computed at -24.5 dB for highly tapered illumination function	Yes: by the use of several feed horns on the scan circle	Spherical-abberation-correcting horns or line source feeds; rotary joints or waveguide switches	Determined mainly by bearings and rotary joints or by waveguide switches	Relatively complex	About same as parabolic torus	
	No	Yes: by use of crossed-slot elements and polarization processing	Estimated at 90% by Aerojet General			Yes: with addition of multiple feeding and phasing networks	Waveguide feeds, orthomode transducers, branch-line phase shifters	Determined mainly by phase shifters and drivers	Complex	90 pounds for 39 x 39 x ¼-inch array (including phase shifters, drivers and receiver)	Expensive ($1.1 MS/channel)
	Yes: two frequencies	No: one polarization at each frequency				Yes: with addition of multiple feeding and phasing networks	Waveguide feed, orthomode transducers, branch-line phase shifters	Determined mainly by phase shifters and drivers	Complex		Expensive
	Yes: two frequencies	No: one polarization at each frequency		Controllable by control of aperture distribution		Yes: with addition of multiple feeding and phasing networks	Separate waveguide feed for each array, Branch-line phase shifters	Determined mainly by phase shifters and driver	Complex		Expensive

requency and one polarization.

(Continued next page)

TA

Antenna Type	Applicable Scan Techniques	Multiple-Frequency Capability	Dual-Polarization Capability	Beam Efficiency	Sidelobe Levels	Cross-Polarization Isolation	Multiple-Beam Capability	Feeding Techniques	Reliability in Operation	Complexity
REFLECTORS										
1. Offset Paraboloid	Mechanical: by moving reflector and feed together	Yes: two to three bands from one corrugated conical horn	Yes: determined by feed design	Computed at 90% for geometry given in Section 3.3	Computed at -19 to -23 dB in elevation; -24 to -33 dB in azimuth	Estimated below -20 dB for geometry given in Section 3.3	No	Horns, waveguide transmission lines, and rotary joints	Determined mainly by bearings and rotary joint	Relatively simple
2. Parabolic Torus	Mechanical: by movement of feed. Electrical: by switching feeds	Yes: two to three bands by use of corrugated conical horns	Yes: determined by feed design	Needs special feed pattern in scan plane to achieve high efficiency	Needs special feed in scan plane to achieve low sidelobes	Unknown	Yes: by the use of several feed horns on the scan circle	Spherical-abberation-correcting horns or line source feeds; rotary joints or waveguide switches	Determined mainly by bearings and rotary joint or by waveguide switches	Relatively complex
3. Spherical Reflector	Mechanical: by movement of feed Electrical: by switching feeds	Yes: two to three bands by use of corrugated conical horns	Yes: determined by feed design	Needs special feed pattern in both planes to achieve high efficiency	Needs special feed pattern in both planes to achieve low sidelobes	Computed at -24.5 dB for highly tapered illumination function	Yes: By the use of several feed horns on the scan circle	Spherical-abberation-correcting horns or line source feeds; rotary joints or waveguide switches	Determined mainly by bearings and rotary joints or by waveguide switches	Relatively complex
PHASE SCANNED ARRAYS										
1. Square Waveguide Branchline	Electronic	No	Yes: by use of crossed-slot elements and polarization processing	Estimated at 90% by Aerojet General			Yes: with addition of multiple feeding and phasing networks	Waveguide feeds, orthomode transducers, branch-line phase shifters	Determined mainly by phase shifters and drivers	Complex
2. Rectangular Waveguide Branchline - crossed slots	Electronic	Yes: two frequencies	No: one polarization at each frequency				Yes: with addition of multiple feeding and phasing networks	Waveguide feed, orthomode transducers, branch-line phase shifters	Determined mainly by phase shifters and drivers	Complex
3. Rectangular Waveguide Branchline - Interleaved arrays	Electronic	Yes: two frequencies	No: one polarization at each frequency		Controllable by control of aperture distribution		Yes: with addition of multiple feeding and phasing networks	Separate waveguide feed for each array, Branch-line phase shifters.	Determined mainly by phase shifters and driver	Complex

*A channel indicates operation at one frequency and one polarization.

1 FOLDOUT FRAME

2 FOLDOUT FRAME

(Table 5-1, concluded)

icable Scan chniques	Multiple-Frequency Capability	Dual-Polarization Capability	Beam Efficiency	Sidelobe Levels	Cross-Polarization Isolation	Multiple-Beam Capability	Feeding Techniques	Reliability in Operation	Complexity	Weight	Relative Cost
onic	Yes: up to three frequencies (possibly four if one array can be used for both 18 and 21 GHz)	No: one polarization at each frequency		Controllable by control of aperture distribution; element spacing may be a limiting factor		Yes: with addition of multiple feeding and phasing networks	Separate feed system for each array; corporate feeding	Determined by phase shifters and drivers	Complex		Expensive
nical	Yes	No		Controllable by control of aperture distribution		No	Waveguide feeds and rotary joints	Determined by bearing and rotary joints	Moderately complex	Array structure relatively light	Moderate
nical	No	Yes: by use of crossed slots and polarization processing		Controllable by control of aperture distribution		No	Waveguide corporate feeds, magic-tees connected to branch lines	Determined by bearing and rotary joints	Relatively simple	Array structure relatively light	Moderate
nical: by ent of entire a or by move- f feed; ical: by ing feeds	No	Yes: determined by feed design	Should be at least comparable to that of reflectors	Controlled by aperture illumination taper		Yes: by use of multiple feeds	Horns, waveguide transmission lines and rotary joints, switches, or variable power dividers	Determined mainly by bearing and rotary joints, switches, or power dividers	Relatively complex	Lens structure heavier than array structure	Moderate Moderately expensive
nical: by ent of entire a or by move- f feed; ical: by ing feeds	No	Yes: determined by feed design and lens element	May be lower than reflectors due to cable loss in lens	Controlled by aperture illumination taper		Yes: by use of multiple feeds	Horns, waveguide transmission lines and rotary joints, switches, or variable power dividers	Determined mainly by bearing and rotary joints, switches, or power dividers	Complex	Relatively heavy	Moderately expensive Expensive

2 FOLDOUT FRAME

Preceding page blank

3 FOLDOUT FRAME

ORIGINAL PAGE IS
OF POOR QUALITY

Antenna Type	Applicable Scan Techniques	Multiple-Frequency Capability	Dual-Polarization Capability	Beam Efficiency	Sidelobe Levels	Cross Polarization Isolation	Multiple Beam Capability	Feeding Techniques	Reliability in Operation	Complexity
4. Interleaved Elements	Electronic	Yes: up to three frequencies (possibly four if one array can be used for both 18 and 21 GHz)	No: one polarization at each frequency		Controllable by control of aperture distribution; Element spacing may be a limiting factor		Yes: with addition of multiple feeding and phasing networks	Separate feed system for each array; corporate feeding	Determined by phase shifters and drivers	Complex
MECHANICALLY SCANNED ARRAYS										
1. Multimode-Multifrequency	Mechanical	Yes	No		Controllable by control of aperture distribution		No	Waveguide feeds and rotary joints	Determined by bearing and rotary joints	Moderately complex
2. Multimode-dual polarized	Mechanical	No	Yes: by use of crossed slots and polarization processing		Controllable by control of aperture distribution		No	Waveguide corporate feeds, magic-tees connected to branch lines	Determined by bearing and rotary joints	Relatively simple
LENSES										
1. Waveguide (square guide)	Mechanical: by movement of entire antenna or by movement of feed; Electrical: by switching feeds	No	Yes: determined by feed design	Should be at least comparable to that of reflectors	Controlled by aperture illumination taper		Yes: by use of multiple feeds	Horns, waveguide transmission lines and rotary joints, switches, or variable power dividers	Determined mainly by bearing and rotary joints, switches, or power dividers	Relatively complex
2. Bootlace	Mechanical: by movement of entire antenna or by movement of feed; Electrical: by switching feeds	No	Yes: determined by feed design and lens element	May be lower than reflectors due to cable loss in lens	Controlled by aperture illumination taper		Yes: by use of multiple feeds	Horns, waveguide transmission lines and rotary joints, switches, or variable power dividers	Determined mainly by bearing and rotary joints, switches, or power dividers	Complex

APPENDIX A
DIAGONAL ROW SPACING CALCULATIONS

It can be shown that the diagonal row spacing in the triangular-grid element arrangement shown in Figure 2-9 is always exactly equal to one freespace wavelength for rectangular waveguide with infinitely thin walls when the array is designed to radiate a broadside beam. This relation is true regardless of the "a" dimension of the waveguide as long as the cutoff point is not reached and only the TE_{10} mode is assumed to propogate. The proof is as follows.

The geometry relating row spacing, s, to the cutoff wavelength, λ_c, and the guide wavelength, λ_g, is given in Figure A-1. The right triangles ACD and ABC are similar and have a common angle, α. The expressions

$$\sin \alpha = s/\lambda_c \tag{A-1}$$

and

$$\tan \alpha = \lambda_g/\lambda_c \tag{A-2}$$

can be written from inspection of Figure A-1. Equation (A-1) is solved for s,

$$s = \lambda_c \sin\alpha \tag{A-3}$$

and Equation (A-2) is solved for α,

$$\alpha = \tan^{-1} (\lambda_g/\lambda_c) \tag{A-4}$$

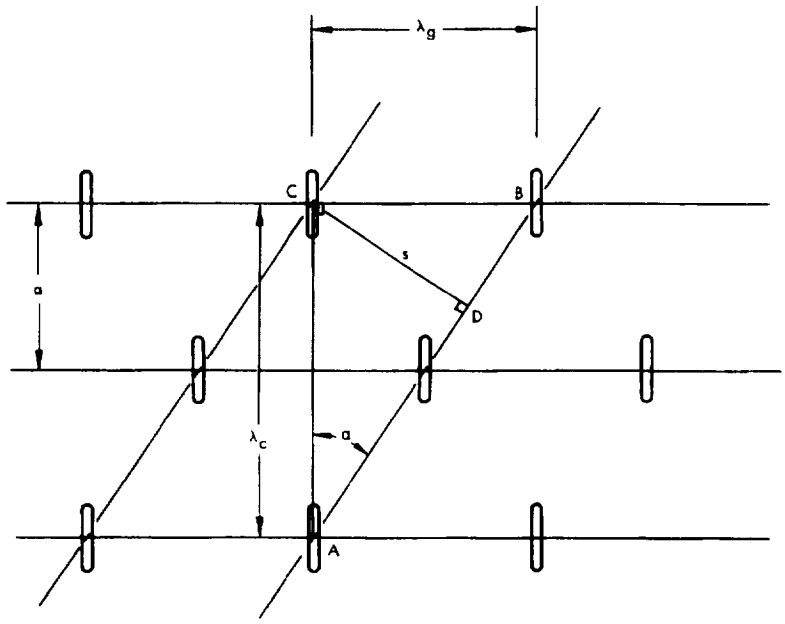

Figure A-1. Geometry for determination of row spacing, s, in terms of other waveguide parameters.

Substitution of Equation (A-4) into (A-3) for α then gives

$$s = \lambda_c \sin \tan^{-1}\left[(\lambda_g/\lambda_c)\right] \qquad \text{(A-5)}$$

The formula for λ_g in terms of λ_c and λ_o (freespace wavelength) for "empty" (not loaded with dielectric material or any periodic structure) rectangular waveguide is customarily given as

$$\lambda_g = \frac{\lambda_0}{\sqrt{1 - (\lambda_0/\lambda_c)^2}}$$

This equation is often rewritten as

$$\frac{1}{\lambda_0^2} = \frac{1}{\lambda_c^2} + \frac{1}{\lambda_g^2} \tag{A-6}$$

The terms in Equation (A-6) can be related to the sides of a right triangle as shown in Figure A-2. From this triangle it is apparent that

$$\tan\theta = \frac{1/\lambda_c}{1/\lambda_g} = \lambda_g/\lambda_c$$

$$\theta = \tan^{-1}(\lambda_g/\lambda_c) \tag{A-7}$$

Substitution of Equation (A-7) into Equation (A-5) for $\tan^{-1}(\lambda_g/\lambda_c)$ yields

$$s = \lambda_c \sin\theta \tag{A-8}$$

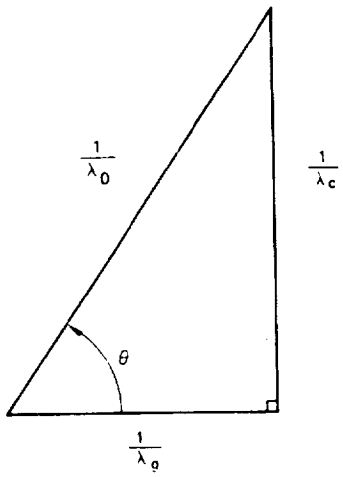

Figure A-2. Geometrical representation of equation relating pertinent wavelengths in a waveguide.

From Figure A-2, it can be seen that

$$\sin \theta = \frac{1/\lambda_c}{1/\lambda_0} = \lambda_0/\lambda_c \qquad \text{(A-9)}$$

Substitution of Equation (A-9) into Equation (A-8) gives

$$s = \lambda_c (\lambda_0/\lambda_c) = \lambda_0$$

and it is thus proved that the row spacing, s, is always equal to λ_0 under the conditions outlined above.

APPENDIX B
BEAM POSITION IN ANTENNA COORDINATES

For some antenna configurations it may be desirable to fix the antenna boresight axis along the ground track and to scan the beam relative to the boresight by motion of a feed or by switching among multiple feeds. In that case it is necessary to determine the required beam positions relative to the boresight position. These positions may be specified in terms of azimuth angle, α, and an elevation angle, ϵ, as illustrated in Figure B-1.

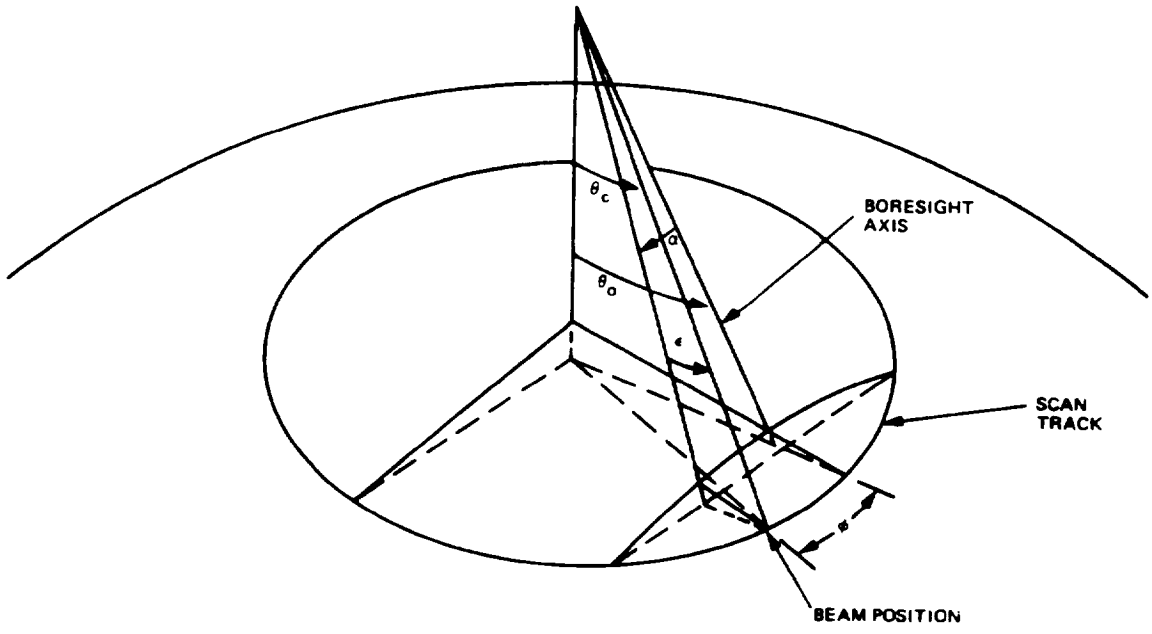

Figure B-1. Scan coordinates of fixed antenna with boresight axis at θ_0.

These angles are a function of the scan angle ϕ, the cone angle θ_c, and the boresight angle θ_o. The relationships are given as follows.

$$\sin \epsilon = \sin \theta_c \cos \theta_0 \cos \phi - \cos \theta_c \sin \theta_0$$

$$\tan \alpha = \frac{\sin \theta_c \sin \phi}{\sin \theta_c \sin \theta_0 \cos \phi + \cos \theta_c \cos \theta_0}$$

The angle θ_0 should be picked to minimize the elevation scan angle. It will generally be selected to provide elevation scans above and below boresight so that the beam is not scanned too far off-axis. One possibility is to make the scans above and below the boresight equal. Another possibility is to put the boresight at the angle that gives zero elevation scan at the maximum azimuth scan, θ_s. The first condition is given by

$$\tan \theta_0 = \tan \theta_c \frac{(1 + \cos \phi_s)}{2}$$

and the second condition by

$$\tan \theta_0 = \tan \theta_c \cos \phi_s$$

For the first condition, for θ_c = 45 degrees and ϕ_s = 35 degrees, θ_0 is 42.29 degrees. For this case the values of α and ϵ versus ϕ are given in Figure B-2a. The ϵ versus α is plotted in Figure B-2b.

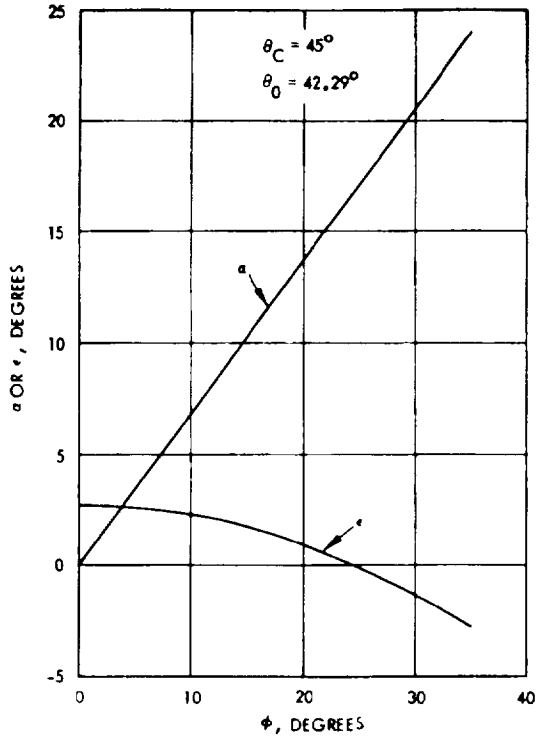

a. Azimuth and elevation angles versus beam position on scan track

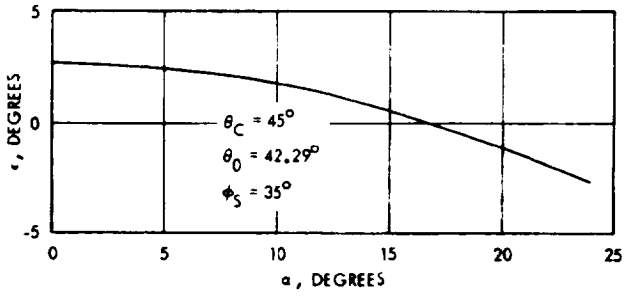

b. Elevation angle versus azimuth angle for scan on 45-degree cone

Figure B-2. Scan coordinates relative to boresight axis.

REFERENCES

Aerojet (1971). A 37-GHz High Resolution Radiometer Study, Task 1: Tradeoff Study, Report No. 3003R-1, Aerojet General Corporation, December.

Aerojet (1974). A 37-GHz High Resolution Radiometer Study, Final Report on Contract Report No. 1742FR-1A, Aerojet Electrosystems Company, February. NAS5-21676.

Agrawal, V.D., and W.A. Imbriale (1976). "Experimental and Theoretical Design of Dichroic Surface for a Spacecraft Antenna" AP-S International Symposium Digest, 105-108.

Ajioka, J.S., D.M. Joe, R. Tang, and N.S. Wong (1974). "Arbitrarily Polarized Slot Radiators in Bifurcated Waveguide Arrays," IEEE Trans. on Antennas and Propagation, AP-22, 196-200, March.

Amitay, N., and H. Zucker (1972). "Compensation of Spherical Reflector Aberrations by Planar Array Feeds," IEEE Trans. on Antennas and Propagation, AP-20, 49-56.

Arnaud, J.A. and F.A. Pelow, "Resonant-Grid Quasi-Optical Diplexers," Bell Syst. Tech. Journ., 54, No. 2, February 1, 1975, 263-283.

Ashmead, J. and A.B. Pippard (1946). "The Use of Spherical Reflectors as Microwave Scanning Aerials, "Journal IEE (London), 93, Pt. III-A, 627-632.

Baldwin, R., and P.A. McInnes (1973). "Radiation Patterns of Dielectric Loaded Rectangular Horns," IEEE Trans. on Antennas and Propagation, AP-21, 375-376, May.

Bokurka, V.J., (1975). "Dual Frequency Band Feed with Partially Dielectric Loaded Grooves," Electronic Letters, 11, 376-378; 7 August.

Born and Wolf, Principles of Optics, Sec. 4.5.1, 166-168, Pergamon Press, 1959.

Boynes, J.E., and J.H. Provencher (1972). "Experimental Results of a Multi-frequency Array Antenna," IEEE Trans. on Antenna and Propagation, AP-20, 106-107, January.

Brown, J. (1953). "Artificial Dielectrics Having Refractive Indices Less Than Unity," Proc. IEE (London), 100, Pt. 4, Monograph No. 62R, 51-62, May.

Carne, A., and J. Brown (1958). "Theory of Reflections from the Rodded-Type Artificial Dielectric," Proc. IEE (London), 106B, Paper No. 274R, 107-115, November.

Chen, C.C. (1973). "Transmission of Microwaves through Perforated Flat Plates of Finte Thickness," IEEE Trans. on Microwave Theory and Techniques, MTT-21, 1-6.

Chen, C.C. (1971). "Diffraction of Electromagnetic Waves by a Conducting Screen Perforated Periodically with Circular Holes, IEEE Trans. On Microwave Theory and Technique, MTT-19, 457-481, May

Clarricoats, P.J.B., and P.K. Saha (1971). "Propagation and Radiation Behaviour of Corrugated Feeds," Parts 1 and 2, Proc. IEE (London), 118, 1167-1186, September.

Dion, A. (1969). A Variable-Coverage Communications Antenna, Report TR-4-11, MIT Lincoln Laboratories.

Frey, F. (1976). A 5-Frequency Radiometer Antenna System Feed Horn, NASA/GSFC Contract NAS5-20637, Comsat Labs, Clarksburg, Md. 20794; June.

Goebels, F.J., and R.K. Anderson (1970). "A Dual-Band Slot Array Technique," IEEE Trans. On Antennas and Propagation, AP-18, 282-284, March.

Goebels, F.J., and T.S. Fong (1965). "Four Independent Beams from a Single Linear Array," IEEE Trans. on Antennas and Propagation, AP-13, 683-691.

Goodall, E.G.Z., and J.A.C. Jackson (1959). "Transmission of Electromagnetic Waves through Wire Gratings (Experimental)," Marconi Review, 22, 91-98.

Gustincic, J.J. (1974). Spherical Reflector Feasibility Study, Final Report on JPL Contract No. 560080, December.

Hansen, R.C. (1964), Microwave Scanning Antennas, Vol. 1, Academic Press, N.Y, 180.

Hansen, R.C. (1974). Design Tradeoff Study for a Spherical Antenna System for SIMS, Final Report on JPL Contract No. 954104, December.

Holtzman, J.C. (1968). "A Dual Band Array." IEEE Trans. on Antennas and Propagation, AP-16, 603; Patent No. 3,243,818, assigned to Hughes Aircraft Company.

Hsiao, J.K. (1971). "Analysis of Interleaved Arrays of Waveguide Elements," IEEE Trans. on Antennas and Propagation, AP-19, 729-735, November.

Hughes (1964). Manned Spacecraft Deep Space Antenna Study, Final Report on Contract NAS9-2099, Report No. P64-51, Hughes Aircraft Company, April.

Hyde, G. (1968). "Studies of the Focal Region of a Spherical Reflector: Stationary Phase Evaluation," IEEE Trans. on Antennas and Propagation, AP-16, 646-656, November.

Kummer, W.H., and A.F. Seaton (1973). Broadband Techniques for Waveguide Lenses, Patent Disclosure No. 63183, Hughes Aircraft Company.

Li, T. (1959). "A Study of Spherical Reflectors as Wide-Angle Scanning Antennas," IRE Trans. on Antennas and Propagation, AP-7, 223-226.

Love, A.W. (1976). "Electromagnetic Horn Antennas" IEEE Press, New York, New York 10017.

Love, A.W. (1973). "Scale Model Development of a High Efficiency Dual-Polarized Line Feed for the Arecibo Spherical Reflector," IEEE Trans. on Antennas and Propagation, AP-21, 626-639, September.

Love, A.W., and J.J. Gustincic (1968). "Line Source Feed for a Spherical Reflector," IEEE Trans. on Antennas and Propagation, AP-16, 132-134, January.

Luebbers, R.J., and B.A. Munk, (1975). "Cross Polarization Losses in Periodic Arrays of Loaded Slots," IEEE Trans. on Antennas and Propagation, Vol. AP-23, No. 2, March 1975, 159-164.

Meier, R., and R.K. Thomas (1972). Multi-Beam, Multi-Frequency Microwave Radiometer Antenna, Technical Information Series Report No. 72SD254, General Electric Space Division, November.

Mentzer, C.A., and L. Peters, Jr. (1974). "Properties of Cutoff Corrugated Surfaces for Corrugated Horn Design," IEEE Trans. on Antennas and Propagation, AP-22, 191-196, March.

Miller, J.R. and B.J. Forman (1966). "A Planar Array with Four Independent Beams," IEEE Trans. on Antennas and Propagation, AP-14, 560-565.

Munk, B.A. and R.J. Luebbers, (1974). "Reflection Properties of Two-Layer Dipole Arrays," IEEE Trans. on Antennas and Propagation, Vol. AP-22, No. 6, November 1974, 776-773.

Pascalar, H.G. (1974). "Millimeter Wave Passive Sensing from Satellites," Proc. of 1974 Millimeter Waves Techniques Conference, 2, F-5-18 to F5-21, Naval Electronics Laboratory Center, San Diego, CA.

Pelton, E.L. and B.A. Munk (1974). "A Streamlined Metallic Radome," IEEE Trans. on Antennas and Propagation, AP-22, No. 6, November 1974, 799-803.

Potter, P.D. (1973). Efficient Antenna Systems: A New Computer Program for the Design and Analysis of High Performance Conical Feedhorns, Technical Report No. 32-1526, Jet Propulsion Laboratory.

Roberts, C. (1973). Private Communication, GTE Sylvania.

Rotman, W. (1962). "Plasma Simulation by Artifical Dielectrics and Parallel-Plate Media," IRE Trans. on Antennas and Propagation, AP-10, 82-95, January.

Ruze, J. (1966). "Antenna Tolerance Theory," Proc. IEEE, 54, 633-640.

Saleh, A.A.M., and R.A. Semplak, (1976). "A Quasi-Optical Polarization-Independent Diplexer for Use in Beam Feed Systems of Millimeter-Wave Antennas," IEEE Trans. on Antennas and Propagation, AP-24, 780-785; November.

SAMSO (1973). Advanced General Purpose Forces Satellite Antenna Study, Final Report, SAMSO-TR-74-71, Hughes Aircraft Company, December.

Satoh, T. (1972). "Dielectric Loaded Horn Antenna," IEEE Trans. on Antennas and Propagation, AP-20, 199-201, March.

Schennum, G.H. (1973). "Frequency Selective Surfaces for Multiple Frequency Antennas"; Microwave Journal 16, 55-57, May.

Seaton, A.F. (1971). Virtual-Wall Slot Circularly Polarized Planar Array Antenna, Patent No. 3599216, assigned to Hughes Aircraft Company, August.

Skwirzynshi, J.K., and J.C. Thackray (1959). "Transmission of Electromagnetic Waves through Wire Gratings (Theory)," Marconi Review, 22, 77-90.

Sletten, C.J. (1969). "Reflector Antennas," Antenna Theory, Part 2, R.E. Collin and F.J. Zucker, eds., McGraw-Hill Book Company, Inc.

Strider, C.A. (1974). "Millimeter-Wave Planar Arrays," Proc. of 1974 Millimeter-Waves Techniques Conference, 1, B6-1 to B6-11, Naval Electronics Laboratory Center, San Diego, CA.

TDRSS (1975). TDRSS Users Guide, Revision 2, STDN No. 101.2 Goddard Space Flight Center, National Aeronautics and Space Administration, May.

Tsandoulos, G.N. and W.D. Fitzgerald (1972). "Aperture Efficiency Enhancement in Dielectrically Loaded Horns," IEEE Trans. on Antennas and Propagation, AP-20, 69-74, January.

Wesley, R.W. and C.Y. Tomita (1971). X-band Constrained Lens Radar Antenna, AFAL-TR-71-229, August.

Zvic, F. (1975). "Very Wideband Corregated Horns," Electronic Letters, 11, 131-133, 2 March.